DIFFERENT AUTOPILOT DESIGNS AND THEIR PERFORMANCE COMPARISON FOR GUIDED MISSILES

A THESIS SUBMITTED TO
THE GRADUATE SCHOOL OF NATURAL AND APPLIED SCIENCES
OF
THE MIDDLE EAST TECHNICAL UNIVERSITY

BY

ÖZGÜR ATEŞOĞLU

IN PARTIAL FULFILLMENT OF THE REQUIREMENTS FOR THE DEGREE OF
MASTER OF SCIENCE
IN
THE DEPARTMENT OF AERONAUTICAL ENGINEERING

DECEMBER 1996

Approval of the Graduate School of Natural and Applied Sciences.

Prof. Dr. Tayfur ÖZTÜRK
Director

I certify that this thesis satisfies all the requirements as a thesis for the degree of Master of Science.

Prof. Dr. Yalçın GÖĞÜŞ
Head of Department

This is to certify that we have read this thesis and that in our opinion it is fully adequate, in scope and quality, as a thesis for the degree of Master of Science.

Prof. Dr. Kemal ÖZGÖREN
Co.- Supervisor

Assoc. Prof. Mehmet Ş. KAVSAOĞLU
Supervisor

Examining Committee Members

Assoc. Prof. Ozan TEKİNALP
Assoc. Prof. Mehmet Ş. KAVSAOĞLU
Prof. Dr. M. Kemal ÖZGÖREN
Dr. Murat EREN
Assoc. Prof. Ömer MORGÜL

ABSTRACT

DIFFERENT AUTOPILOT DESIGNS AND THEIR PERFORMANCE COMPARISON FOR GUIDED MISSILES

ATEŞOĞLU, Özgür
M. S., Department of Aeronautical Engineering
Supervisor: Assoc. Prof. Mehmet Ş. KAVSAOĞLU
Co-Supervisor: Prof. Dr. M. Kemal ÖZGÖREN

December 1996, 118 pages

In this thesis, modeling, guidance, control, and flight simulations of an inertially guided missile are made. For a typical canard controlled missile, one guidance methodology for tracking a predefined trajectory and two different autopilot designs are presented.

The guidance design is made by using the inverse dynamics methodology, in order to null the error between the desired and the actual trajectories of the missile.

The autopilots are designed using two different methods. The first autopilot is designed by applying a pole and zero placement technique. The second one is designed by applying the optimal control method with a prescribed degree of stability.

The performances of the two autopilots are demonstrated using six degrees of freedom simulations for a pre - specified trajectory considering the same disturbances such as thrust misalignment, randomly distributed side wind and random aerodynamic derivative perturbations. Their performances are examined, compared, and discussed.

Keywords : Missile dynamics, Flight simulation, Guided missile, Guidance and control, Missile autopilots, Canard control, Pole and zero placement, Optimal control with prescribed stability, Side wind disturbance, Thrust misalignment, Aerodynamic derivative perturbation.

ÖZ

GÜDÜMLÜ FÜZELER İÇİN FARKLI OTOPİLOT TASARIMLARI VE PERFORMANS KARŞILAŞTIRMALARI

ATEŞOĞLU, Özgür
Yüksek Lisans, Havacılık Mühendisliği Bölümü
Tez Yöneticisi: Doç. Dr. Mehmet Ş. KAVSAOĞLU
Ortak Tez Yöneticisi: Prof. Dr. M. Kemal ÖZGÖREN

Aralık 1996, 118 sayfa

Bu tezde, ataletsel güdümlü bir füzenin modellenmesi, güdümü, kontrolu ve uçuş benzetimleri yapılmıştır. Ön kanatçık kontrollu tipik bir füze için önceden belirlenmiş bir yörüngeyi takip eden bir güdüm metodu ve iki farklı otopilot tasarımları sunulmuştur.

Güdüm tasarımı, istenen yörünge ile gerçek yörünge arasındaki hatayı sıfırlamak amacıyla evrik dinamik yöntemi kullanılarak yapılmıştır.

Otopilot tasarımları farklı iki yöntem kullanılarak yapılmıştır. Birinci otopilot bir kutup ve sıfır yerleştirme tekniği kullanılarak tasarlanmıştır. İkincisi ise, önceden belirlenmiş bir kararlılık derecesini sağlayan optimal kontrol yöntemi ile tasarlanmıştır.

Her iki otopilotun performansları, önceden belirlenen bir yörünge için altı serbestlik dereceli ortam bilgisayar benzetimleri kullanılarak, itki kaçıklığı, yanal rüzgar ve aerodinamik veri bozunumu gibi bozucu etkiler altında sunulmuştur.Bu performanslar incelenmiş, karşılaştırılmış, ve tartışılmıştır.

Anahtar Kelimeler : Füze dinamiği, Uçuş benzetimi, Güdümlü füze, Güdüm ve kontrol, Füze otopilotları, Ön kanatçıkla yöneltme, Kutup ve sıfir yerlştirme, Belirtilmiş kararlılık dereceli optimal kontrol, Yanal rüzgar saptırması, İtki vektörü kaçıklığı, Aerodinamik türev perturbasyonu.

To My Father, Mother and Elder Sister,

Ömer, Perihan Ateşoğlu and Özlem Kuyucuoğlu,

for their endless love, support and patience throughout my life…

ACKNOWLEDGEMENT

I would like to express my sincere thanks and appreciation to my supervisor Assoc. Prof. Dr. Mehmet Ş. KAVSAOĞLU for his support and understanding and to my co-supervisor Prof. Dr. M. Kemal ÖZGÖREN for his support, suggestions and encouragement during the preparation of this thesis.

TÜBİTAK SAGE and my colleagues at TÜBİTAK SAGE and my group coordinator Dr. Murat EREN is greatly acknowledged.

I would like to express my thanks to all of the colleagues at TÜBİTAK - S.A.G.E. - E.G.T.G.; Taner İNCİ, Feza GÖKIŞIK, Aytekin ÖZKAN, Hüseyin TÜRKOĞLU, Naci ORHAN, Alper ÜNVER, Armağan ERGÜN, Sefa HAZIR.

This study is carried out at Defense Industries Research and Development Institute, Electronics and Guidance Technologies Research Group, TÜBİTAK - SAGE. The support provided by TÜBİTAK - SAGE is greatly acknowledged.

TABLE OF CONTENTS

LIST OF TABLES

LIST OF FIGURES

LIST OF SYMBOLS

a, b	relative weightings among canard deflection pairs
a, b, c, d, e	relative weightings among state variables and input for autopilot 2
a, b, c, e, f, g, t	transfer functions polynomial coefficients for the design of autopilot 1
a_x, a_y, a_z	acceleration components in body fixed reference frame
a'_x, a'_y, a'_z	body acceleration components without gravitational acceleration components
$a'_{xb}, a'_{yb}, a'_{zb}$	body acceleration components without gravity acceleration components in body fixed reference frame
$a'_{xe}, a'_{ye}, a'_{ze}$	body acceleration components without gravity acceleration components in earth fixed reference frame
a_{xm}, a_{ym}, a_{zm}	measured acceleration components in body fixed reference frame
a_y, a_z	normal accelerations of the missile in y and z directions
a_{yd}, a_{zd}	desired normal accelerations in y and z directions
a_z^*	reference normal acceleration in z direction
$a_z^{*''}$	reference normal acceleration in z direction for autopilot 2
A	maximum cross sectional area of the missile
$\hat{A}$	system matrix for the linearized dynamics of the missile
$\hat{A}'$	system matrix for the modified linear dynamics of the missile
$\hat{A}''$	system matrix for autopilot 2
$\bar{b}$	control vector for the linearized dynamics of the missile

$\bar{b}'$	control vector for the modified linear dynamics of the missile
c_{ij}	elements of transformation matrix $\hat{C}^{(i,j)}$
$\bar{c}'$	output vector for the modified linear dynamics of the missile
C	speed of sound
C_i	aerodynamic force and moment coefficients
$C_{i,j}^{(a,b)}$	cosine of the angle between the i th axis of reference frame a and j th axis of reference frame b
$C_{i\theta_i}(M)$	partial derivative of i th aerodynamic force or moment with respect to flight parameter θ_i
$\hat{C}^{(i,j)}$	orthonormal transformation matrix from frame j to i
d	diameter of the missile
d_1	disturbance coming from nonlinearity on roll dynamics
$\bar{e}$	column vector used in performance index for autopilot 2
$\bar{e}$	error vector for the desired and instantaneous positions of the missile in Y and Z directions
$\vec{F}$	net force acting on the missile body
F_0	unrolled missile frame
F_1	rolled missile frame
F_{ax}, F_{ay}, F_{az}	components of force occuring only due to aerodynamic effects acting on the missile in the body fixed reference frame
F_x, F_y, F_z	components of net force acting on the missile in the body fixed reference frame
g_x, g_y, g_z	gravity components in body fixed reference frame
$\bar{g}$	column vector used in the formation of optimal input
G_a	transfer function for accelerometers
G_g	transfer function for gyroscopes
$\bar{G}(s)$	transfer matrix for the linearized dynamics of the missile

h	altitude
H	Hamiltonian of the performance index
$\vec{H}$	angular momentum of the missile
I_{ij}	elements of inertia matrix
$\hat{I}$	identity matrix
I_0	initial rotational inertia before the consumption of the propellant
I_1	final rotational inertia after the consumption of the propellant
Imp	impulse at any instant
Imp_{total}	total impulse
$\breve{J}$	inertia dyadic
$\hat{J}$	inertia matrix
$\hat{\bar{J}}$	performance index for autopilot 2
kdp, kdy, kpp, kpy	coefficients for the error vector dynamics $\bar{e}$
$\bar{k}$	column vector for autopilot 2 controller gains
K^*	amplifying gain for $\hat{Q}_0$
K_a, K_q, K_z, K_δ	autopilot 1 and autopilot 2 controller gains
K_p, K_ϕ	roll autopilot controller gains
K_r	ratio of autopilot 1 gain K_z to K_a
K_t	autopilot 2 controller gain
l	length of the missile
l_a	distance of accelerometers from the nose
L, M, N	components of moment occuring only due to aerodynamic effects acting on the missile in the body fixed reference frame
L_T, M_T, N_T	components of thrust moment acting on the missile in the body fixed reference frame
$L_{\theta_i}, M_{\theta_i}, N_{\theta_i}$	short hand notations with respect to flight parameter θ_i for rotational linear dynamics of the missile

m	mass of the missile
m_0	initial mass before the consumption of the propellant
m_1	final mass after the consumption of the propellant
M	Mach number
$\vec{M}$	net moment acting on the missile body
M_x, M_y, M_z	components of net moment acting on the missile in the body fixed reference frame
N', M'	compensated aerodynamic moments for changing center of mass
p, q, r	components of angular velocity in the body fixed reference frame with respect to the earth fixed reference frame
p_4	fourth pole of the closed loop of autopilot 1
$\hat{P}$	matrix found from the solution of algebraic Riccati equation
Q_d	dynamic pressure
$\hat{Q}$	weighting matrix used in canard deflection minimization
$\hat{Q}$	weighting matrix for the state vector for autopilot 2
$\hat{Q}_0$	weighting matrix used for different relative weightings among state variables for autopilot 2
$\bar{r}^{(0)}$	commanded canard deflection column vector in the unrolled missile frame
$\bar{r}^{(1)}$	commanded canard deflection column vector in the rolled missile frame
$\bar{r}$	forcing vector for inverse dynamics guidance logic
$\bar{r}^{(i)}$	any vector in coordinate frame (i)
R	universal gas constant
R	weighting value for the input for autopilot 2
$\hat{R}_i(\theta_k)$	successive elementary rotation along i th axis by θ_k
t	time
t_{boost}	final time of the boost phase

T	thrust force
T	temperature
T_0	temperature at sea level
T_x, T_y, T_z	components of thrust force acting on the missile in the body fixed reference frame
u_r, v_r, w_r	relative velocity components of the missile in case of wind in the body fixed reference frame
U_{wx}, U_{wy}, U_{wz}	components of wind velocity in the body fixed reference frame
V_{wx}, V_{wy}, V_{wz}	components of wind velocity in the earth fixed reference frame
$\vec{V}_T$	total velocity of the missile
x, y, z	axes of body fixed reference frame
x_{c0}	initial mass center position before the consumption of the propellant
x_{c1}	final mass center position after the consumption of the propellant
$\bar{x}$	state vector for the linearized dynamics of the missile
$\bar{x}'$	state vector for the modified linear dynamics of the missile
$\bar{x}''$	state vector for autopilot 2
X, Y, Z	axes of earth fixed reference frame
X_s, Y_s, Z_s	axes of stability reference frame
X_w, Y_w, Z_w	axes of wind reference frame
y_c	distance between the rolling body axis to the area center of one fin panel
Y_d, Z_d	desired positions of the missile in Y and Z directions
Y_{θ_i}, Z_{θ_i}	short hand notations with respect to flight parameter θ_i for transitional linear dynamics of the missile
z	state variable in the modified linear dynamics of the missile
z_i	i th zero of the closed loop transfer function of autopilot 1

Greek Letters

α	angle of attack
α	predefined stability degree
β	side slip angle
β_p	arccosine of damping ratio of denominator dynamics for autopilot 1
β_z	arccosine of damping ratio of numerator dynamics for autopilot 1
γ	specific heat ratio
δ_1, δ_2	thrust misalignment angles
$\delta_1, \delta_2, \delta_3, \delta_4$	four canard deflections
δ_a	effective aileron deflection
δ_{ac}	commanded aileron deflection in the unrolled missile frame
δ'_{ac}	commanded aileron deflection in the rolled missile frame
δ_c	commanded fin deflection for control actuation system
δ_e	effective elevator deflection
δ_{ec}	commanded elevator deflection in the unrolled missile frame
δ'_{ec}	commanded elevator deflection in the rolled missile frame
δ_r	effective rudder deflection
δ_{rc}	commanded rudder deflection in the unrolled missile frame
δ'_{rc}	commanded rudder deflection in the rolled missile frame
$\Delta_d(s)$	denominator polynomial for closed loop of autopilot 1
$\Delta_{dr}(s)$	denominator polynomial for closed loop of roll autopilot
$\Delta_n(s)$	numerator polynomial for closed loop of autopilot 1
ζ_a	damping ratio of accelerometer dynamics
ζ_c	damping ratio of control actuation system dynamics

ζ_g	damping ratio of gyroscope dynamics
ζ_p	damping ratio of denominator dynamics for autopilot 1
ζ_r	damping ratio of numerator dynamics for roll autopilot
ζ_z	damping ratio of numerator dynamics for autopilot 1
η	input for the modified linear dynamics of the missile
η''	input for autopilot 2
η''^{o}	optimal input value for autopilot 2
θ_{i0}	trim values of the flight parameters
$\theta_{i,j}$	angle between the i th axis of reference frame a and j th axis of reference frame b
$\hat{\kappa}_1$	matrix used for formation of $\overline{g}$
$\overline{\kappa}_2$	column vector used for formation of $\overline{g}$
ξ_p	damping ratio of pitch plane error dynamics
ξ_y	damping ratio of yaw plane error dynamics
ρ_0	air density at sea level
ϕ, θ, ψ	Euler angles
$\hat{\Phi}$	$\overline{g}$ transition matrix
$\overline{\psi}$	costate vector for the Hamiltonian of the performance index for autopilot 2
$\overline{\omega}$	column vector composed of components of the angular velocity of the body frame with respect to the earth frame
$\tilde{\omega}$	skew symmetric matrix composed of components of the angular velocity of the body frame with respect to the earth frame
ω_{na}	natural frequency of accelerometer dynamics
ω_{nc}	natural frequency of control actuation system dynamics
ω_{ng}	natural frequency of gyroscope dynamics
ω_{np}	natural frequency of denominator dynamics for autopilot 1
ω_{np}	natural frequency of pitch plane error dynamics
ω_{nr}	natural frequency of numerator dynamics for roll autopilot

ω_{ny}	natural frequency of yaw plane error dynamics
ω_{nz}	natural frequency of numerator dynamics for autopilot 1

CHAPTER 1

INTRODUCTION

Missile guidance system is the system that realizes the determination and control of its position. This system is composed of navigation, guidance and control. The components of navigation, guidance and control system for inertial guidance is seen in Figure 1.1.

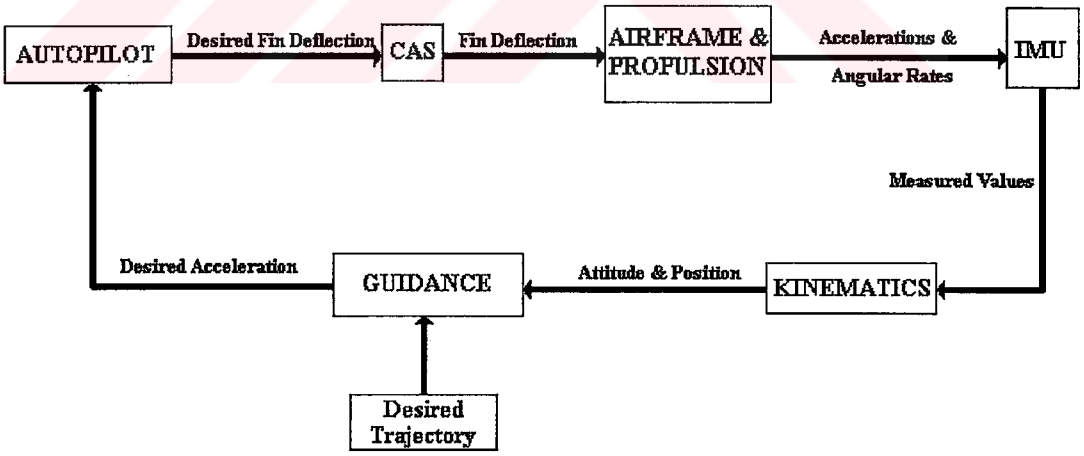

Figure 1.1 Navigation, Guidance and Control System for Inertial Guidance

Navigation system provides the velocity, position and attitude of the missile with respect to an inertial reference frame. Navigation computation is done

with the help of the signals coming from accelerometers and gyroscopes which are configured as a gimbaled or strapdown system in the inertial measurement unit. The whole system is called inertial navigation system.

The flight control system stabilizes the missile with respect to the guidance commands generated throughout the flight. This stabilization is done in pitching, yawing and rolling motions of the missile. The flight control system generates its own commands for control mechanisms, in order to properly execute the guidance commands.

The guidance system provides the necessary flight path dynamics in order to achieve the mission objective of the missile. In the case of fixed target intercept, the guidance system is preprogrammed to guide the missile on a predefined desired trajectory. This is called inertial guidance.

There are different kinds of guidance as; command guidance, homing guidance and preset guidance. Throughout this study a preset guidance method is investigated. With a preset guidance system, the missile is guided along a predefined flight trajectory to the target position. With the help of the inertial measurement unit, the actual position of the missile is found and compared with the predefined trajectory. Necessary control commands are generated to null the error between the predefined and actual trajectory. This kind of preset guidance is inertial guidance.

The reference frame in inertial guidance is stabilized within the missile. This can be done both physically or analytically. In inertial platform gimbaled systems, there is a platform which is always aligned with the inertial reference by means of gimbal drive systems. On this platform, accelerometer triads are mounted. Since the platform is aligned with the inertial reference, by means of the gyroscopes, the accelerometer triad senses the accelerations in the inertial reference frame. With correction for gravity and double integration of the measured acceleration values, position determination is possible. Figure 1.2 shows position determination for

gimbaled platform systems. In strapdown inertial systems, accelerometers and gyroscopes are mounted directly to the vehicle. Outputs of these measuring devices are the acceleration and angular velocity vectors with respect to the inertial frame expressed by their components in the body coordinate system. These outputs have to be transformed to inertial frame via a transformation matrix generated between two frames. Figure 1.3 shows position determination for strapdown systems. The inertial sensors in strapdown systems has to have a very large dynamic range, since they are subjected to entire vehicle dynamics. In autopilot studies, outputs of strapdown systems can be used directly. Throughout this study, strapdown inertial navigation system is considered.

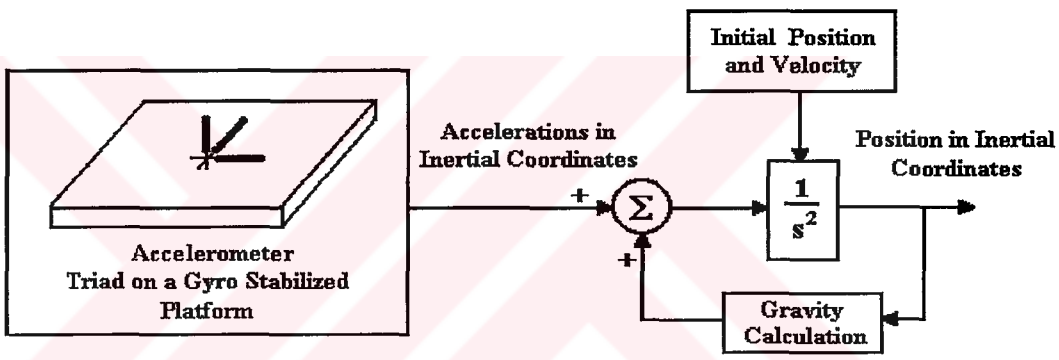

Figure 1.2 Position Determination for Gimbaled Platform Systems

Inertial navigation system functions' are sensing, computing and outputting. The gyroscopes and accelerometers sense the angular velocity and acceleration. Their outputs are used in the computer which is generating velocity, position and attitude information. Outputs of the inertial navigation system are used in flight control system.

The autopilot closes the loop in flight control system to achieve required stability and performance characteristics. The autopilot consists of compensation networks (controllers) designed to process sensor signals and

guidance commands in order to provide actuator system commands which cause the desired missile response.

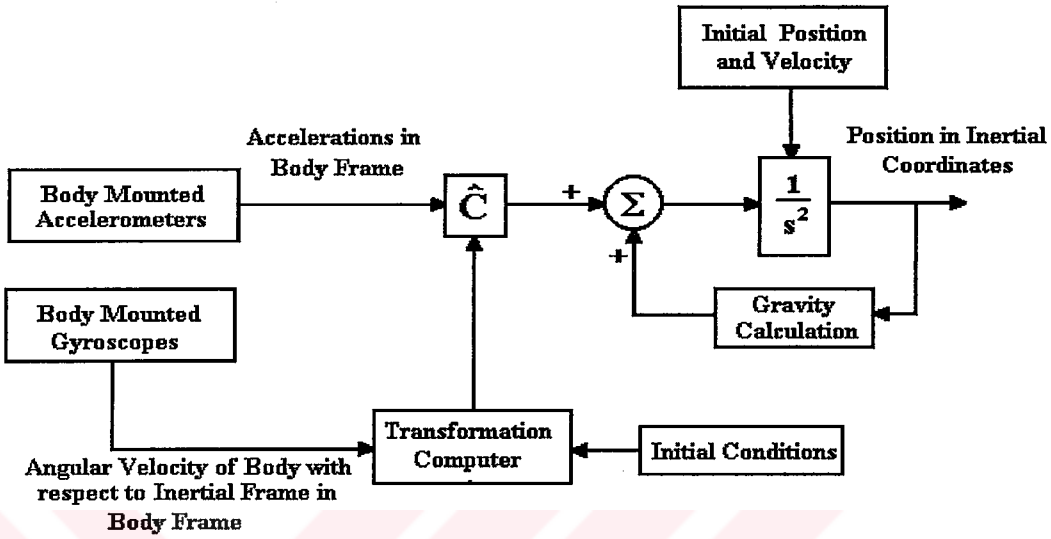

Figure 1.3 Position Determination for Strapdown Systems

The autopilot controllers are functions of airframe design, flight environment, sensor and control actuator characteristics. Since the airframe has time varying characteristics, the controllers require time varying coefficients. Also some nonlinearities should be integrated within the controllers. Typically Laplace domain design techniques are used to design the required controller. Algorithms are developed to compute appropriate controller coefficients over the operating regime of the autopilot. Flight simulations are then used to evaluate the effect of nonlinearities, coupling effects and time varying characteristics on autopilot design.

The autopilot closed loop is essentially another component in the guidance closed loop system. Hence the autopilot stability and performance characteristics have major interference effect on guidance loop stability and performance. It is desired that, the bandwidth of the closed loop autopilot be much greater than the bandwidth of the guidance loop.

The purpose of the autopilot can be summarized as follows; controlling the missile dynamic stability for all phases of flight, controlling the aerodynamic loads on the missile to attain guidance objectives, compatibility with guidance loop, decoupling the pitch and yaw control channels, reducing the effects of disturbances and noise.

The autopilot types in conventional use are; rate command, acceleration command, velocity command, angle of attack command and attitude command. Also damping with rate feedback as stability augmentation can be integrated with these types of autopilots [1].

There are some constraints on the design of the autopilot. These constraints are trajectory constraints, guidance constraints and airframe constraints [1]. Trajectory constraints are launch conditions, staging, re - entry, winds, Mach number range, dynamic pressure range and maximum normal accelerations. Guidance constraints are steering commands accuracy, resolution, response time and bandwidth, compatibility with guidance modes, mode switching transients as initialization, magnitude and recovery time, hardware constraints, stability and attitude angles, angular rates and accelerations. Airframe constraints are aerodynamic parameters, aeroelastic effects, body parameters, control vane parameters, propulsion, thrust levels and allocated size, weight and location of autopilot components.

Autopilot design cycle can be summarized as shown in Figure 1.4 [2].

In this thesis two different acceleration autopilot design techniques are applied for a generic canard controlled inertially guided surface to surface missile. The dynamics and control simulation of this missile is made by considering the overall missile dynamics, navigation, guidance and autopilot loops in six degrees of freedom modeling.

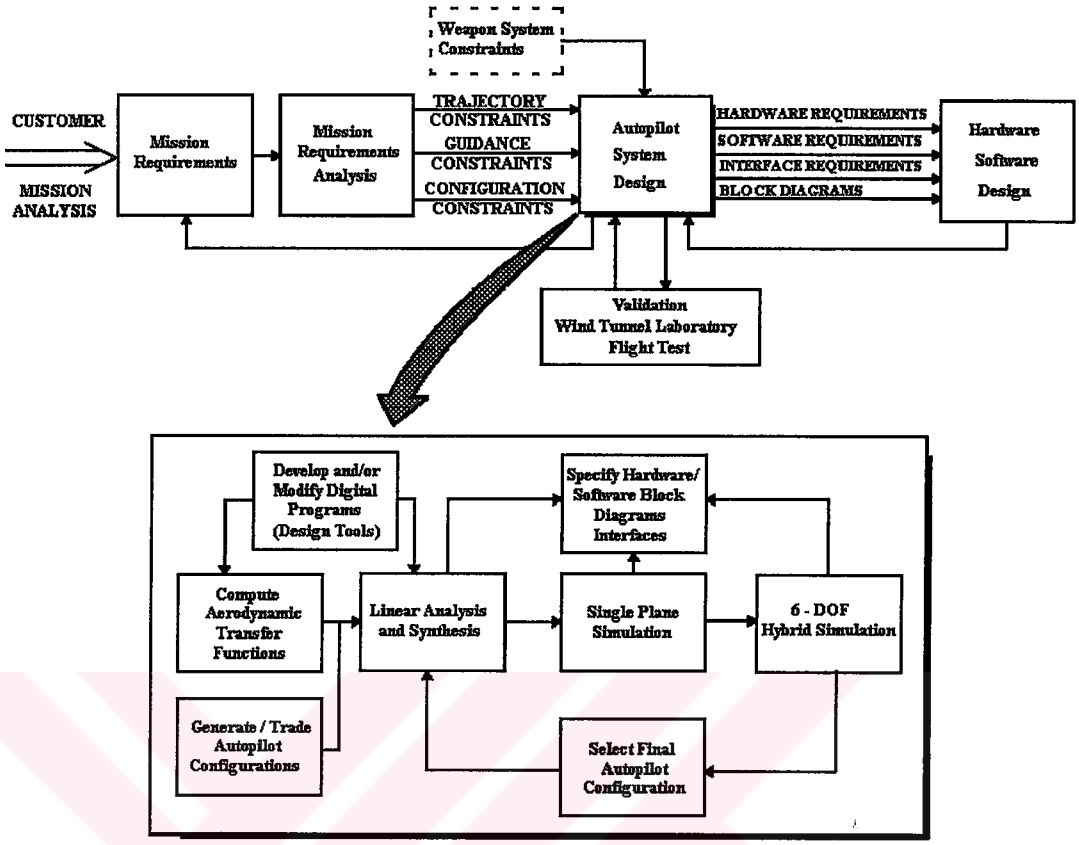

Figure 1.4 Autopilot Design Cycle

In Chapter 2, the equations of motion for a rigid missile are derived and obtained. These came out to be six kinematic and six dynamic first order nonlinear coupled first order differential equations. Numerical solution of these equations, with appropriate initial conditions, leads to the velocity, position and attitude of the missile in flight.

In Chapter 3, modeling of aerodynamic forces and moments acting on the missile are made. The aerodynamic coefficient conventions for a stable canard controlled missile are given in longitudinal and yaw planes of flight.

In Chapter 4, the missile model is linearized and the derivation of the missile linearized dynamics transfer functions are made for longitudinal, lateral and rolling aspects of flight.

In Chapter 5, guidance design using nonlinear inverse dynamics scheme is applied. In order to track the pre - specified trajectory, the reference accelerations in longitudinal and yaw planes are derived symbolically as functions of missile's total velocity component in the direction of its range, missile's body acceleration component excluding gravitation in the direction of its central line, elements of direction cosine matrix, and reference trajectories in longitudinal and lateral directions.

In Chapter 6, two different types of autopilot design techniques are studied for the missile under consideration and two longitudinal and lateral acceleration autopilots are designed. The roll reversal phenomena is examined for the missile under study and a roll attitude autopilot is designed.

In Chapter 7, the six degrees of freedom simulations are made for these two autopilots for a predefined desired trajectory. Throughout these simulations two of the autopilots are subjected to some external disturbances as side wind and thrust misalignments. Also random aerodynamic derivative perturbation is done on the missile six degrees of freedom model to see the robustness of the designed autopilot to uncertainties in the missile frame modeling. The simulations are made on HP - UX 9.01 environment on Apollo 9000/720 workstation using Integrated Systems Inc., $Matrix_x$ Product Family, Xmath and SystemBuild Modules [3], [4].

In Chapter 8, after the simulations, the performance of the two autopilots are discussed and compared. The overall study is discussed and recommendations for future studies are made.

In Appendix, modeling of other components that make up the overall six degrees of freedom model are given. These are variable mass and inertia model, thrust misalignment model, sensor models, strapdown model, control actuation system model including aerodynamic surface arrangements and roll resolving, wind model and effect of center of gravity change.

All of the presented work in this thesis is done using the belonging hardware and software supplies in Defense Industries Research and Development Institute, Electronics and Guidance Technologies Research Group, TÜBİTAK - SAGE.

CHAPTER 2

THE EQUATIONS OF MOTION

The equations of motion of a rigid missile are composed of twelve nonlinear first order differential equations. Six of them are kinematic equations and the other six are dynamic equations. The kinematic equations of the missile can be derived from the geometry and the dynamic equations can be derived using Newtonian Mechanics.

2.1 Reference frames

Here two reference frames are used to describe the motion of the missile, which are both right handed and orthogonal. These reference frames are fixed to the earth and to the missile's body. The earth fixed reference frame can be assumed to be inertial because the range of the missile is short compared to the radius of the earth and motion of the missile is much faster compared to the earth motion. The axes of this 'pseudo' inertial reference frame are X, Y, and Z. Here X axis points towards north, Z axis points downwards to earth's center, and the Y axis is the complementing orthogonal axis found by the right hand rule. Body fixed reference frame has its origin at the missile's center of mass and its axes are x, y, and z. or X_b, Y_b, and Z_b. These reference frames are shown in Figure 2.1.

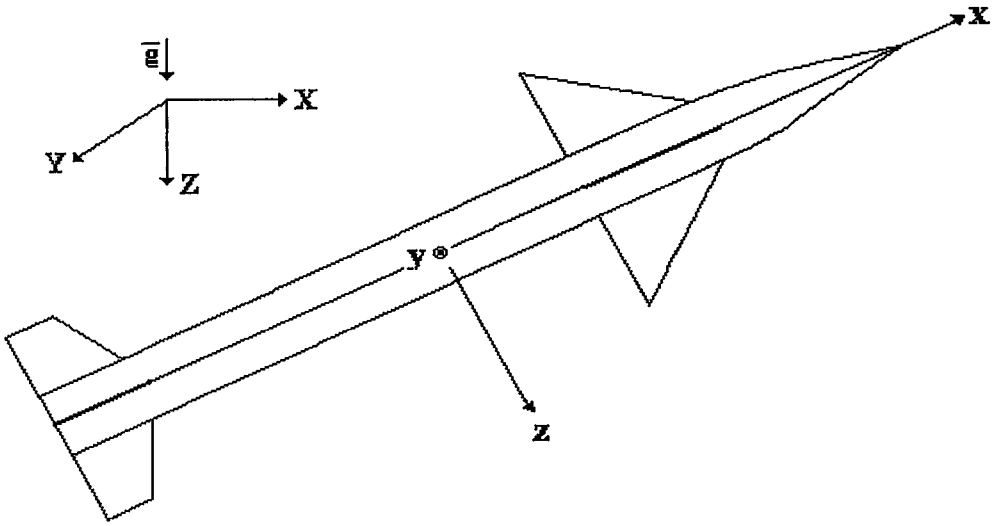

Figure 2.1. Earth Axes and Body Axes

Any vector $\vec{r}$ can be expressed in different coordinate frames as different column vectors. These column vectors can be related by using a linear transformation between the specified coordinate frames. Such a transformation can be represented as,

$$\bar{r}^{(a)} = \hat{C}^{(a,b)}\bar{r}^{(b)} \tag{2.1}$$

$\hat{C}^{(a,b)}$ is an orthogonal transformation matrix which represents a transformation from frame F_b to frame F_a. Since the matrix is an orthanormal one the following properties hold,

$$\hat{C}^{(a,b)} = \hat{C}^{(b,a)-1} = \hat{C}^{(b,a)T} \tag{2.2}$$

Let $\vec{u}_i^{(a)}$ and $\vec{u}_j^{(b)}$ be the ith unit basis vector of reference frame F_a and j^{th} unit basis vector of reference frame F_b. Then the element at the ith row and the jth column of matrix $\hat{C}^{(a,b)}$ can be expressed as,

$$C_{i,j}^{(a,b)} = \cos\left(\theta_{i,j}\right) \tag{2.3}$$

where

$$\theta_{i,j} = \left\{\vec{u}_i^{(a)} \rightarrow \vec{u}_j^{(b)}\right\} \tag{2.4}$$

Using the above equalities, the transformation between the body and the earth axes can be written as,

$$\begin{Bmatrix} X \\ Y \\ Z \end{Bmatrix} = \hat{C}^{(e,b)} \begin{Bmatrix} x \\ y \\ z \end{Bmatrix} \tag{2.5}$$

Here $\hat{C}^{(e,b)}$ is the direction cosine matrix and can be expressed uniquely using a set of Euler Angles.

2.1.1 Euler Angles

Rotational transformation between two reference frames can be expressed by successive basic rotation matrices. In flight mechanics applications it is customary to use a 3 - 2 - 1 rotated frame based Euler transformation sequence.

The Euler angles are denoted as, ψ : "yaw angle", θ : "pitch angle", and ϕ : "roll angle". A 3 - 2 - 1 rotated frame based sequence can be produced by using these three angles in three successive elementary rotations. This can be seen more clearly in Figure 2.2.

The elementary rotation matrices and the resulting transformation matrix are given below :

$$\hat{R}_3(\psi) = \begin{bmatrix} c\psi & -s\psi & 0 \\ s\psi & c\psi & 0 \\ 0 & 0 & 1 \end{bmatrix} \tag{2.6}$$

$$\hat{R}_2(\theta) = \begin{bmatrix} c\theta & 0 & s\theta \\ 0 & 1 & 0 \\ -s\theta & 0 & c\theta \end{bmatrix} \tag{2.7}$$

$$\hat{R}_1(\phi) = \begin{bmatrix} 1 & 0 & 0 \\ 0 & c\phi & -s\phi \\ 0 & s\phi & c\phi \end{bmatrix} \tag{2.8}$$

$$\hat{C}^{(e,b)} = \hat{R}_3(\psi).\hat{R}_2(\theta).\hat{R}_1(\phi) \tag{2.9}$$

$$\hat{C}^{(e,b)} = \begin{bmatrix} c\theta c\psi & s\phi s\theta c\psi - c\phi s\psi & c\phi s\theta c\psi + s\phi s\psi \\ c\theta s\psi & s\phi s\theta s\psi + c\phi c\psi & c\phi s\theta s\psi - s\phi c\psi \\ -s\theta & s\phi c\theta & c\phi c\theta \end{bmatrix} \tag{2.10}$$

In the above equations s and c denote sine and cosine respectively. 3 - 2 - 1 rotation sequence has a singularity for $\theta = \pm 90^{0}$. At these θ values, ψ and ϕ values cannot be differentiated from each other and singularity occurs. In order to remove this singularity different formulations has to be done. In our application, this singularity does not take place, since vertical flight is not achieved in any phase of the flight.

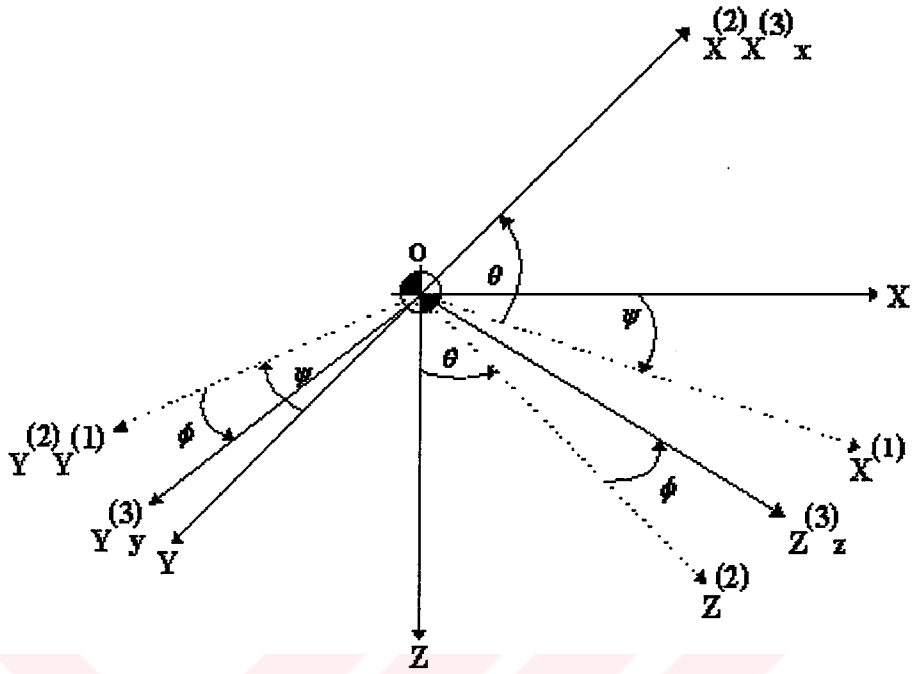

Figure 2.2. Reference Frames and Euler Angles

2.2 Kinematic Equations

The position and the attitude of the missile with respect to the earth frame is found by solving the kinematic equations given in this section.

2.2.1 Translational Kinematics

The velocity components in the earth reference frame and in the body reference frame are related as,

$$\begin{bmatrix} \dot{X} \\ \dot{Y} \\ \dot{Z} \end{bmatrix} = \hat{C}^{(e,b)} \begin{bmatrix} u \\ v \\ w \end{bmatrix} \tag{2.11}$$

where X , Y , Z are the coordinates of the mass center of the missile in the earth frame. u , v , w denote the components of the missile's absolute velocity in the missile reference frame and $\hat{C}^{(e,b)}$ is the transformation matrix from the body frame to the earth frame.

2.2.2 Rotational Kinematics

The rotational kinematic equations relate the time rate of change of the Euler Angles to the angular rates of the missile body. Letting,

$$\hat{C} = \hat{C}^{(e,b)} \tag{2.12}$$

and using the identity

$$\hat{C}^T \hat{C} = \hat{I}, \tag{2.13}$$

it is seen that,

$$\frac{d}{dt}\left(\hat{C}^T \hat{C}\right) = \frac{d}{dt}\left(\hat{I}\right) = \hat{0} \tag{2.14}$$

$$\hat{C}^T \dot{\hat{C}} = -\dot{\hat{C}}^T \hat{C} \tag{2.15}$$

$$\hat{C}^T \dot{\hat{C}} = -\left(\hat{C}^T \dot{\hat{C}}\right)^T \tag{2.16}$$

The above equation indicates that $\hat{C}^T \dot{\hat{C}}$ is a skew symmetric matrix and so there exists a skew symmetric matrix $\tilde{\omega}$ generated from a column $\overline{\omega}$ such that $\tilde{\omega} = \hat{C}^T \dot{\hat{C}}$. $\overline{\omega}$ is composed of the components of the angular velocity of the

body frame with respect to the earth frame represented at the body frame. More explicitly,

$$\overline{\omega} = \begin{bmatrix} p \\ q \\ r \end{bmatrix}, \tag{2.17}$$

and the corresponding skew symmetric matrix is

$$\widetilde{\omega} = \begin{bmatrix} 0 & -r & q \\ r & 0 & -p \\ -q & p & 0 \end{bmatrix} \tag{2.18}$$

Solving $\hat{C}^T\dot{\hat{C}} = \widetilde{\omega}$ for the Euler angle rates, the rotational kinematic equations are found as,

$$\dot{\psi} = \left(q.\sin\phi + r.\cos\phi\right) / \cos\theta \tag{2.19}$$

$$\dot{\theta} = q.\cos\phi - r.\sin\phi \tag{2.20}$$

$$\dot{\phi} = p + \left(q.\sin\phi + r.\cos\phi\right).\tan\theta \tag{2.21}$$

Once the p , q , r are known ψ , θ , ϕ can be found by integrating the above three differential equations.

2.3 Dynamic Equations

The dynamic equations of motion can be found from Newton's Second Law of Motion for rigid bodies which states that the time rate of change of the momentum is equal to the net force applied on the body and the time rate of

change of the angular momentum is equal to the net moment applied on the body. For the translational and the rotational dynamics, the equations can be written as,

$$\vec{F} = \frac{d}{dt}\left(m.\vec{V}_T\right)\Big]_I \tag{2.22}$$

$$\vec{M} = \frac{d}{dt}\left(\vec{H}\right)\Big]_I \tag{2.23}$$

In these equations $\vec{F}$ and the $\vec{M}$ are the net force and the net moment acting on the missile body. $\vec{H} = \breve{J}.\vec{\omega}$ is the angular momentum of the missile, where $\breve{J}$ is the inertia dyadic. $\vec{V}_T$ is the total velocity of the missile and m is the mass of the missile. $\Big]_I$ indicates that the differentiation of the related vectors are done in the inertial frame. Since the mass and the moment of inertia changes more slowly when compared with the translational and rotational velocities, they can be assumed to be quasi-constant during the derivation of dynamic equations.

2.3.1 Translational Dynamics

The translational dynamic equation is,

$$\vec{F} = m.\frac{d}{dt}\left(\vec{V}_T\right)\Big]_I \tag{2.24}$$

It is more convenient to express this equation in the body frame. So, it can be written again as

$$\vec{F} = m.\left\{\frac{d}{dt}\left(\vec{V}_T\right)\Big]_B + \vec{\omega} \times \vec{V}_T\right\} \tag{2.25}$$

where $]_B$ indicates that the differentiation is done in the body frame. In the body frame, the relevant vectors will be represented by the following columns :

$$\overline{\omega} = \begin{bmatrix} p \\ q \\ r \end{bmatrix} \tag{2.26}$$

$$\overline{V}_T = \begin{bmatrix} u \\ v \\ w \end{bmatrix} \tag{2.27}$$

$$\overline{F} = \begin{bmatrix} F_x \\ F_y \\ F_z \end{bmatrix} \tag{2.28}$$

Thus, the translational dynamic equations are found as

$$\dot{u} = F_x / m - w.q + v.r \tag{2.29}$$

$$\dot{v} = F_y / m - u.r + w.p \tag{2.30}$$

$$\dot{w} = F_z / m - v.p + u.q \tag{2.31}$$

These equations can be written in a compact form as shown below,

$$\begin{bmatrix} \dot{u} \\ \dot{v} \\ \dot{w} \end{bmatrix} = -\widetilde{\omega}.\begin{bmatrix} u \\ v \\ w \end{bmatrix} + \begin{bmatrix} F_x / m \\ F_y / m \\ F_z / m \end{bmatrix} \tag{2.32}$$

F_x, F_y, F_z are the components of the total force acting on the body expressed in the body frame, including the aerodynamic, thrust, and the gravitational forces.

2.3.2 Rotational Dynamics

The same procedure in translational dynamics equation, is applied to the rotational dynamics equation. The inertia dyadic can be expressed in the body frame by the following matrix,

$$\hat{J} = \begin{bmatrix} I_x & -I_{xy} & -I_{xz} \\ -I_{xy} & I_y & -I_{yz} \\ -I_{xz} & -I_{yz} & I_z \end{bmatrix} \tag{2.33}$$

I_{xy}, I_{yz}, I_{xz}, are the product of inertia terms, and taken to be zero since the missile under consideration is symmetric so that the body axes are principal. Also due to the rotational symmetry of the missile I_y, I_z, terms are taken to be equal to each other. Thus, the inertia matrix that is going to be used in the equations is taken in a simplified form as,

$$\hat{J} = \begin{bmatrix} I_x & 0 & 0 \\ 0 & I_y & 0 \\ 0 & 0 & I_y \end{bmatrix} \tag{2.34}$$

The rotational dynamics equation is,

$$\vec{M} = \frac{d}{dt}\left(\vec{H}\right)\Big]_I \tag{2.35}$$

Again, it is more convenient to express this equation in the body frame. So, it can be written again as

$$\vec{M} = \frac{d}{dt}\left(\vec{H}\right)\Big]_B + \vec{\omega} \times \vec{H} \tag{2.36}$$

On the other hand, $\breve{J}$ is constant in the body frame according to the constant mass assumption. So,

$$\vec{M} = \breve{J}.\left\{\frac{d}{dt}(\vec{\omega})\Big]_B\right\} + \vec{\omega} \times \breve{J}.\vec{\omega} \tag{2.37}$$

where $\Big]_B$ denotes differentiation done in the body frame.

Taking $\overline{\omega}$ as in Equation (2.17), and

$$\overline{M} = \begin{bmatrix} M_x \\ M_y \\ M_z \end{bmatrix} \tag{2.38}$$

The rotational dynamic equations are found as,

$$\dot{p} = M_x / I_x \tag{2.39}$$

$$\dot{q} = M_y / I_y + r.p.(I_y - I_x) / I_y \tag{2.40}$$

$$\dot{r} = M_z / I_y + p.q.(I_x - I_y) / I_y \tag{2.41}$$

M_x, M_y, M_z, are the components of the total moment acting on the body about its mass center expressed in the body frame, including the aerodynamic, thrust, and the gravitational moments.

CHAPTER 3

MODELING OF AERODYNAMIC FORCES AND MOMENTS

3.1 Modeling of Aerodynamics

In Chapter 2 forces and moments acting on the missile body are given as,

$$\overline{F} = \begin{bmatrix} F_x \\ F_y \\ F_z \end{bmatrix} \tag{3.1}$$

$$\overline{M} = \begin{bmatrix} M_x \\ M_y \\ M_z \end{bmatrix} \tag{3.2}$$

These forces and moments include the aerodynamic, thrust, and the gravitational effects. These forces and moments can be rewritten as,

$$\overline{F} = \begin{bmatrix} F_{ax} + m.g_x + T_x \\ F_{ay} + m.g_y + T_y \\ F_{az} + m.g_z + T_z \end{bmatrix} \tag{3.3}$$

$$\overline{M} = \begin{bmatrix} L + L_T \\ M + M_T \\ N + N_T \end{bmatrix} \tag{3.4}$$

In the above equations F_{ax}, F_{ay}, F_{az}, L, M ,N, are the forces and the moments which only occur due to aerodynamic effects on the missile in flight. g_x, g_y, g_z, are the body frame components of the gravitational acceleration which is assumed to have a constant magnitude and to be oriented directly towards the earth center. T_x, T_y, T_z are the thrust force components and L_T, M_T, N_T are the thrust moment components. T_y, T_z, M_T and N_T are zero unless there is thrust misalignment and L_T is zero unless the nozzle has spiral grooves. The gravity components can be found by applying a linear transformation on the gravity acceleration vector. This is,

$$\begin{bmatrix} g_x \\ g_y \\ g_z \end{bmatrix} = \hat{C}^T . \begin{bmatrix} 0 \\ 0 \\ g \end{bmatrix} \tag{3.5}$$

Aerodynamic forces and the moments can be expressed as,

$$\begin{bmatrix} F_{ax} \\ F_{ay} \\ F_{az} \end{bmatrix} = Q_d . A . \begin{bmatrix} C_x \\ C_y \\ C_z \end{bmatrix} \tag{3.6}$$

$$\begin{bmatrix} L \\ M \\ N \end{bmatrix} = Q_d . A . d . \begin{bmatrix} C_l \\ C_m \\ C_n \end{bmatrix} \tag{3.7}$$

In the above equations Q_d, is the dynamic pressure, A, is the maximum cross-sectional area of the missile, d, is the missile diameter. The C_i terms

are the dimensionless aerodynamic force and moment coefficients which are designated as,

C_x : Axial force coefficient.

C_y : Side force coefficient.

C_z : Normal force coefficient

C_l : Rolling moment coefficient

C_m : Pitching moment coefficient

C_n : Yawing moment coefficient

Dynamic pressure is expressed as,

$$Q_d = \frac{1}{2}.\rho.V_T{}^2 \tag{3.8}$$

where

$$V_T = \sqrt{\left(u^2 + v^2 + w^2\right)} \tag{3.9}$$

ρ is the air density and it changes with the altitude h, as,

$$\rho = \begin{Bmatrix} \rho_0.(1 - 0.00002256.h)^{4.256} & \text{for } h \leq 10000\text{m.} \\ 0.412.e^{-0.000151.(h-10000)} & \text{for } h > 10000\text{m.} \end{Bmatrix} \tag{3.10}$$

Here ρ_0 is the air density at sea level (1.223kg/m^3). These formulas are obtained by curve fitting to the density variation in the ICAO standard atmosphere,[5].

The aerodynamic force and moment coefficients are basically functions of the Mach number, M, which is a dimensionless number defined as the

ratio of the flight vehicle's velocity to the speed of sound at the altitude at which the vehicle is at flight. It is expressed as

$$M = \frac{V_T}{C} \tag{3.11}$$

where C is the speed of sound, i.e.

$$C = \sqrt{(\gamma . R . T)} \tag{3.12}$$

In the above equations γ is the specific heat ratio of the air which is taken to be equal to 1.4,and R is the universal air gas constant which is taken to be equal to 287 J/kg.K. T is the ambient temperature which also changes with altitude, and can be expressed as

$$T = \begin{Bmatrix} T_0 . (1 - 0.00002256 . h) & \text{for } h \leq 10000\text{m.} \\ 0.7744 . T_0 & \text{for } h > 10000\text{m.} \end{Bmatrix} \tag{3.13}$$

Here T_0 is the temperature at sea level and it is equal to 293 K. These formulas are also obtained by curve fitting to the temperature variation in the ICAO standard atmosphere,[5].

Throughout the flight, some flight angles are introduced to describe the motion of the missile. These angles are the angle of attack (α), and the side slip angle (β). The definition of these angles can be seen in Figure 3.1. They lead to the definitions of stability and wind axes which are also shown in the same figure.

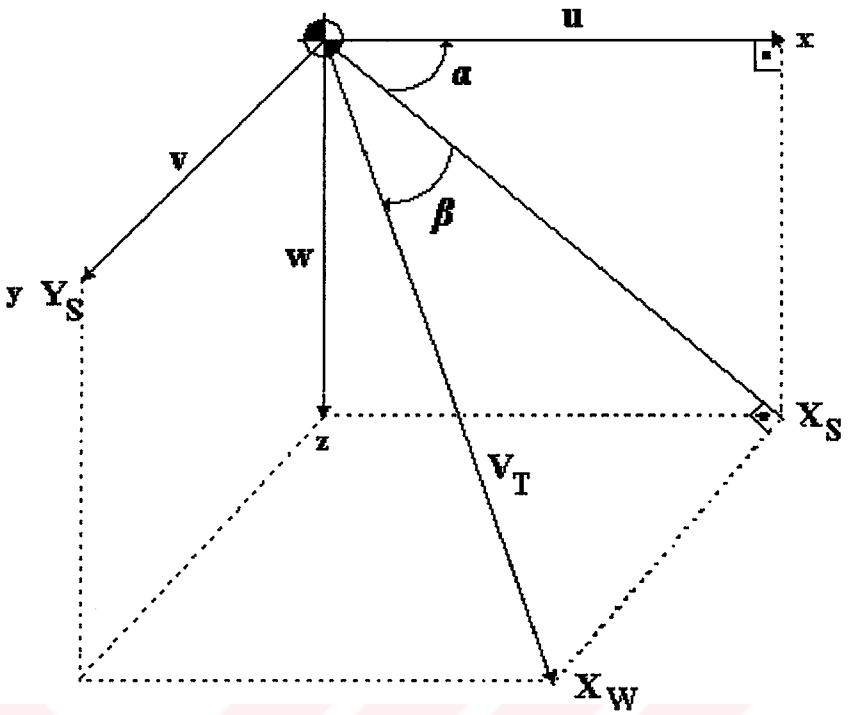

Figure 3.1 Definition of α, β, Stability Axes X_s, Y_s and the Wind Axes X_w.

The stability and wind axes can be found by means of following rotations :

From body to stability axes,

$$\hat{C}^{(b,s)} = \begin{bmatrix} \cos\alpha & 0 & \sin\alpha \\ 0 & 1 & 0 \\ -\sin\alpha & 0 & \cos\alpha \end{bmatrix} \tag{3.14}$$

From stability to wind axes,

$$\hat{C}^{(s,w)} = \begin{bmatrix} \cos\beta & -\sin\beta & 0 \\ \sin\beta & \cos\beta & 0 \\ 0 & 0 & 1 \end{bmatrix} \tag{3.15}$$

Using the total velocity V_T, and its components in the body axes, the angles α and β can be expressed as

$$\alpha = \arctan\left(\frac{w}{u}\right) \tag{3.16}$$

$$\beta = \arcsin\left(\frac{v}{V_T}\right) \tag{3.17}$$

Since w, v values are much smaller when compared with the u value, u value can be taken to be equal to the V_T value and the above equations can be written as

$$\alpha \cong \frac{w}{u} \tag{3.18}$$

$$\beta \cong \frac{v}{u} \tag{3.19}$$

The aerodynamic coefficients C_i are also functions of flight parameters such as the angle of attack, the side slip angle, the control surface deflections (δ_e, δ_r, δ_a), the body angular rates p, q, r and the time rate of change of the angle of attack and the side slip angle, in addition to the Mach number. The subscripts e, r, a of the δ terms denote the elevator, rudder, aileron deflections, respectively. These deflections are provided by the control surfaces. For more details see Appendix.

C_i can be shown as

$$C_i = C_i\left(M, \alpha, \beta, \delta_e, \delta_r, \delta_a, p, q, r, \dot{\alpha}, \dot{\beta}\right) \tag{3.20}$$

The aerodynamic coefficients are found using wind tunnel tests, computational fluid dynamics methods and some semi-empirical methods [6].

In the flight mechanics model in simulations, the aerodynamic coefficients are taken to be non-linear functions of flight parameters. But, in order to use in the autopilot studies, they can be linearized by using the Taylor series expansion around the trim values of the flight parameters as in Equation (3.21).

$$\begin{aligned} C_i\left(M,\alpha,\beta,\delta_e,\delta_r,\delta_a,p,q,r,\dot{\alpha},\dot{\beta}\right) &= C_{i0}(M) + C_{i\alpha}(M).\alpha + C_{i\beta}(M).\beta \\ &+ C_{i\delta_e}(M).\delta_e + C_{i\delta_r}(M).\delta_r + C_{i\delta_a}(M).\delta_a + C_{ip}(M).p.\frac{d}{2.V_T} + C_{iq}(M).q.\frac{d}{2.V_T} \\ &+ C_{ir}(M).r.\frac{d}{2.V_T} + H.O.T. \end{aligned} \tag{3.21}$$

In the above equation H.O.T. stands for the higher order terms in the Taylor series expansion and $d/2.V_T$ term is included as a multiplier to the dynamic aerodynamic derivatives to make the final product dimensionless.

A useful short hand notation is used for the above aerodynamic derivatives. This is shown as,

$$C_{i\theta_i}(M) = \left.\frac{\partial C_i}{\partial \theta_i}\right|_{\theta_i=\theta_{i0}} \quad \text{and} \quad C_{i\dot{\theta}_i}(M) = \left.\frac{\partial C_i}{\partial(\dot{\theta}_i.\frac{d}{2.V_T})}\right|_{\dot{\theta}_i=\dot{\theta}_{i0}}$$

The aerodynamic derivative values are taken at the trim values of the flight parameters and they are kept only as a non-linear function of the Mach number.

Since along the flight path of the missile $\alpha, \beta, \delta_e, \delta_r, \delta_a, p, q, r, \dot{\alpha}, \dot{\beta}$ will be small, the trim values used in this thesis are $\alpha_0 = \beta_0 = \delta_{e0} = \delta_{r0} = \delta_{a0} = 0$ and $p_0 = q_0 = r_0 = \dot{\alpha}_0 = \dot{\beta}_0 = 0$. With these values, $C_{i0} = 0$ for all i except i = x.

Thus, in order to use in the autopilot design studies, the dimensionless aerodynamic coefficients can be expressed linearly as shown below,

$$C_x = C_{x0}(M) \tag{3.22}$$

$$C_y = C_{y\beta}(M).\beta + C_{y\delta}(M).\delta_r + C_{yr}.r.\frac{d}{2.V_T} \tag{3.23}$$

$$C_z = C_{z\alpha}(M).\alpha + C_{z\delta}(M).\delta_e + C_{zq}.q.\frac{d}{2.V_T} \tag{3.24}$$

$$C_l = C_{l\delta}(M).\delta_a + C_{lp}.p.\frac{d}{2.V_T} \tag{3.25}$$

$$C_m = C_{m\alpha}(M).\alpha + C_{m\delta}(M).\delta_e + C_{mq}(M).q.\frac{d}{2.V_T} \tag{3.26}$$

$$C_n = C_{n\beta}(M).\beta + C_{n\delta}(M).\delta_r + C_{nr}(M).r.\frac{d}{2.V_T} \tag{3.27}$$

Maple-Synge rotational symmetry analysis on linear transverse aerodynamic forces and moments for a missile which has a symmetry with respect to its y, and z axis shows that [7],

$$C_{z\alpha} = C_{y\beta} \tag{3.28}$$

$$C_{z\delta} = C_{y\delta} \tag{3.29}$$

$$C_{zq} = -C_{yr} \tag{3.30}$$

$$C_{m\alpha} = -C_{n\beta} \tag{3.31}$$

$$C_{m\delta} = -C_{n\delta} \tag{3.32}$$

$$C_{mq} = C_{nr} \tag{3.33}$$

This rotational symmetry analysis can be understood more clearly with the help of sign convention analysis in the pitch and yaw planes.

Positive canard deflection convention can be taken as the one which creates a clockwise rolling moment when viewed from the aft of the missile [6]. This is shown in Figure 3.2.

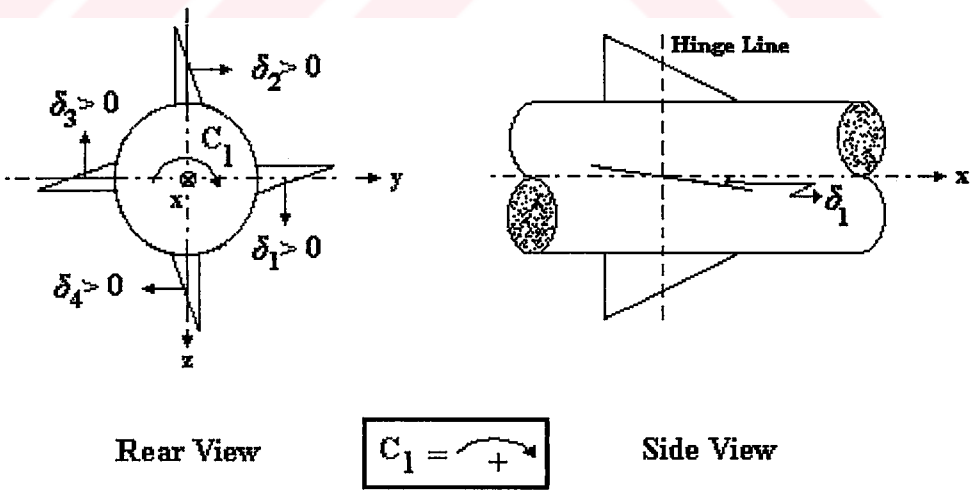

Figure 3.2. Convention for a Positive Canard Deflection

For a stable canard controlled missile, the sign conventions in pitch and yaw planes are shown in Figure 3.3 and 3.4.

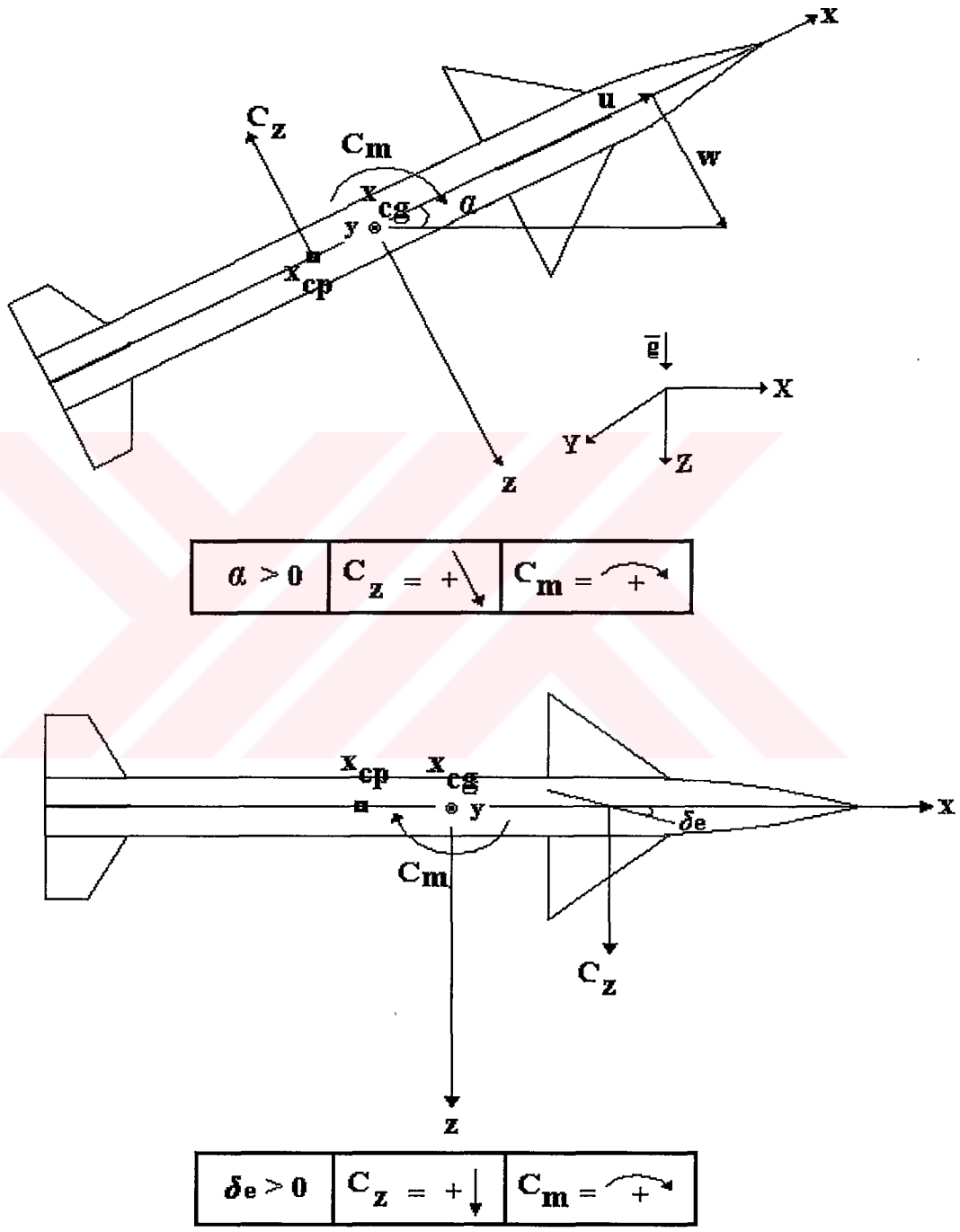

Figure 3.3. Aerodynamic Coefficient Conventions for a Stable Canard Controlled Missile in Pitch Plane

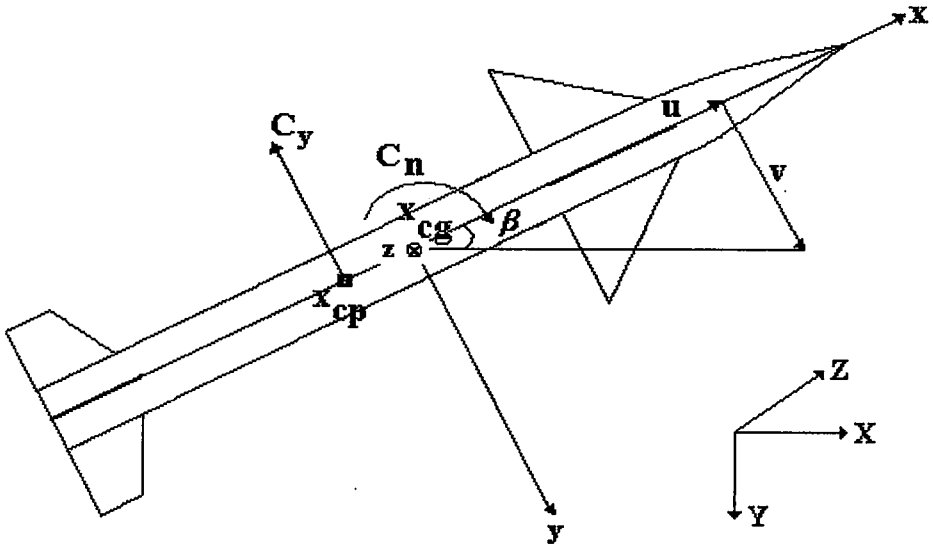

$\beta > 0$	$C_y = +$	$C_n = +$

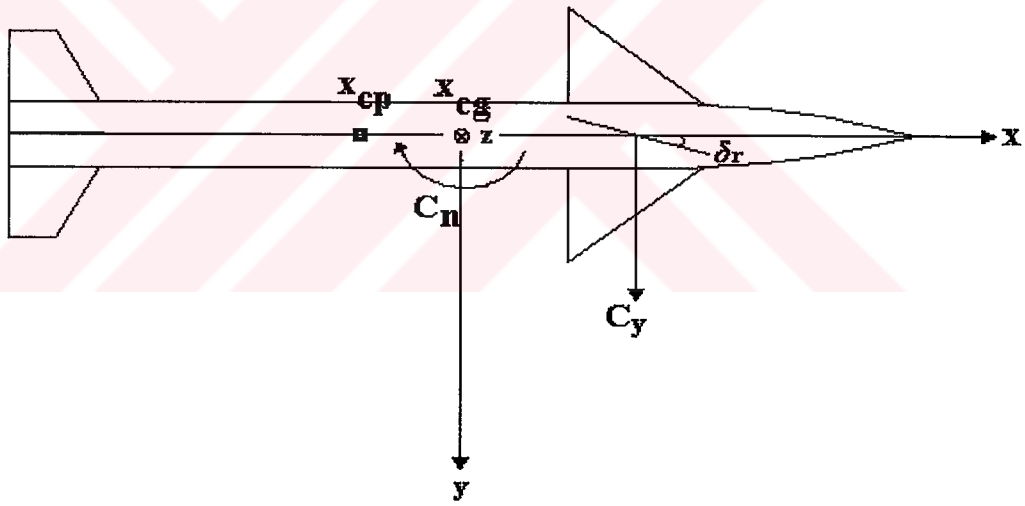

$\delta_r > 0$	$C_y = +$	$C_n = +$

Figure 3.4. Aerodynamic Coefficient Conventions for a Stable Canard Controlled Missile in Yaw Plane

With the help of the Figure 3.3 and 3.4, the inequalities $C_{m\alpha} < 0$, $C_{m\delta} < 0$, $C_{z\alpha} < 0$, $C_{z\delta} > 0$ and $C_{n\beta} > 0$, $C_{n\delta} > 0$, $C_{y\beta} < 0$, $C_{y\delta} > 0$ hold.

Also with the help of the Figure 3.1, for the roll motion, the inequality $C_{l\delta} > 0$ holds.

The dynamic aerodynamic derivatives show the damping characteristics of the missile. Their conventions will be shown as, $C_{mq} < 0$, $C_{zq} < 0$, $C_{lp} < 0$ and $C_{nr} < 0$, $C_{yr} > 0$.

CHAPTER 4

LINEARIZATION OF THE MISSILE MODEL

Non-linear equations describing the dynamics and kinematics of the missile are used in the simulations. For the control system design, these equations need to be simplified and linearized. These linearized equations describe the linear dynamics and stability characteristics of the missile. Using this linearized dynamics, any type of guidance and control scheme can easily be applied on the system. The controller designed for the linearized dynamics works properly for the small amplitude motions of the missile around the equilibrium condition of the linearized missile dynamics Throughout the flight, missile deviates from these equilibrium conditions due to some external disturbances such as, winds, gusts, thrust misalignments and, etc. But these deviations can be rejected by the autopilot servo loop due to its robustness properties.

4.1 Linearization Of Equations

Linearization of the dynamic and kinematic equations of motion can be done by using the following assumptions;

•Ambient density, ambient temperature, the speed of the missile and hence the Mach number are assumed to be constant.

•Angle of attack, side slip angle and the fin deflection angle are assumed to be small.

•Rolling motion is assumed to be very small. (i.e. $p \cong 0$, with $\phi \cong 0$).

•Components of gravitational acceleration in the yaw and the pitch planes are assumed to be external disturbances.

First assumption indicates that, the aerodynamic force and moment derivatives at trim conditions are constant. Second assumption is the major assumption that brings linearity on the equations. This assumption is originating from the fact that the velocity components w, and v remain small. Using this assumption angle of attack and the side slip angle can be used as motion variables instead of w and v. Third assumption is used to uncouple the motion in the pitch and the yaw planes to analyze the motions independently. This assumption is valid throughout the flight, since the roll control dynamics which has a reference roll angle being equal to zero, is designed to be faster than the pitch and the yaw control dynamics. Fourth assumption also helps to get rid of the non-linearity in the dynamics.

Linearization process can be done by rewriting the Equation (3.3) and 3.4, as follows ;

$$\begin{bmatrix} \dot{u} \\ \dot{v} \\ \dot{w} \end{bmatrix} = \begin{bmatrix} r.v - q.w + F_{ax}/m + g_x \\ -r.u + p.w + F_{ay}/m + g_y \\ q.u - p.v + F_{az}/m + g_z \end{bmatrix} \tag{4.1}$$

$$\begin{bmatrix} \dot{p} \\ \dot{q} \\ \dot{r} \end{bmatrix} = \begin{bmatrix} L/I_x \\ M/I_y + r.p.(I_y - I_x)/I_y \\ N/I_y + p.q.(I_x - I_y)/I_y \end{bmatrix} \tag{4.2}$$

In Equation (4.1) and (4.2) the thrust force and moment components occurring in Equations (3.3) and (3.4) are not included, since the design of lateral, longitudinal and roll autopilots will be done for the flight after the boost phase.

Using the assumptions that, v << u, and w << u, i.e. $u \cong V_T$, and $\dot{u} \cong \dot{V}_T \cong 0$, the following dynamic equations can be obtained. In these equations, it is also assumed that the roll autopilot can keep $p \cong 0$.

Longitudinal Dynamics:

$$\dot{w} = q.u + F_{az} / m + g_z \tag{4.3}$$

$$\dot{q} = M / I_y \tag{4.4}$$

Lateral Dynamics:

$$\dot{v} = -u.r + F_{ay} / m + g_y \tag{4.5}$$

$$\dot{r} = N / I_y \tag{4.6}$$

Roll Dynamics:

$$\dot{p} = L / I_x \tag{4.7}$$

This kind of an approximation is called 'short period approximation' in flight control systems literature.[8]. This approximation is almost true for the flight of the missile after the boost phase.

Using $p \cong 0$ assumption also with $\phi \cong 0$ in the kinematic Equations (2.19) and (2.20), the following equations will be obtained :

$$\dot{\theta} = q \tag{4.8}$$

$$\dot{\psi} = r / \cos\theta \tag{4.9}$$

Using the small angle and small velocity assumption in the Equations (3.18) and (3.19), the time derivatives of angle of attack and side-slip angle can be written as follows :

$$\dot{\alpha} \cong \frac{\dot{w}}{u} \tag{4.10}$$

$$\dot{\beta} \cong \frac{\dot{v}}{u} \tag{4.11}$$

Rewriting the simplified translational dynamic equations with the above formulations, they will take the following forms :

$$\dot{\alpha} = q + F_{az} / (m.u) + g_z / u \tag{4.12}$$

$$\dot{\beta} = -r + F_{ay} / (m.u) + g_y / u \tag{4.13}$$

The aerodynamic forces and the moments in the above equations can be linearized by using the Equations (3.23), (3.24), (3.26), and (3.27).

$$\dot{\alpha} = q + Q_d.A.(C_{z\alpha}.\alpha + C_{z\delta}.\delta_e + C_{zq}.q.\frac{d}{2.V_T}) / (m.u) + g_z / u \tag{4.14}$$

$$\dot{q} = Q_d.A.d.(C_{m\alpha}.\alpha + C_{m\delta}.\delta_e + C_{mq}.q.\frac{d}{2.V_T})/I_y \tag{4.15}$$

and

$$\dot{\beta} = -r + Q_d.A.(C_{y\beta}.\beta + C_{y\delta}.\delta_r + C_{yr}.r.\frac{d}{2.V_T})/(m.u) + g_y/u \tag{4.16}$$

$$\dot{r} = Q_d.A.d.(C_{n\beta}.\beta + C_{n\delta}.\delta_r + C_{nr}.r.\frac{d}{2.V_T})/I_y \tag{4.17}$$

In the above equations, the following short hand notations can be used:

$$Z_\alpha = \frac{Q_d.A}{m}.C_{z\alpha} \tag{4.18}$$

$$Z_\delta = \frac{Q_d.A}{m}.C_{z\delta} \tag{4.19}$$

$$Z_q = \frac{Q_d.A}{m}.(\frac{d}{2.V_T}).C_{zq} \tag{4.20}$$

$$Y_\beta = \frac{Q_d.A}{m}.C_{y\beta} \tag{4.21}$$

$$Y_\delta = \frac{Q_d.A}{m}.C_{y\delta} \tag{4.22}$$

$$Y_r = \frac{Q_d.A}{m}.(\frac{d}{2.V_T}).C_{yr} \tag{4.23}$$

$$M_\alpha = \frac{Q_d.A.d}{I_y}.C_{m\alpha} \tag{4.24}$$

$$M_\delta = \frac{Q_d.A.d}{I_y}.C_{m\delta} \tag{4.25}$$

$$M_q = \frac{Q_d.A.d}{I_y}.(\frac{d}{2.V_T}).C_{mq} \tag{4.26}$$

$$N_\beta = \frac{Q_d.A.d}{I_y}.C_{n\beta} \tag{4.27}$$

$$N_\delta = \frac{Q_d.A.d}{I_y}.C_{n\delta} \tag{4.28}$$

$$N_r = \frac{Q_d.A.d}{I_y}.(\frac{d}{2.V_T}).C_{nr} \tag{4.29}$$

Using the above short hand notations, linearized dynamics of the missile can be written as;

$$\dot{\alpha} = q + \frac{Z_\alpha}{u}.\alpha + \frac{Z_\delta}{u}.\delta_e + \frac{Z_q}{u}.q + \frac{g_z}{u} \tag{4.30}$$

$$\dot{q} = M_\alpha.\alpha + M_\delta.\delta_e + M_q.q \tag{4.31}$$

and

$$\dot{\beta} = -r + \frac{Y_\beta}{u}.\beta + \frac{Y_\delta}{u}.\delta_r + \frac{Y_r}{u}.r + \frac{g_y}{u} \tag{4.32}$$

$$\dot{r} = N_\beta.\beta + N_\delta.\delta_r + N_r.r \tag{4.33}$$

Taking the gravitational acceleration components as external disturbances on the system and ignoring them for the design of the autopilot servo characteristics, the linearized dynamics of the missile in the pitch plane is expressed as;

$$\dot{\alpha} = \frac{Z_\alpha}{u}.\alpha + (\frac{Z_q}{u} + 1).q + \frac{Z_\delta}{u}.\delta_e \tag{4.34}$$

$$\dot{q} = M_\alpha.\alpha + M_q.q + M_\delta.\delta_e \tag{4.35}$$

$$\dot{\theta} = q \tag{4.36}$$

And the yaw plane equations will be;

$$\dot{\beta} = \frac{Y_\beta}{u}.\beta + (\frac{Y_r}{u} - 1).r + \frac{Y_\delta}{u}.\delta \tag{4.37}$$

$$\dot{r} = N_\beta.\beta + N_r.r + N_\delta.\delta_r \tag{4.38}$$

$$\dot{\psi} = \frac{r}{\cos\theta} \tag{4.39}$$

4.2 Transfer Function Derivations

In the linearized equations θ, ψ values need not be taken as states, since they are obtainable by free integration of q and $r/\cos\theta$. If these equations are written in matrix form, the following equations will be obtained :

$$\begin{bmatrix}\dot{\alpha}\\ \dot{q}\end{bmatrix}=\begin{bmatrix}\frac{Z_\alpha}{u} & (\frac{Z_q}{u}+1)\\ M_\alpha & M_q\end{bmatrix}.\begin{bmatrix}\alpha\\ q\end{bmatrix}+\begin{bmatrix}\frac{Z_\delta}{u}\\ M_\delta\end{bmatrix}.\delta_e \tag{4.40}$$

$$\begin{bmatrix}\dot{\beta}\\ \dot{r}\end{bmatrix}=\begin{bmatrix}\frac{Y_\beta}{u} & (\frac{Y_r}{u}-1)\\ N_\beta & N_r\end{bmatrix}.\begin{bmatrix}\beta\\ r\end{bmatrix}+\begin{bmatrix}\frac{Y_\delta}{u}\\ N_\delta\end{bmatrix}.\delta_r \tag{4.41}$$

From the above equations it is seen that the linear dynamics of the missile is in the customary form $\dot{\bar{x}}=\hat{A}.\bar{x}+\bar{b}.\delta$, both for the pitch and the yaw planes.

For the pitch plane,

$$\bar{x}=\begin{bmatrix}\alpha\\ q\end{bmatrix},\ \hat{A}=\begin{bmatrix}\frac{Z_\alpha}{u} & (\frac{Z_q}{u}+1)\\ M_\alpha & M_q\end{bmatrix},\ \bar{b}=\begin{bmatrix}\frac{Z_\delta}{u}\\ M_\delta\end{bmatrix},\ \delta=\delta_e \tag{4.42}$$

For the yaw plane,

$$\bar{x}=\begin{bmatrix}\beta\\ r\end{bmatrix},\ \hat{A}=\begin{bmatrix}\frac{Y_\beta}{u} & (\frac{Y_r}{u}-1)\\ N_\beta & N_r\end{bmatrix},\ \bar{b}=\begin{bmatrix}\frac{Y_\delta}{u}\\ N_\delta\end{bmatrix},\ \delta=\delta_r \tag{4.43}$$

$\hat{I}$ being the identity matrix, the transfer matrix can be found as follows:

$$\frac{\bar{x}(s)}{\delta_e(s)}=\bar{G}(s)=(s.\hat{I}-\hat{A})^{-1}.\bar{b} \tag{4.44}$$

This equation, written explicitly, leads to

$$\begin{bmatrix}\alpha(s)\\ q(s)\end{bmatrix}=\begin{bmatrix}\dfrac{\frac{Z_\alpha}{u}.s+(M_\delta.(\frac{Z_q}{u}+1)-\frac{Z_\delta}{u}.M_q)}{s^2-(M_q+\frac{Z_\alpha}{u}).s+(\frac{Z_\alpha}{u}.M_q-M_\alpha.(\frac{Z_q}{u}+1))}\\ \dfrac{M_\delta.s+(\frac{M_\alpha.Z_\delta}{u}-\frac{M_\delta.Z_\alpha}{u})}{s^2-(M_q+\frac{Z_\alpha}{u}).s+(\frac{Z_\alpha}{u}.M_q-M_\alpha.(\frac{Z_q}{u}+1))}\end{bmatrix}.\delta_e(s) \qquad (4.45)$$

If the same approach is applied to the yaw plane, the corresponding equation will be,

$$\begin{bmatrix}\beta(s)\\ r(s)\end{bmatrix}=\begin{bmatrix}\dfrac{\frac{Y_\delta}{u}.s+(N_\delta.(\frac{Y_r}{u}-1)-\frac{Y_\delta}{u}.N_r)}{s^2-(N_r+\frac{Y_\beta}{u}).s+(\frac{Y_\beta}{u}.N_r-N_\beta.(\frac{Y_r}{u}-1))}\\ \dfrac{N_\delta.s+(\frac{N_\beta.Y_\delta}{u}-\frac{N_\delta.Y_\beta}{u})}{s^2-(N_r+\frac{Y_\beta}{u}).s+(\frac{Y_\beta}{u}.N_r-N_\beta.(\frac{Y_r}{u}-1))}\end{bmatrix}.\delta_r(s) \qquad (4.46)$$

The transfer functions which relate the normal acceleration of the missile both in pitch and yaw planes can be found by using the Equations (4.47) and (4.48) as shown below :

$$a_z = u.(\dot{\alpha} - q) \qquad (4.47)$$

$$a_y = u.(\dot{\beta} + r) \qquad (4.48)$$

Taking the Laplace Transform of the above equations with zero initial conditions, and dividing both sides of the equations with $\delta_e(s)$ and $\delta_r(s)$ respectively, the following transfer functions are obtained :

$$\frac{a_z(s)}{\delta_e(s)} = u.(\frac{\alpha(s)}{\delta_e(s)}.s - \frac{q(s)}{\delta_e(s)}) \tag{4.49}$$

$$\frac{a_y(s)}{\delta_r(s)} = u.(\frac{\beta(s)}{\delta_r(s)}.s + \frac{r(s)}{\delta_r(s)}) \tag{4.50}$$

These transfer functions are explicitly expressed as;

$$\frac{a_z(s)}{\delta_e(s)} = \frac{Z_\delta.s^2 + (Z_q.M_\delta - M_q.Z_\delta).s + (-M_\alpha.Z_\delta + Z_\alpha.M_\delta)}{s^2 - (M_q + \frac{Z_\alpha}{u}).s + (\frac{Z_\alpha}{u}.M_q - M_\alpha.(\frac{Z_q}{u} + 1))} \tag{4.51}$$

$$\frac{a_y(s)}{\delta_r(s)} = \frac{Y_\delta.s^2 + (Y_r.N_\delta - N_r.Y_\delta).s + (N_\beta.Y_\delta - Y_\beta.N_\delta)}{s^2 - (N_r + \frac{Y_\beta}{u}).s + (\frac{Y_\beta}{u}.N_r - N_\beta.(\frac{Y_r}{u} - 1))} \tag{4.52}$$

The linearized roll dynamics can be written by using the Equations (2.21) and (2.39). Since r and θ are not functions of p or ϕ in the linear dynamics, and since $\phi \cong 0$ as assumed before, $(q.\sin\phi + r.\cos\phi).\tan\theta$ term in Equation (2.21) can be treated as a disturbance on the roll dynamics and thus ignored for the design of the roll autopilot servo characteristics.

For convenience, the following short hand notations can be used :

$$L_\delta = \frac{Q_d.A.d}{I_x}.C_{l\delta} \tag{4.53}$$

$$L_p = \frac{Q_d.A.d}{I_x}.(\frac{d}{2.V_T}).C_{lp} \tag{4.54}$$

Then, the linearized roll dynamics can be written as

$$\dot{p} = L_p . p + L_\delta . \delta_a \tag{4.55}$$

$$\dot{\phi} = p \tag{4.56}$$

Taking the Laplace Transform of the above equations with zero initial conditions, the following transfer functions are obtained for the linearized roll dynamics :

$$\frac{p(s)}{\delta_a(s)} = \frac{L_\delta}{s - L_p} \tag{4.57}$$

$$\phi(s) = \frac{p(s)}{s} \tag{4.58}$$

CHAPTER 5

GUIDANCE DESIGN

For guided missiles it is important to increase the probability of hit, and decrease the miss distance. For that reason some kind of guidance system is installed on the missile depending on the design and the accuracy requirements of the missile. This guidance varies in a wide range, due to the mission of the missile. In any guidance application, the function of the guidance system is to send commands to the missile control system (autopilot), which also generates and sends commands to the control actuation system to achieve the desired movement of the missile.

Throughout this chapter design of a guidance scheme for a canard controlled, surface to surface and inertially guided missile is proposed. The aim of the designed guidance system is to generate the desired acceleration to follow a given desired trajectory in both of the pitch and yaw planes throughout the flight. This reference acceleration signal is generated in a way to correct the discrepancy between the position of the missile which is obtained by the strapdown algorithm in the inertial navigation system (INS), and the pre-programmed desired trajectory. Reference acceleration signal is sent to the longitudinal and lateral autopilots which generate the desired canard deflection commands, using this reference acceleration signal and the acceleration of the missile which is measured by the accelerometers both in the lateral and the longitudinal directions. The autopilots also use the rate

gyro signals as additional feedback inputs. Design of the autopilots and the guidance can be accomplished independently, since the autopilot loop is designed to be an inner loop dynamics, and the guidance is designed to be an outer loop dynamics which requires a frequency response characteristics with a much smaller bandwidth when compared with that of the autopilot. In this chapter, the guidance system is designed by using the nonlinear inverse dynamics principle as explained below.

Taking the desired trajectories in the pitch and yaw planes as functions of the range X as, $Z_d = Z_d(X)$, and $Y_d = Y_d(X)$, following error vector can be written;

$$\bar{e} = \begin{bmatrix} Z - Z_d \\ Y_d - Y \end{bmatrix} \tag{5.1}$$

In the above expression Z, Y are the positions at which the missile is instantaneously located in the earth frame. The time derivative of the error vector can be expressed as

$$\dot{\bar{e}} = \begin{bmatrix} \dot{Z} - \frac{\partial Z_d}{\partial x}.\dot{X} \\ \frac{\partial Y_d}{\partial x}.\dot{X} - \dot{Y} \end{bmatrix} \tag{5.2}$$

or

$$\dot{\bar{e}} = \begin{bmatrix} -\frac{\partial Z_d}{\partial x} & 0 & 1 \\ \frac{\partial Y_d}{\partial x} & -1 & 0 \end{bmatrix} . \begin{bmatrix} \dot{X} \\ \dot{Y} \\ \dot{Z} \end{bmatrix} \tag{5.3}$$

Let

$$\hat{G} = \begin{bmatrix} -\dfrac{\partial Z_d}{\partial x} & 0 & 1 \\ \dfrac{\partial Y_d}{\partial x} & -1 & 0 \end{bmatrix} \tag{5.4}$$

Then

$$\dot{\bar{e}} = \hat{G}.\hat{C}.\begin{bmatrix} u \\ v \\ w \end{bmatrix} \tag{5.5}$$

Differentiating with respect to time once again, it is obtained that

$$\ddot{\bar{e}} = \dot{\hat{G}}.\hat{C}.\begin{bmatrix} u \\ v \\ w \end{bmatrix} + \hat{G}.\dot{\hat{C}}.\begin{bmatrix} u \\ v \\ w \end{bmatrix} + \hat{G}.\hat{C}.\begin{bmatrix} \dot{u} \\ \dot{v} \\ \dot{w} \end{bmatrix} \tag{5.6}$$

Using $\dot{\hat{C}} = \hat{C}.\tilde{\omega}$, the second time derivative of the error vector can be written as

$$\ddot{\bar{e}} = \dot{\hat{G}}.\begin{bmatrix} \dot{X} \\ \dot{Y} \\ \dot{Z} \end{bmatrix} + \hat{G}.\hat{C}.\tilde{\omega}.\begin{bmatrix} u \\ v \\ w \end{bmatrix} + \hat{G}.\hat{C}.(-\tilde{\omega}.\begin{bmatrix} u \\ v \\ w \end{bmatrix} + \begin{bmatrix} F_{ax}/m \\ F_{ay}/m \\ F_{az}/m \end{bmatrix} + \begin{bmatrix} g_x \\ g_y \\ g_z \end{bmatrix}) \tag{5.7}$$

Note that the mass center acceleration components of the missile in the body frame excluding gravity, can be represented as

$$\begin{bmatrix} a'_x \\ a'_y \\ a'_z \end{bmatrix} = \begin{bmatrix} F_{ax}/m \\ F_{ay}/m \\ F_{az}/m \end{bmatrix} \tag{5.8}$$

So,

$$\ddot{\bar{e}} = \dot{\hat{G}}.\begin{bmatrix}\dot{X}\\ \dot{Y}\\ \dot{Z}\end{bmatrix} + \hat{G}.\hat{C}.\begin{bmatrix}a'_x\\ a'_y\\ a'_z\end{bmatrix} + \hat{G}.\begin{bmatrix}0\\ 0\\ g\end{bmatrix} \tag{5.9}$$

or

$$\ddot{\bar{e}} = \begin{bmatrix}-\dfrac{\partial^2 Z_d}{\partial x^2}.\dot{X}^2\\ \dfrac{\partial^2 Y_d}{\partial x^2}.\dot{X}^2\end{bmatrix} + \begin{bmatrix}-\dfrac{\partial Z_d}{\partial x} & 0 & 1\\ \dfrac{\partial Y_d}{\partial x} & -1 & 0\end{bmatrix}.\hat{C}.\begin{bmatrix}a'_x\\ a'_y\\ a'_z\end{bmatrix} + \begin{bmatrix}g\\ 0\end{bmatrix} \tag{5.10}$$

Let the error vector dynamics be required to obey the following equation :

$$\ddot{\bar{e}} + \begin{bmatrix}kdp & 0\\ 0 & kdy\end{bmatrix}.\dot{\bar{e}} + \begin{bmatrix}kpp & 0\\ 0 & kpy\end{bmatrix}.\bar{e} = \bar{0} \tag{5.11}$$

where

$$\begin{bmatrix}kdp & 0\\ 0 & kdy\end{bmatrix} = \begin{bmatrix}2.\xi_p.\omega_{np} & 0\\ 0 & 2.\xi_y.\omega_{ny}\end{bmatrix} \tag{5.12}$$

$$\begin{bmatrix}kpp & 0\\ 0 & kpy\end{bmatrix} = \begin{bmatrix}\omega_{np}^2 & 0\\ 0 & \omega_{ny}^2\end{bmatrix} \tag{5.13}$$

In the above equations ω_{np}, ξ_p are the error dynamics parameters for the pitch plane and ω_{ny}, ξ_y are the error dynamics parameters for the yaw plane.

Equation (5.11) can be rewritten as

$$\ddot{\bar{e}} = \bar{r} = -\begin{bmatrix} kdp & 0 \\ 0 & kdy \end{bmatrix} . \dot{\bar{e}} - \begin{bmatrix} kpp & 0 \\ 0 & kpy \end{bmatrix} . \bar{e} \tag{5.14}$$

with

$$\bar{r} = \begin{bmatrix} r_1 \\ r_2 \end{bmatrix} \tag{5.15}$$

Let the transformation matrix $\hat{C}$ be written in open form as;

$$\hat{C} = \begin{bmatrix} c_{11} & c_{12} & c_{13} \\ c_{21} & c_{22} & c_{23} \\ c_{31} & c_{32} & c_{33} \end{bmatrix} \tag{5.16}$$

Let the desired accelerations in y and z directions be determined such that the required error dynamics be realized. That is;

$$\begin{bmatrix} r_1 \\ r_2 \end{bmatrix} = \begin{bmatrix} -\dfrac{\partial^2 Z_d}{\partial x^2} . \dot{X}^2 \\ \dfrac{\partial^2 Y_d}{\partial x^2} . \dot{X}^2 \end{bmatrix} + \begin{bmatrix} a_1 & b_1 & c_1 \\ a_2 & b_2 & c_2 \end{bmatrix} . \begin{bmatrix} a'_x \\ a_{yd} \\ a_{zd} \end{bmatrix} + \begin{bmatrix} g \\ 0 \end{bmatrix} \tag{5.17}$$

where;

$$\begin{bmatrix} a_1 & b_1 & c_1 \\ a_2 & b_2 & c_2 \end{bmatrix} = \begin{bmatrix} -\dfrac{\partial Z_d}{\partial x} & 0 & 1 \\ \dfrac{\partial Y_d}{\partial x} & -1 & 0 \end{bmatrix} . \begin{bmatrix} c_{11} & c_{12} & c_{13} \\ c_{21} & c_{22} & c_{23} \\ c_{31} & c_{32} & c_{33} \end{bmatrix} \tag{5.18}$$

and a_{yd}, a_{zd} are the desired accelerations in the yaw and pitch planes respectively. From Equation (5.17) the desired accelerations are found as

$$\begin{bmatrix} a_{zd} \\ a_{yd} \end{bmatrix} = \begin{bmatrix} \dfrac{r_1 + \dfrac{\partial^2 Z_d}{\partial x^2}.\dot{X}^2 - g - (a_1.a'_x + b_1.a_{yd})}{c_1} \\ \dfrac{r_2 - \dfrac{\partial^2 Y_d}{\partial x^2}.\dot{X}^2 - (a_2.a'_x + c_2.a_{zd})}{b_2} \end{bmatrix} \tag{5.19}$$

which can also be arranged as

$$\begin{bmatrix} a_{zd} \\ a_{yd} \end{bmatrix} = \begin{bmatrix} \dfrac{b_2.(-r_1 - \dfrac{\partial^2 Z_d}{\partial x^2}.\dot{X}^2 + g) + b_1.(r_2 - \dfrac{\partial^2 Y_d}{\partial x^2}.\dot{X}^2) + a'_x.(b_2.a_1 - b_1.a_2)}{b_1.c_2 - c_1.b_2} \\ \dfrac{c_2.(r_1 + \dfrac{\partial^2 Z_d}{\partial x^2}.\dot{X}^2 - g) - c_1.(r_2 - \dfrac{\partial^2 Y_d}{\partial x^2}.\dot{X}^2) + a'_x.(-c_2.a_1 + c_1.a_2)}{b_1.c_2 - c_1.b_2} \end{bmatrix} \tag{5.20}$$

There is a restriction for the solution to exist. Denominator of the acceleration expressions must be nonzero, that is

$$b_1.c_2 \neq c_1.b_2 \tag{5.21}$$

If the expressions of b_1, c_1, b_2 and c_2 are put in Equation (5.21), with $\cos(\theta) \neq 0$ the singularity condition reduces to

$$(\frac{\partial Y_d}{\partial X}).\sin\psi - (\frac{\partial Z_d}{\partial X}).\tan\theta \neq -\cos\psi \tag{5.22}$$

With $(\frac{\partial Y_d}{\partial X}) = \tan\psi_d$ and $(\frac{\partial Z_d}{\partial X}) = -\tan\theta_d / \cos\psi_d$, Figure 5.1, the condition reduces further to

$$\cos(\psi - \psi_d) + \tan\theta . \tan\theta_d \neq 0 \tag{5.23}$$

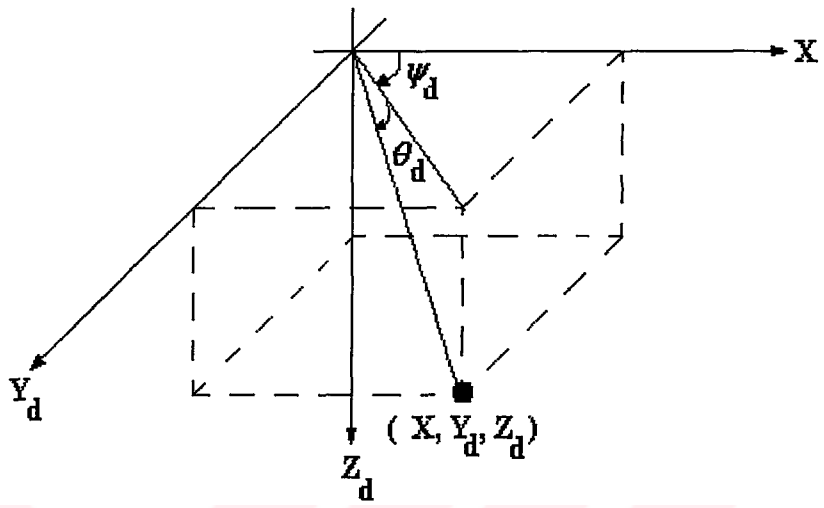

Figure 5.1 θ_d and ψ_d Angles

Thus, if $\psi = \psi_d$, $\tan\theta . \tan\theta_d \neq -1$, i.e. $\theta \neq \theta_d \pm \pi / 2$; and if $\theta = 0$ or $\theta_d = 0$, $\cos(\psi - \psi_d) \neq 0$, i.e. $\psi \neq \psi_d \pm \pi / 2$.

If the singularity condition is achieved or approached in the flight, prescribed values of maximum and minimum accelerations that the missile frame can physically achieve will be the outputs of the guidance algorithm, by means of a limiter in the output of the guidance loop.

CHAPTER 6

AUTOPILOT DESIGN

6.1 Longitudinal and Lateral Autopilot Design

Missile longitudinal and lateral autopilots are the control systems whose reference inputs are the normal acceleration commands in the pitch and yaw planes. These autopilots use normal accelerations and angular rates as feedback measurements. The output of the autopilots are the necessary control surface deflections to correct the acceleration error. If the missile is assumed to have no rolling motion, the lateral and longitudinal autopilots can be decoupled and designed in pitch and yaw planes independently. Here design of two different autopilots for the same generic canard controlled missile are presented. Since the missile under consideration is symmetric, lateral and longitudinal autopilots are identical except for the sign differences in the control gains. Since the design technique is the same for both of the pitch and yaw autopilots, the design of the two different autopilots is explained in the following sections considering the longitudinal dynamics only.

6.1.1 State Space Formulation

The state space equation for the pitch plane is

$$\begin{bmatrix} \dot{\alpha} \\ \dot{q} \end{bmatrix} = \begin{bmatrix} \frac{Z_\alpha}{u} & (\frac{Z_q}{u}+1) \\ M_\alpha & M_q \end{bmatrix} . \begin{bmatrix} \alpha \\ q \end{bmatrix} + \begin{bmatrix} \frac{Z_\delta}{u} \\ M_\delta \end{bmatrix} . \delta_e \tag{6.1}$$

In this matrix equation, the state variables α and q are the angle of attack and the pitching rate, respectively.

The normal acceleration of the missile in the pitch plane can be found from the following equation :

$$a_z = u.(\dot{\alpha} - q) \tag{6.2}$$

A controller on the normal acceleration of the missile using the state variables in Equation (6.1) and Equation (6.2) can be designed. But in this design, the normal acceleration is not a state variable and also the design techniques which use full state feedback procedures cannot be applied, since there does not exist a sensor mounted on the missile to measure the angle of attack state.

In order to have all the states directly observable by means of sensors mounted in the inertial measurement unit of the missile, a state transformation can be applied on the system using Equation (6.1) and (6.2) as shown below:

$$\alpha = \frac{1}{Z_\alpha}.(a_z - Z_q.q - Z_\delta.\delta_e) \tag{6.3}$$

The coefficients Z_α, Z_q and Z_δ are slowly varying compared to the attitude dynamics of the missile. So, treating them as constants, the derivative of Equation (6.3) leads to the following equation :

$$\dot{\alpha} = \frac{1}{Z_\alpha}.(\dot{a}_z - Z_q.\dot{q} - Z_\delta.\dot{\delta}_e) \tag{6.4}$$

Expressing $\dot{q}$ in terms a_z, q, and δ_e gives

$$\dot{q} = \frac{M_\alpha}{Z_\alpha}.a_z + (M_q - \frac{M_\alpha.Z_q}{Z_\alpha}).q + (M_\delta - \frac{M_\alpha.Z_\delta}{Z_\alpha}).\delta_e \tag{6.5}$$

Plugging Equation (6.5) in Equation (6.4) and using Equation (6.2), the following expression can be obtained for the time derivative of the normal acceleration :

$$\begin{aligned}\dot{a}_z &= (\frac{Z_q.M_\alpha}{Z_\alpha} + \frac{Z_\alpha}{u}).a_z + (-\frac{M_\alpha.Z_q^{\,2}}{Z_\alpha} + Z_q.M_q + Z_\alpha).q \\ &+ (-\frac{Z_q.M_\alpha.Z_\delta}{Z_\alpha} + Z_q.M_\delta).\delta_e + Z_\delta.\dot{\delta}_e\end{aligned} \tag{6.6}$$

Taking $\dot{\delta}_e = \eta$ in Equation (6.6), a new state space equation can be formed as $\dot{\bar{x}} = \hat{A}.\bar{x} + \bar{b}.\eta$, where

$$\bar{x} = \begin{bmatrix} a_z \\ q \\ \delta_e \end{bmatrix} \tag{6.7}$$

$$\hat{A} = \begin{bmatrix} \frac{Z_q.M_\alpha}{Z_\alpha} + \frac{Z_\alpha}{u} & Z_\alpha + Z_q.M_q - \frac{M_\alpha.Z_q^{\,2}}{Z_\alpha} & Z_q.M_\delta - \frac{Z_q.M_\alpha.Z_\delta}{Z_\alpha} \\ \frac{M_\alpha}{Z_\alpha} & M_q - \frac{M_\alpha.Z_q}{Z_\alpha} & M_\delta - \frac{M_\alpha.Z_\delta}{Z_\alpha} \\ 0 & 0 & 0 \end{bmatrix} \tag{6.8}$$

$$\bar{b} = \begin{bmatrix} Z_\delta \\ 0 \\ 1 \end{bmatrix} \tag{6.9}$$

Since the normal acceleration is to be controlled, an integral control action would be desirable. So, a fourth state variable z is introduced to the system as the integral of the error between the reference acceleration and the measured acceleration. The corresponding state equation is

$$\dot{z} = a_z^* - a_z \tag{6.10}$$

Then the new state space equation taking a_z^* as an input term will be

$$\dot{\bar{x}}' = \hat{A}'.\bar{x}' + \bar{b}'.\eta + \bar{c}'.a_z^* \tag{6.11}$$

where,

$$\bar{x}' = \begin{bmatrix} a_z \\ q \\ \delta_e \\ z \end{bmatrix} \tag{6.12}$$

$$\hat{A}' = \begin{bmatrix} \hat{A} & \bar{0} \\ \begin{bmatrix} -1 & 0 & 0 \end{bmatrix} & 0 \end{bmatrix} \tag{6.13}$$

$$\bar{b}' = \begin{bmatrix} \bar{b} \\ 0 \end{bmatrix} \tag{6.14}$$

$$\bar{c}' = \begin{bmatrix} \bar{0} \\ 1 \end{bmatrix} \tag{6.15}$$

6.1.2 Controller Design Using Pole and Zero Placement (Autopilot 1)

The gains of the controller has to be determined to satisfy the desired performance characteristics of the autopilot. For that reason a controller is designed which generates the control input $\eta(t)$ according to the following equation:

$$\eta(t) = K_a . e(t) + K_z . z(t) + K_q . q(t) + K_\delta . \delta_e(t) \tag{6.16}$$

where,

$$e(t) = a_z^*(t) - a_z(t) \tag{6.17}$$

and

$$z(t) = \int_0^t e(\tau). d\tau \tag{6.18}$$

Note that although $\eta(t)$ is treated as the control variable, the actual steering input to the missile dynamics is the state variable $\delta_e(t)$, i.e.

$$\delta_e(t) = \int_0^t \eta(\tau). d\tau \tag{6.19}$$

This can be seen more clearly in the block diagram representation shown in Figure 6.1.

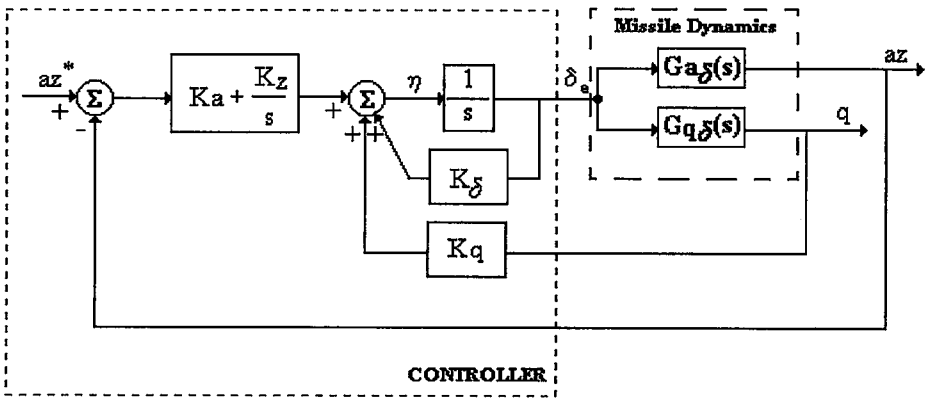

Figure 6.1 Block Diagram Representation of Autopilot 1.

Using the linearized missile dynamics and the transfer functions which are derived in Chapter 4, following equations can be written :

$$\frac{q(s)}{\delta_e(s)} = \frac{M_\delta . s + (\frac{M_\alpha . Z_\delta}{u} - \frac{M_\delta . Z_\alpha}{u})}{s^2 - (M_q + \frac{Z_\alpha}{u}).s + (\frac{Z_\alpha}{u}.M_q - M_\alpha.(\frac{Z_q}{u} + 1))} \tag{6.20}$$

$$\frac{a_z(s)}{\delta_e(s)} = \frac{Z_\delta . s^2 + (Z_q . M_\delta - M_q . Z_\delta).s + (-M_\alpha . Z_\delta + Z_\alpha . M_\delta)}{s^2 - (M_q + \frac{Z_\alpha}{u}).s + (\frac{Z_\alpha}{u}.M_q - M_\alpha.(\frac{Z_q}{u} + 1))} \tag{6.21}$$

For the sake of brevity, these equations can be written as follows :

$$\frac{q(s)}{\delta_e(s)} = \frac{f.s + g}{s^2 + a.s + b} = G_{q\delta}(s) \tag{6.22}$$

$$\frac{a_z(s)}{\delta_e(s)} = \frac{c.s^2 + t.s + e}{s^2 + a.s + b} = G_{a\delta}(s) \tag{6.23}$$

Applying block diagram algebra, the closed loop autopilot transfer function will be obtained as

$$\frac{a_z(s)}{a_z^*(s)} = \frac{K_a.c.s^3 + (K_z.c + K_a.t).s^2 + (K_z.t + K_a.e).s + K_z.e}{s^4 + (a - K_\delta + K_a.c).s^3 + (K_a.t + b + K_z.c - K_\delta.a - K_q.f).s^2 + (-K_\delta.b + K_a.e - K_q.g + K_z.t).s + K_z.e} \tag{6.24}$$

or

$$\frac{a_z(s)}{a_z^*(s)} = \frac{\Delta_n(s)}{\Delta_d(s)} \tag{6.25}$$

$\Delta_n(s)$ can be factored as

$$\Delta_n(s) = (K_a.s + K_z).(c.s^2 + t.s + e) \tag{6.26}$$

From Equation (6.26), it can be seen that only one of the three zeros can be controlled by proper adjustments of K_z and K_a. The other two zeros are determined by c, t and e values, which comes from the nature of the uncontrolled missile dynamics. Thus, two zeros of the closed loop transfer function $\frac{a_z(s)}{a_z^*(s)}$ are fixed by the missile dynamics. Taking $\frac{K_z}{K_a} = K_r$, the three zeros of the numerator dynamics are found as follows :

$$z_1 = -K_r \tag{6.27}$$

$$z_{2,3} = \frac{-t \pm j.\sqrt{4.c.e - t^2}}{2.c} = -\omega_{nz}.(\zeta_z \pm j.\sqrt{1 - \zeta_z^2}) \tag{6.28}$$

z_2 and z_3 values are calculated for different Mach numbers ranging between 0.1 and 3.

The ω_{nz} values are all satisfactory enough to design an autopilot whose cut off frequency can be assigned to a value which is smaller than these values. By the application of such an assignment, there will not be any sensible effect of the numerator dynamics up to the cut off frequency of the autopilot. This behavior can be best seen in Figure 6.4 which shows the Bode magnitude and phase plots of the closed loop transfer function of the autopilot.

Since the frequency characteristics of the second and third zeros are satisfactory, the first zero can also placed such that $z_1 = -\omega_{nz}$. Thus, a Butterworth pattern of zero placement will be obtained for the numerator. This is shown in Figure 6.2.

On the other hand, $z_1 = -K_r$. So,

$$K_r = \omega_{nz} = (\frac{e}{c})^{1/2} \tag{6.29}$$

For the denominator, four poles are to be placed. The dominant first three of them are again placed in Butterworth pattern and the fourth one is placed as a recessive real pole. Complex conjugate pair property is preferred for the dominant poles in order to have faster response characteristics. So, with $p_{1,2} = -\omega_{np}.(\zeta_p \pm j.\sqrt{1-\zeta_p^2})$, $p_3 = -\omega_{np}$, $p_4 = -p$ the desired characteristics polynomial will be

$$\begin{aligned}\Delta_d(s) &= s^4 + [(2.\zeta_p + 1).\omega_{np} + p].s^3 \\ &+ [(2.\zeta_p + 1).\omega_{np}^2 + (2.\zeta_p + 1).\omega_{np}.p].s^2 \\ &+ [(2.\zeta_p + 1).\omega_{np}^2.p + \omega_{np}^3].s + \omega_{np}^3.p\end{aligned} \tag{6.30}$$

On the other hand, according to Equation (6.24),

$$\begin{aligned}\Delta_d(s) &= s^4 + (a - K_\delta + K_a.c).s^3 \\ &+ (K_a.t + b + K_z.c - K_\delta.a - K_q.f).s^2 \\ &+ (-K_\delta.b + K_a.e - K_q.g + K_z.t).s + K_z.e\end{aligned} \tag{6.31}$$

Equating the zeroth order coefficients of the polynomials, the fourth pole can be related to the other parameters as

$$p_4 = -p = -(\frac{K_r.e}{\omega_{np}^{\ 3}}).K_a \tag{6.32}$$

By using the above equation, p can be eliminated from the remaining equations and three equations for three unknowns (K_δ, K_a, K_q) are left by equating the coefficients of the polynomials.

For convenience, let

$$v = (\frac{K_r.e}{\omega_{np}^{\ 3}}) \tag{6.33}$$

Then, the following linear equation set can be written :

$$\begin{bmatrix} -1 & c - v & 0 \\ -a & t + K_r.c - v.(2.\zeta_p + 1).\omega_{np} & -f \\ -b & e + K_r.t - v.(2.\zeta_p + 1).\omega_{np}^{\ 2} & -g \end{bmatrix} . \begin{Bmatrix} K_\delta \\ K_a \\ K_q \end{Bmatrix} = \begin{bmatrix} (2.\zeta_p + 1).\omega_{np} - a \\ (2.\zeta_p + 1).\omega_{np}^{\ 2} - b \\ \omega_{np}^{\ 3} \end{bmatrix} \tag{6.34}$$

Assigning ω_{np} and ζ_p properly as desired, the values of K_δ, K_a, K_q can be found. Also K_z is found from $K_z = K_a.K_r$. After thus finding the four

control gains, $p_4 = -\frac{K_z . e}{\omega_{np}^{\ 3}}$ has to be checked that, it has not come out to be closer to the imaginary axis than the dominant complex conjugate pole pairs which are stated by ω_{np} and ζ_p values. The tuning of p_4 can be achieved by assigning proper values for ω_{np} and ζ_p.

The zero placement for the numerator and the pole placement for the denominator can be seen in Figures 6.2 and 6.3.

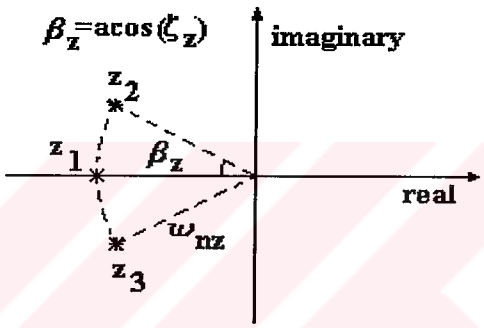

Figure 6.2 Zero Placement for Numerator.

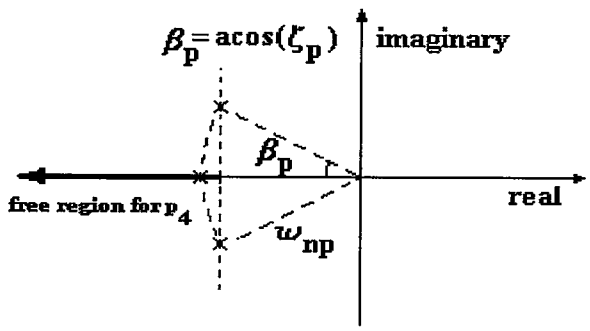

Figure 6.3 Pole Placement for Denominator Dynamics.

The pole and zero placement for the missile under consideration is done for Mach numbers between 0.1 and 3, in which the generic missile is most probably to operate.

The corresponding gains for the controller in the autopilot are found using Equation (6.34), and integrated in the six degrees of freedom simulations for a gain scheduling with respect to Mach number variation.

Designed autopilot is also checked in frequency domain by plotting the Bode Diagrams of the autopilot closed loop transfer function at a Mach number equal to 1.5. This can be seen in Figure 6.4. This plot is satisfactory as far as the bandwidth requirement for the autopilot servo loop is concerned.

Application of this design technique leads to the partial adjustments of both numerator and denominator dynamics. Only one of the three zeros and three of the four poles can be placed. Here it should be admitted that it has been possible to achieve satisfactory numerator and denominator dynamics, because the parameters a, b, c, e, f, g, t of the uncontrolled missile dynamics happen to have favorable values for all Mach numbers greater than 0.7 which cover almost all of the flight duration.

After the design of the longitudinal autopilot, the lateral autopilot is designed in the same way and also integrated into the six degrees of freedom simulations with the proper sign conventions for the controller gains.

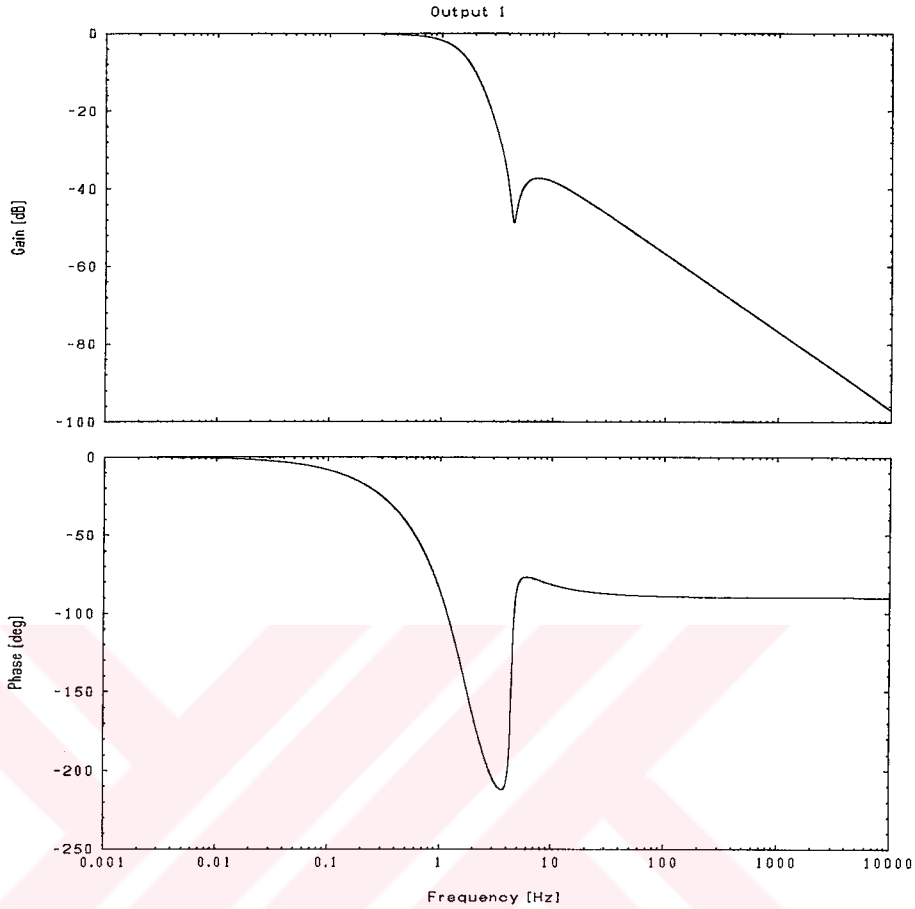

Figure 6.4 Bode Plot of the Autopilot 1 Closed Loop at M=1.5.

6.1.3 Controller Design Using Optimal Control with Prescribed Degree of Stability (Autopilot 2)

In this procedure, a quadratic performance index minimization scheme is applied on the system with a prescribed degree of stability. This prescribed degree of stability is imposed on the system in a way to modify the decay rate of states in the time domain. This also means to have the autopilot closed loop poles at the left hand side of a predefined stability border in the complex plane. This is done by

applying the following new transformation on the modified system given by Equation (6.11), as shown in [8].

$$\bar{x}''(t) = e^{\alpha t}.\bar{x}'(t) \tag{6.35}$$

$$\eta''(t) = e^{\alpha t}.\eta(t) \tag{6.36}$$

$$a_z^{*''}(t) = e^{\alpha t}.a_z^{*}(t) \tag{6.37}$$

This transformation will end up in a new state space system as described below:

$$\dot{\bar{x}}''(t) = \alpha.e^{\alpha t}.\bar{x}'(t) + e^{\alpha t}.\dot{\bar{x}}'(t) \tag{6.38}$$

$$\dot{\bar{x}}'' = \alpha.\bar{x}'' + e^{\alpha t}.(\hat{A}'.\bar{x}' + \bar{b}'.\eta + \bar{c}'.a_z^{*}) \tag{6.39}$$

$$\dot{\bar{x}}'' = \alpha.\bar{x}'' + \hat{A}'.\bar{x}'' + \bar{b}'.\eta'' + \bar{c}'.a_z^{*''} \tag{6.40}$$

$$\dot{\bar{x}}'' = \hat{A}''.\bar{x}'' + \bar{b}'.\eta'' + \bar{c}'.a_z^{*''} \tag{6.41}$$

where,

$$\hat{A}'' = \alpha.\hat{I} + \hat{A}' \tag{6.42}$$

and $\hat{I}$ denotes the identity matrix.

The performance index to be minimized is taken as

$$\hat{\bar{J}} = \frac{1}{2}.\int_0^{\infty}[(\bar{x}'' - \bar{e}.a_z^{*''})^T.\hat{Q}.(\bar{x}'' - \bar{e}.a_z^{*''}) + \eta''^T.R.\eta''].dt \tag{6.43}$$

where,

$$\bar{e} = \begin{bmatrix} 1 \\ 0 \\ 0 \\ 0 \end{bmatrix} \tag{6.44}$$

The minimization is achieved as described below.

The Hamiltonian associated with the performance index can be written as

$$\begin{aligned} H = \frac{1}{2}.[(\bar{x}'' - \bar{e}.a_z^{*''})^T.\hat{Q}.(\bar{x}'' - \bar{e}.a_z^{*''}) + \eta''^T.R.\eta''] \\ + \bar{\psi}^T.(\hat{A}''.\bar{x}'' + \bar{b}'.\eta'' + \bar{c}'.a_z^{*''}) \end{aligned} \tag{6.45}$$

The optimal control input minimizing the performance index in Equation (6.43) is found as follows :

$$\frac{\partial H}{\partial \eta''} = 0 \rightarrow \eta''^{o} = -R^{-1}.\bar{b}'^T.\bar{\psi} \tag{6.46}$$

The resulting state and costate equations will be

$$\dot{\bar{x}}'' = \frac{\partial H}{\partial \bar{\psi}} = \hat{A}''.\bar{x}'' - \bar{b}'.R^{-1}.\bar{b}'^T.\bar{\psi} + \bar{c}'.a_z^{*''} \tag{6.47}$$

with

$$\overline{x}''(0) = \overline{x}''_0 \tag{6.48}$$

and

$$\dot{\overline{\psi}} = -\frac{\partial H}{\partial \overline{x}''} = -\hat{Q}.\overline{x}'' + \hat{Q}.\overline{e}.a_z^{*''} - \hat{A}''^T.\overline{\psi} \tag{6.49}$$

with

$$\overline{\psi}(\infty) = \overline{0} \tag{6.50}$$

The optimal control can be expressed in feedback form going through the following steps:

Let

$$\overline{\psi} = \hat{P}.\overline{x}'' - \overline{g} \tag{6.51}$$

Then,

$$\dot{\overline{\psi}} = \dot{\hat{P}}.\overline{x}'' + \hat{P}.\dot{\overline{x}}'' - \dot{\overline{g}} \tag{6.52}$$

$$\dot{\overline{x}}'' = \hat{A}''.\overline{x}'' - \overline{b}'.R^{-1}.\overline{b}'^T.\hat{P}.\overline{x}'' + \overline{b}'.R^{-1}.\overline{b}'^T.\overline{g} + \overline{c}'.a_z^{*''} \tag{6.53}$$

$$\dot{\overline{\psi}} = (\dot{\hat{P}} + \hat{P}.\hat{A}'' - \hat{P}.\overline{b}'.R^{-1}.\overline{b}'^T.\hat{P}).\overline{x}'' + \hat{P}.\overline{b}'.R^{-1}.\overline{b}'^T.\overline{g} + \hat{P}.\overline{c}'.a_z^{*''} - \dot{\overline{g}} \tag{6.54}$$

Also, according to Equation (6.49)

$$\dot{\bar{\psi}} = -\hat{Q}.\bar{x}'' + \hat{Q}.\bar{e}.a_z^{*''} - \hat{A}''^T.\hat{P}.\bar{x}'' + \hat{A}''^T.\bar{g} \tag{6.55}$$

Eliminating $\dot{\bar{\psi}}$ between Equations (6.54) and (6.55), two differential matrix equations will be found as

$$\dot{\hat{P}} + \hat{P}.\hat{A}'' - \hat{P}.\bar{b}'.R^{-1}.\bar{b}'^T.\hat{P} + \hat{A}''^T.\hat{P} + \hat{Q} = \hat{0} \tag{6.56}$$

with

$$\hat{P}(\infty) = \hat{0} \tag{6.57}$$

and

$$\dot{\bar{g}} - (\hat{P}.\bar{b}'.R^{-1}.\bar{b}'^T - \hat{A}''^T).\bar{g} - (\hat{P}.\bar{c}' - \hat{Q}.\bar{e}).a_z^{*''} = \bar{0} \tag{6.58}$$

with

$$\bar{g}(\infty) = \bar{0} \tag{6.59}$$

Solution of $\bar{g}$ and $\hat{P}$ will be used in finding the optimal feedback control law as

$$\eta''^o = -R^{-1}.\bar{b}'^T.\hat{P}.\bar{x}'' + R^{-1}.\bar{b}'^T.\bar{g} \tag{6.60}$$

For the solution of $\hat{P}$, since $\hat{A}''$ and $\bar{b}'$ change slowly with time when compared to the missile dynamics, the steady state value is taken as the constant solution. Thus, $\dot{\hat{P}} = 0$ will give the algebraic Riccati Equation as

$$\hat{P}.\hat{A}'' - \hat{P}.\overline{b}'.R^{-1}.\overline{b}'^{T}.\hat{P} + \hat{A}''^{T}.\hat{P} + \hat{Q} = \hat{0} \tag{6.61}$$

and the solution of $\hat{P}$ will be found from this equation.

Solution of $\overline{g}$ will be as described below.

Let Equation (6.58) be re - written as

$$\dot{\overline{g}} = \hat{\kappa}_1.\overline{g} + \overline{\kappa}_2.a_z^{*''} \tag{6.62}$$

with

$$\overline{g}(\infty) = \overline{0} \tag{6.63}$$

where

$$\hat{\kappa}_1 = (\hat{P}.\overline{b}'.R^{-1}.\overline{b}'^{T} - \hat{A}''^{T}) \tag{6.64}$$

$$\overline{\kappa}_2 = (\hat{P}.\overline{c}' - \hat{Q}.\overline{e}) \tag{6.65}$$

Thus,

$$\overline{g}(t) = \int_{\infty}^{t} \hat{\Phi}(t-\tau).\overline{\kappa}_2.a_z^{*''}(\tau).d\tau \tag{6.66}$$

Since $\hat{P}$ is taken to be constant, $\hat{\kappa}_1$ is also constant. So,

$$\hat{\Phi}(t) = e^{\hat{\kappa}_1.t}, \tag{6.67}$$

and

$$\bar{g}(t) = \int_{\infty}^{t} e^{\hat{\kappa}_1.(t-\tau)}.\bar{\kappa}_2.a_z^{*''}(\tau).d\tau \tag{6.68}$$

Since the desired trajectory of the missile is changing slowly with time, the desired acceleration command produced by the guidance algorithm to track this trajectory will also be slowly changing and will have lower frequency characteristics when compared with the autopilot closed loop cut off frequency. Then, $\hat{a}_z^*(t) \cong \text{constant}$ can be taken to give;

$$\bar{g}(t) = \bar{\kappa}_2.a_z^{*''}(t).\int_{\infty}^{t} e^{\hat{\kappa}_1.(t-\tau)}.d\tau = -\hat{\kappa}_1^{-1}.\bar{\kappa}_2.a_z^{*''}(t) \tag{6.69}$$

This will give the feedback control law in a slightly suboptimal manner as

$$\eta'' = -R^{-1}.\bar{b}'^T.\hat{P}.\bar{x}'' + R^{-1}.\bar{b}'^T.(-\hat{\kappa}_1^{-1}.\bar{\kappa}_2).a_z^{*''} \tag{6.70}$$

$$\eta'' = -\bar{k}^T.\bar{x}'' + K_t.a_z^{*''} \tag{6.71}$$

or multiplying both sides by $e^{-\alpha t}$,

$$\eta = -\bar{k}^T.\bar{x}' + K_t.a_z^{*} \tag{6.72}$$

where

$$\bar{k}^T = \begin{bmatrix} K_a & K_q & K_\delta & -K_z \end{bmatrix} \tag{6.73}$$

Writing out $\overline{k}$ and $\overline{x}'$ the optimal control can also be expressed as shown below:

$$\eta(t) = -K_a . a_z(t) - K_q . q(t) - K_\delta . \delta_e(t) + K_z . z(t) + K_t . a_z^* \tag{6.74}$$

where,

$$e(t) = a_z^*(t) - a_z(t) \tag{6.75}$$

and

$$z(t) = \int_0^t e(\tau).d\tau \tag{6.76}$$

Here, again, the actual steering input to the missile dynamics is $\delta_e(t)$, but it happens to be a state variable in the transformed state space system. This can be seen more clearly in the block diagram representation shown in Figure 6.5.

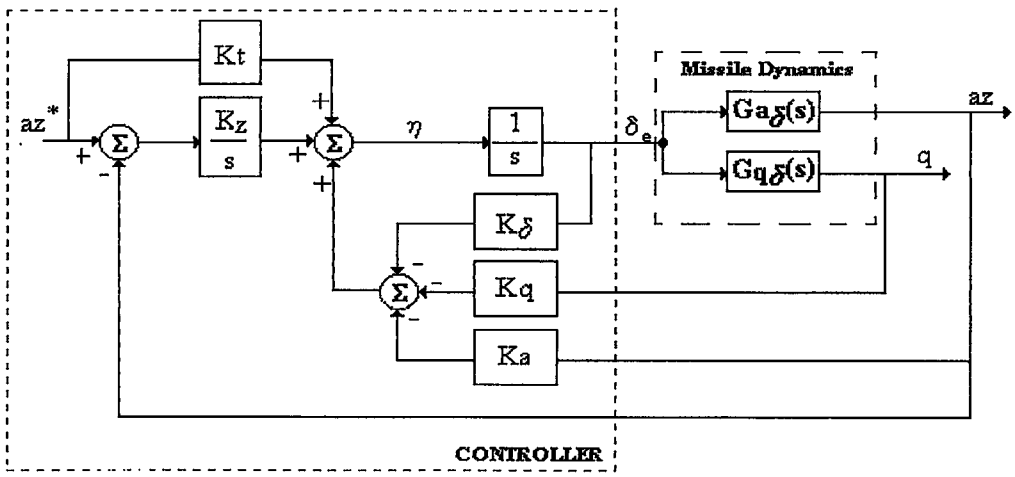

Figure 6.5 Block Diagram Representation of Autopilot 2.

The feedback control law found from the quadratic performance index minimization scheme will end up in

$$\bar{x}'(t) = e^{-\alpha t}.\bar{x}''(t) \tag{6.77}$$

which implies that $\bar{x}'(t)$ will approach zero at least as fast as $e^{-\alpha t}$, as $t \to \infty$.

Usage of the quadratic performance index minimization scheme with prescribed degree of stability will satisfy that, all of the poles of the autopilot closed loop dynamics will be at the left hand side of the line which is parallel to imaginary axis and crossing real axis at (- a) in the complex plane. Here (a) is the predefined stability degree. This is illustrated in Figure 6.6.

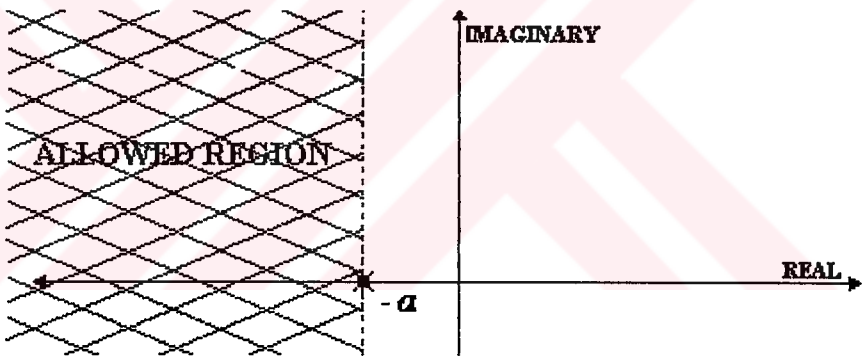

Figure 6.6 Prescribed Stability Degree in Complex Plane.

Next step to finish the design of the controller is to determine $\hat{Q}$, R and the stability degree a to achieve the desired performance characteristics for all Mach numbers during the flight.

Arranging the proper relative weightings in $\hat{Q}$ and R will end up the controller design process. But in all of the quadratic performance index minimization designs, although the minimization of a performance index is satisfied, the achieved

closed loop poles of the system may not be satisfactory. For example, if the dominant closed loop pole is a real one, this may not be a desired characteristic, since the system will then be slower when compared with a complex conjugate dominant pair.

Here, a root locus approach is integrated with the presented approach [9]. This is done by taking the weighting matrix $\hat{Q}$ as $K^*.\hat{Q}_0$ and plotting the closed loop poles as K^* changes. Such plots are repeated for different $\hat{Q}_0$ matrices in order to see the effect of different relative weightings among the state variables. From these root loci graphs, a proper matrix $\hat{Q}_0$ and a proper gain K^* are found in order to have the closed loop poles in the desired locations.

In this procedure, $\hat{Q}_0$ and R will be taken as

$$\hat{Q}_0 = \text{diagonal}(a, b, c, d) \tag{6.78}$$

$$R = e \tag{6.79}$$

For different root locus plots, the weightings a, b, c, d and e are changed gradually as seen in Table 6.1.

Table 6.1 Performance Index Trials for Design

#	a	b	c	d	e
I	1	1	1	1	1
II	100	1	1	1	1
III	1	100	1	1	1
IV	1	1	100	1	1
V	1	1	1	100	1
VI	1	1	100	100	1
VII	1	100	100	100	1
VIII	100	100	100	100	1
IX	1	100	1000	100	1
X	1	100	10000	100	1
XI	1	100	10000	1000	1
XII	1	1000	10000	100	1
XIII	1	100	10000	100	10
XIV	.1	100	10000	100	10
XV	1	100	10000	1000	10
XVI	.1	100	10000	1000	10
XVII	1	1000	10000	100	10
XVIII	.1	1000	10000	100	10

For all combinations in Table 6.1, the gain K^* is changed in the range between 10^{-3} and 10^3 gradually, in order to obtain the root loci graphs. From the root loci obtained this way, it is seen that the first four sets and the set (VIII) give the dominant pole as a real one. A complex conjugate dominant pair tendency is seen in the sets (V), (VI), and (VII) and the sets (X), (XI), and (XII). Natural frequency and damping characteristics of the dominant complex conjugate pole pairs in the sets (X), (XI), and (XII) are seen to be better than those in the sets (V), (VI), and (VII). The autopilot gains found from the sets (X), (XI), and (XII) are examined considering the step response of the linear missile dynamics model in single plane. This examination shows that, transient response has oscillating characteristics and

there exists slightly high overshoot. Thus, the sets (XIII) to (XVIII) are examined in root loci analysis as perturbed versions of the sets (X), (XI) and (XII). Between these six sets the sets (XIV), (XVI) and (XVIII) have come out to be more satisfactory when the natural frequency and damping characteristics of the dominant complex conjugate pole pairs are examined.

The autopilot gains found from these last three sets are again examined considering the step response of the linear missile dynamics model in single plane. By this examination, the weightings are fine tuned in order to improve the transient response characteristics further. As a result, the following weighting set shown in Table 6.2 is found to give apparently the best transient and steady state response performance for a step input.

Table 6.2 Final Weighting Set.

a	b	c	d	e
.1	1000	10000	10	10

This weighting set is again examined using the root locus graphs, and a proper K^* value is found for the final fine tuning. During this procedure, the prescribed degree of stability is taken to be equal to one.

The root locus approach for the Mach number equal to 1.5 can be seen in Figures 6.7 to 6.11. For a fine pole placement, K^* is chosen to be 0.614 for this Mach number.

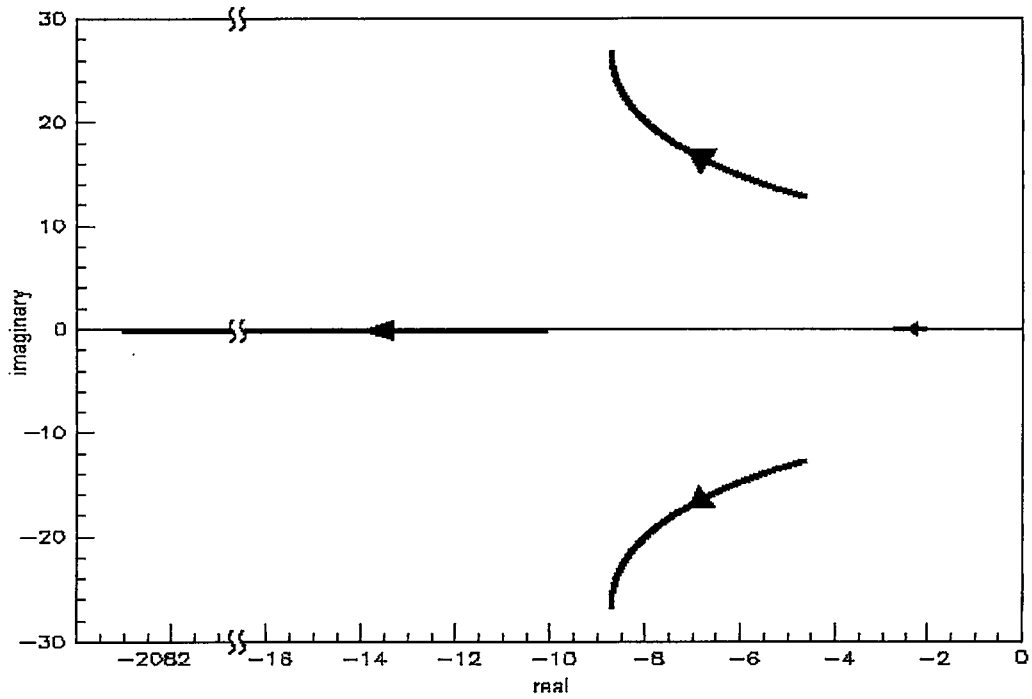

Figure 6.7 Root Locus for Set (III).

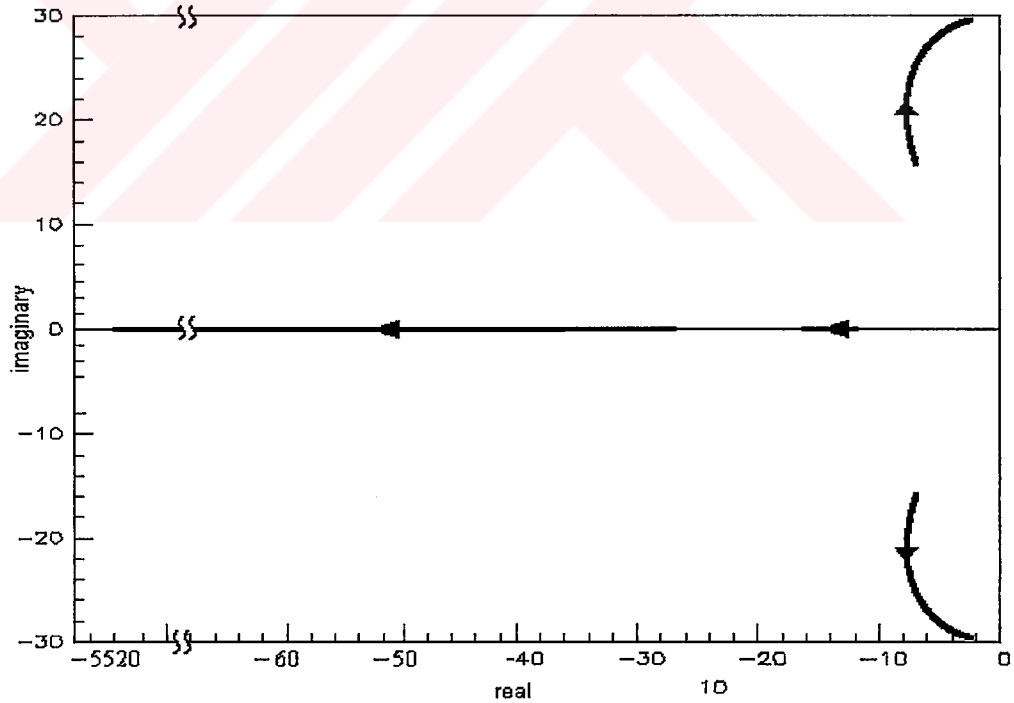

Figure 6.8 Root Locus for Set (VI)

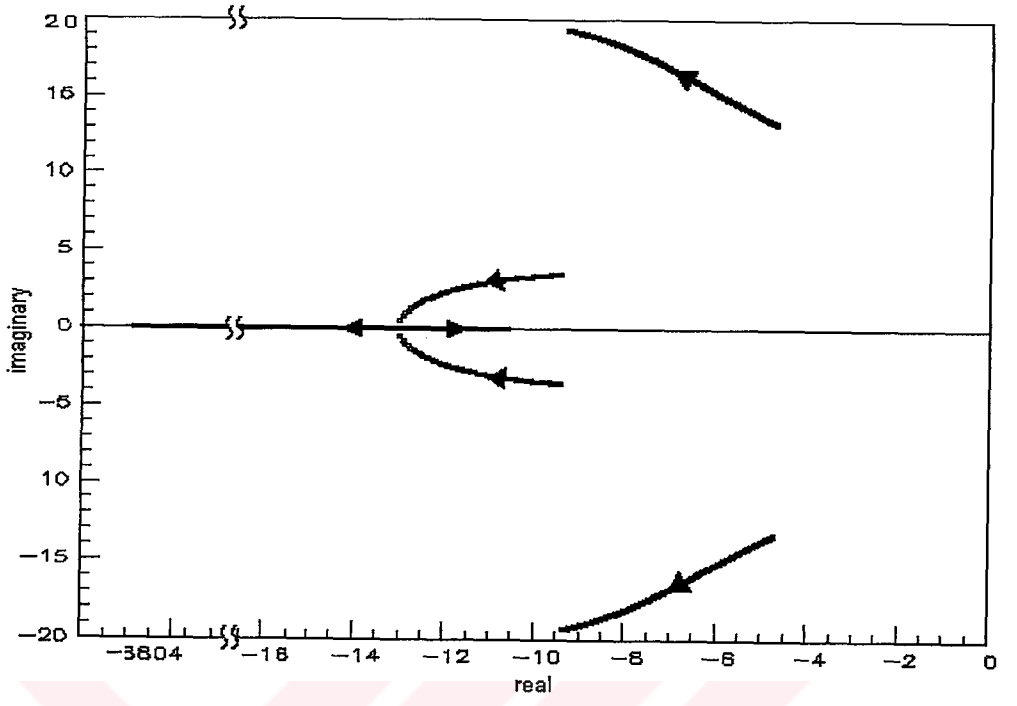

Figure 6.9 Root Locus for Set (X).

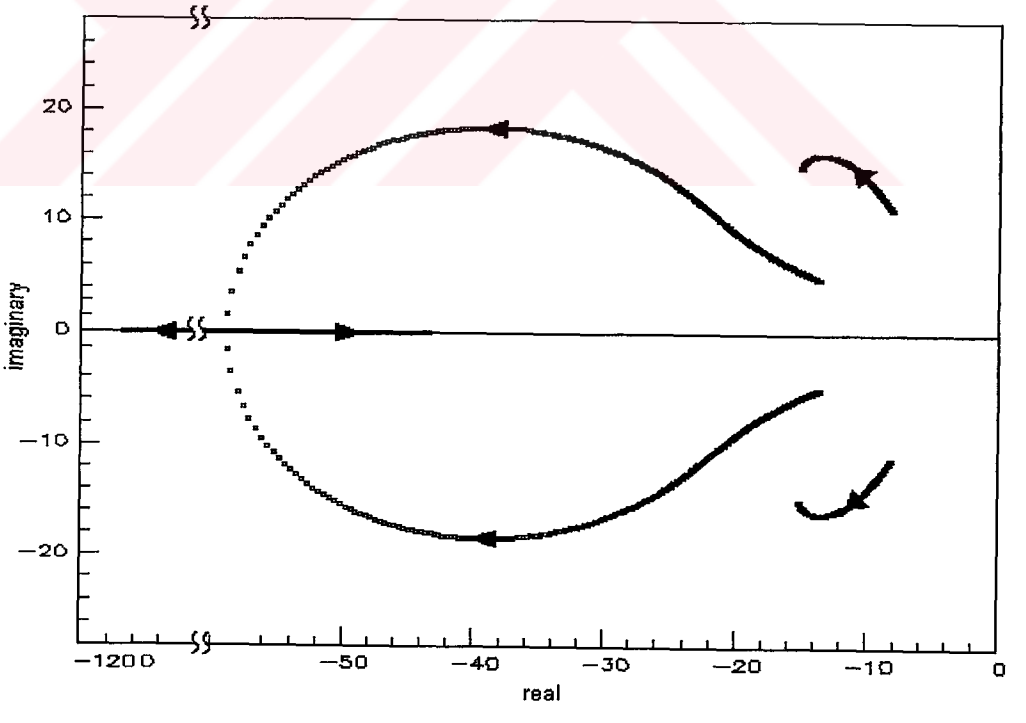

Figure 6.10 Root Locus for Set (XVIII)

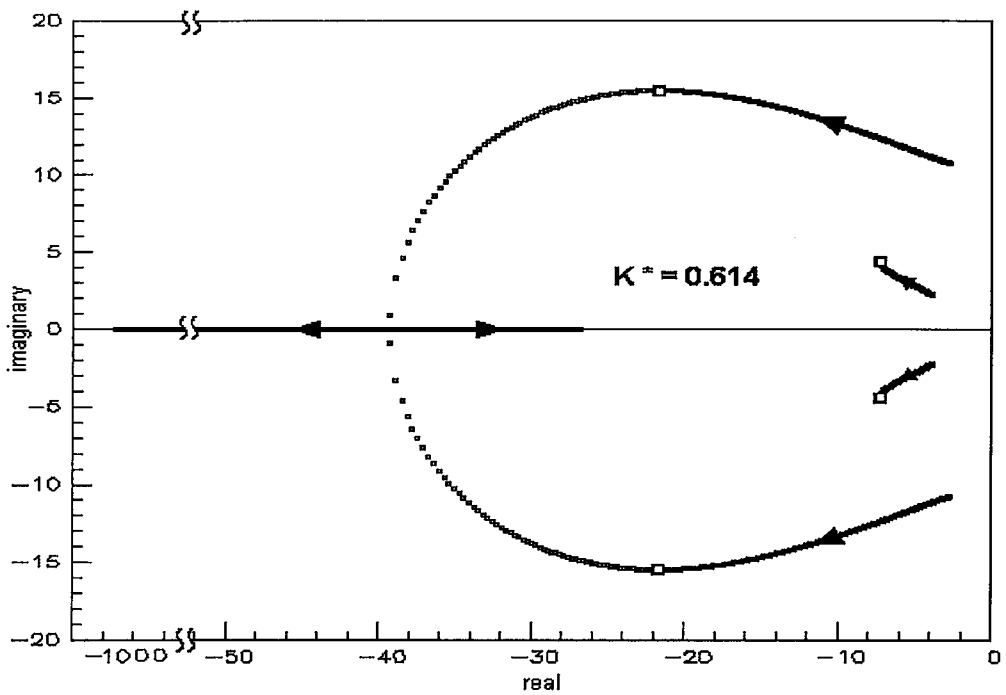

Figure 6.11 Root Locus for the Final Weighting Set.

After the design procedure is finished, the controller gains are found for all Mach numbers ranging between 0.1 and 3 for a gain scheduling in six degrees of freedom simulations. For different Mach numbers, K^* value is taken to be same as the one for Mach number equal to 1.5.

The autopilot designed this way is also checked in frequency domain by plotting the closed loop Bode plot of the autopilot at the Mach number equal to 1.5. This can be seen in Figure 6.12.

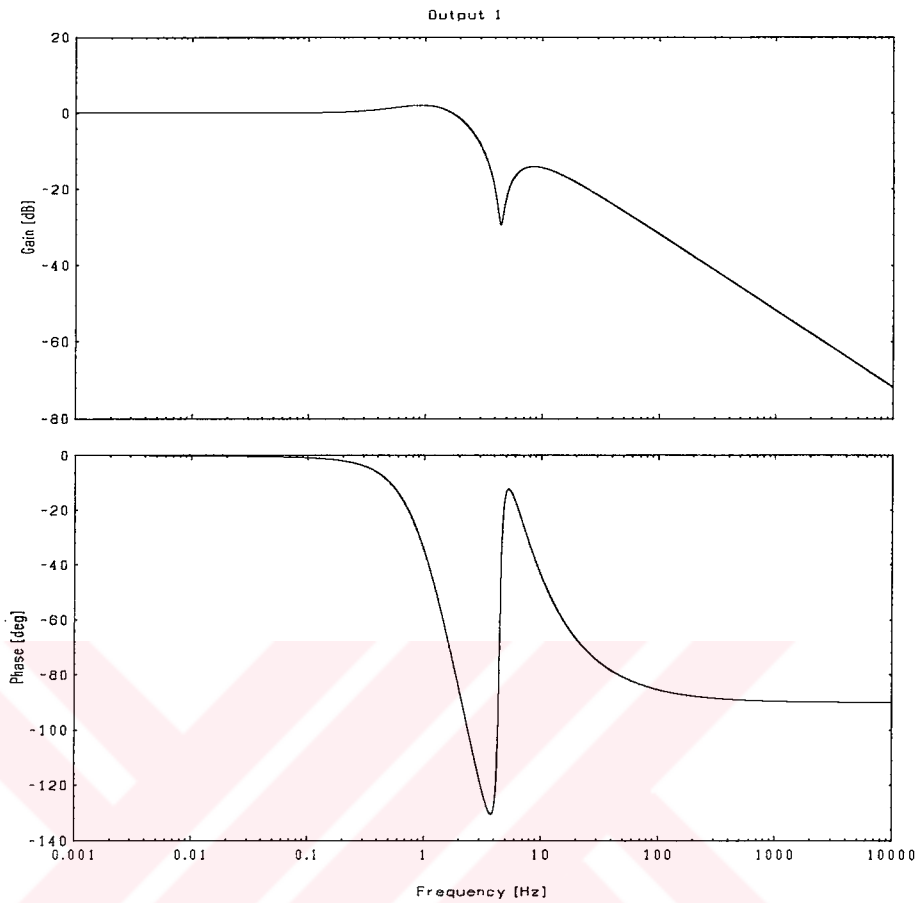

Figure 6.12. Bode Plot of the Autopilot 2 Closed Loop at M=1.5.

After the design of the longitudinal autopilot, the lateral autopilot is designed in the same way and also integrated into the six degrees of freedom simulations with the proper sign conventions for the controller gains.

6.2 Directional (Roll) Autopilot Design

Directional (Roll) autopilot of the missile has a great importance in this study since the lateral and longitudinal autopilots are designed based on the assumption that the rolling motion of the missile is negligibly small. The roll autopilot is an attitude autopilot which tries to keep the missile's roll attitude at zero

degrees. Due to external disturbances and the coupling effect of the pitching and yawing motions which both induce rolling motion, there exists a tendency to roll throughout the flight. The rolled missile is brought to zero roll position by the help of proper aileron deflection signals which are produced by the roll autopilot. The lateral, longitudinal and directional autopilots operate simultaneously during the flight. So, as a rule of thumb the roll autopilot should be much faster than the longitudinal and lateral autopilots. This requirement is necessary to ensure the separation of the yaw and pitch responses of the missile.

The generic missile considered in this study is a canard controlled missile. The missile has four canards and their combinatory motion produces aileron, rudder and elevator deflections to steer the missile in the roll, yaw and pitch planes respectively. Canard control is chosen, since the canards have the advantage of being located far from the tail and the motor sections of the missile. This provides more space for packaging of the control actuation system and the guidance unit. But it is known in the literature that [10], [11], the roll control of vehicles by canard surfaces are rather problematic. This is due to the adverse rolling moments which are induced by differential canard surface deflections. They generate an asymmetric flow field downstream. As a result of this asymmetry, a rolling moment is induced on the tail surfaces, opposing the original one. The magnitude of this adverse moment depends on flight conditions, and very often the net rolling moment is reversed. However, by applying careful aerodynamic design, effective and reliable roll controllable cruciform canard configurations can be obtained.

Due to the studies on roll control of canard controlled missiles [10] [11], simplified vortex sheet models for qualitative design and some guidelines are found. Based on these studies, the following guidelines are found as a rule of thumb :

- "Interdigitated" (+, ×) configuration is mandatory.
- The span and aspect ratio of the canard surfaces must be kept as large as possible considering the physical constraints on the missile.

•Low span and low aspect ratio slender tail fins have to be chosen.

•Roll control has to be done by those canard surfaces which lie in the plane which is perpendicular to the plane in which more steering deflections are made (e.g. generally the pitch plane).

•Roll control has to be preferably done by those canard surfaces which lie in the plane which is perpendicular to the plane in which the angle of attack of the missile remains smaller.

•Effect of the angle of attack in the perpendicular plane can be minimized by taking the canard surface backwards as much as possible.

If these rules of thumb are taken carefully into consideration in the design of the canard surfaces, the roll control of the missile can be achieved successfully without having roll reversal in the flight.

In order to see the roll reversal effect of the canard deflections, a rolling moment study is done on the generic missile under consideration. This study is done by using Missile Datcom [6]. Using Missile Datcom, the roll moment coefficients of the generic missile are found for "in line" (+, +), "interdigitated" (+, ×) and tailless configurations. The roll reversal effect is studied for the "in line" and the "interdigitated" configurations by comparing them with the tailless configuration in which there is no roll reversal effect. These can be seen in Figures 6.13 and 6.14.

From those figures, it can be seen that for the "interdigitated" configuration the roll reversal occurs beyond ± 5 degrees of aileron deflection. But for in line configuration it can be seen that there is always roll reversal for any aileron deflection. Also from Figure 6.14, it can be seen that roll moment efficiency (Cl_δ) of any canard deflection is reduced to one eighth of the tailless configuration. This is due to the interaction of the tail surfaces with the vortex sheet induced by the differential deflection of the canard surfaces. In general, this reduced Cl_δ may not be adequate for the roll control of a missile, and in that case the external configuration

design of the canard surfaces may have to be revised. But in our application, this range of roll moment efficiency turns out to be adequate.

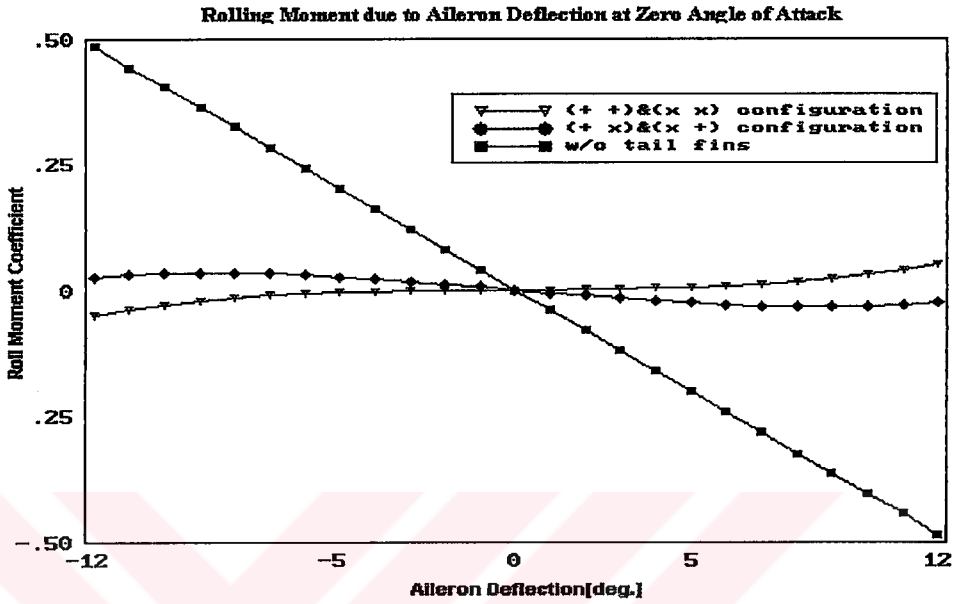

Figure 6.13 Roll Reversal Effect on Roll Moment Coefficient.

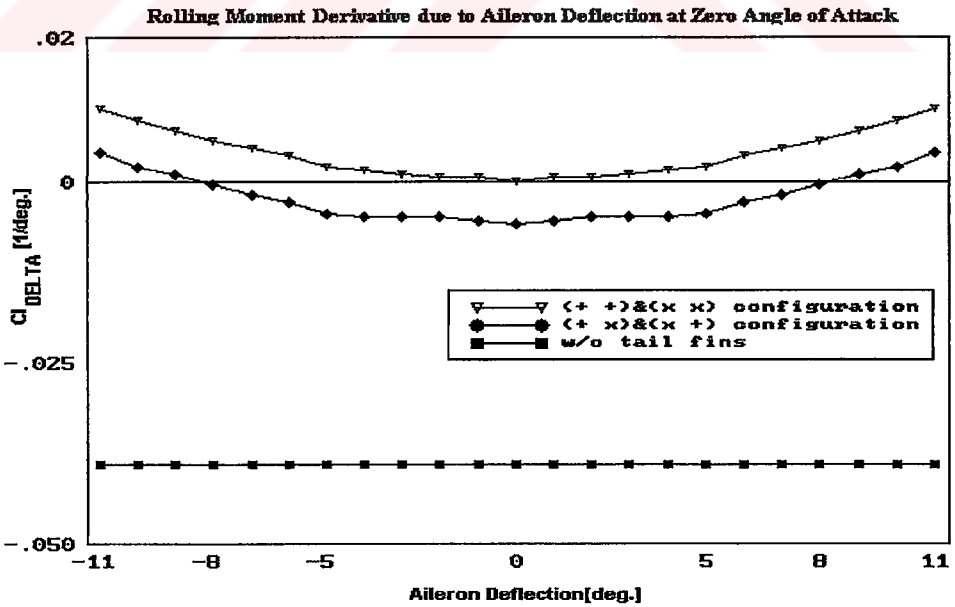

Figure 6.14 Roll Reversal Effect on Roll Moment Coefficient Derivative.

In order to design a roll autopilot, the linearized roll dynamics derived in Chapter 4 is used. The Cl_δ values are found from Missile Datcom. Thus, the L_δ value in Equation (4.53) can be found. In order to find L_p value, Cl_p has to be found. This value is found from Equation (6.80) [12] which is given below :

$$\frac{Cl_p}{Cl_\delta} = -2.15.(\frac{y_c}{d}) \tag{6.80}$$

Here y_c is the distance from the rolling body axis to the area center of one fin panel and d is the diameter of the missile. This correlation is shown to be valid for all missile speeds [12].

The linearized roll dynamics of the missile derived in Chapter 4 can be shown in state space form as

$$\begin{Bmatrix} \dot{p} \\ \dot{\phi} \end{Bmatrix} = \begin{bmatrix} L_p & 0 \\ 1 & 0 \end{bmatrix} . \begin{Bmatrix} p \\ \phi \end{Bmatrix} + \begin{bmatrix} L_\delta \\ 0 \end{bmatrix} . \delta_a + \begin{bmatrix} 0 \\ d_1 \end{bmatrix} \tag{6.81}$$

Here, $d_1 = (q.\sin\phi + r.\cos\phi).\tan\theta$. However, ϕ is to be kept near zero. So, $d_1 \cong r.\tan\theta$. Thus becoming independent of ϕ, d_1 can be treated as a disturbance on the roll dynamics.

A simple full state feedback controller can be designed on this system as shown in Figure 6.15.

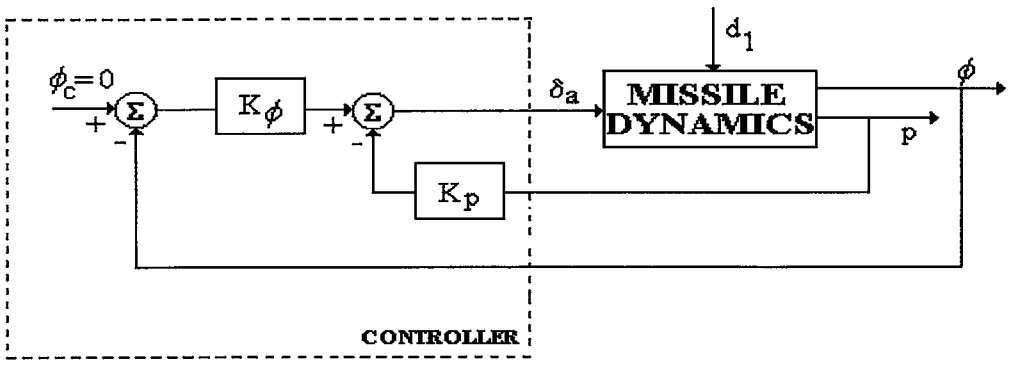

Figure 6.15 Block Diagram Representation of Roll Autopilot.

With $\phi_c = 0$, the controller generates δ_a as

$$\delta_a = -[K_p \quad K_\phi].\begin{Bmatrix} p \\ \phi \end{Bmatrix} \tag{6.82}$$

Then the closed loop system will be represented by

$$\begin{Bmatrix} \dot{p} \\ \dot{\phi} \end{Bmatrix} = \begin{bmatrix} L_p - L_\delta.K_p & -L_\delta.K_\phi \\ 1 & 0 \end{bmatrix}.\begin{Bmatrix} p \\ \phi \end{Bmatrix} \tag{6.83}$$

The characteristic polynomial of this system is

$$\Delta_{dr}(s) = s^2 + (L_\delta.K_p - L_p).s + L_\delta.K_\phi \tag{6.84}$$

Let the characteristic polynomial be of the following desired form :

$$\Delta_{dr} = s^2 + 2.\zeta_r.\omega_{nr} + \omega_{nr}{}^2 \tag{6.85}$$

Hence, the following expressions will be found for the controller gains of the roll autopilot:

$$\begin{Bmatrix} K_p \\ K_\phi \end{Bmatrix} = \begin{bmatrix} \left(2.\zeta_r.\omega_{nr} + L_p\right)/L_\delta \\ \omega_{nr}^{\ 2}/L_\delta \end{bmatrix} \tag{6.86}$$

For a roll stabilized missile the roll autopilot has to be two or three times faster than the lateral and longitudinal autopilots. In our design, this speed for roll autopilot cannot be achieved, since there exists saturation for the aileron deflection. The saturation limit is taken to be $\pm 5^\circ$ for the roll autopilot, since the roll effectiveness (Cl_δ) of the missile, which can be seen in Figure 6.14, decreases rapidly beyond these limits. After few trials, a satisfactory speed that could be achieved at which there is no saturation for specified Cl_δ and Cl_p values is found. And this speed comes out to be adequate for the roll stabilization of the missile under consideration.

Thus, the gains for the roll autopilot are found and integrated into the six degrees of freedom simulations for a gain scheduling with respect to Mach number variation.

CHAPTER 7

SIMULATIONS

The six degrees of freedom simulations are done for the two autopilots designed in Chapter 6 for a given pre - defined desired trajectory. The simulations can be grouped in four different categories. These are no external disturbance, random aerodynamic data perturbation, yaw plane disturbances including both side wind and thrust misalignment and the worst case.

In "no external disturbance" case, there are no external disturbances acting on the missile such as side winds, thrust misalignments, aerodynamic data perturbation and no initial rolling motion. In the "random aerodynamic data perturbation" case, the aerodynamic derivatives that describe the flight dynamics model of the missile are perturbed randomly in order to account for the uncertainties in the computations of Missile Datcom [6], which can be said to be in the range of ± 10 % for all outputs of the program. Ten simulations are made for one perturbation set, in which there are randomly changing perturbation amounts for all of the aerodynamic derivatives independently. In the "yaw plane disturbances" case, the side wind profile and the thrust misalignment model which are explained in Appendix are applied. Two simulations are made for this case, by keeping the direction of the thrust misalignment in the same, and in the opposite direction of the side wind. In the worst case, there are all effects, namely the side wind, the thrust misalignment in the

same direction as the side wind and the aerodynamic data perturbation. The aerodynamic derivatives are perturbed by their maximum deviations (± 10 %). The sign of perturbation is assigned depending on which sense the relevant aerodynamic derivative gets worst. This perturbation scheme can be seen in Table 7.1.

Table 7.1 Worst Aerodynamic Derivative Perturbation

Aerodynamic Derivative	Worst Perturbation Amount	Explanation
Cm_α	- 10 %	Static stability is decreased
Cm_δ	- 10 %	Control effectiveness is decreased
Cm_q	- 10 %	Damping characteristics is decreased
Cz_α	- 10 %	Lifting characteristics is decreased
Cz_δ	- 10 %	Control effectiveness is decreased
Cz_q	- 10 %	Damping characteristics is decreased
Cx	+ 10 %	Air drag is increased
Cl_δ	- 10 %	Control effectiveness is decreased
Cl_p	- 10 %	Damping characteristics is decreased

Initial roll rate of 2.5 r.p.m. is also included in all of the simulations where the performance of lateral control is examined. This is done to see not only the performance of the roll autopilot but also the lateral coupling of roll movements.

The roll autopilot is started to operate one second before the pitch and yaw autopilots are started to operate. The autopilots are not started to operate just at the beginning of the flight, because the missile speed is not yet high enough to realize the steering of the missile with small enough fin deflections remaining within the saturation limits.

The simulations are done for both of the autopilots separately. The results of the simulations are presented in graphical manner in the following sections.

7.1 Desired Trajectory

The desired trajectory is given by specifying the altitude and the cross range as functions of the range. The cross range is always given as zero reference, assuming that the missile azimuth to target alignment is done and the missile is initially in the same plane as the target. In this thesis, the altitude of the missile is given as the sums of three sine functions of range. This is done to provide a trajectory with a gliding phase. The gliding feature is desirable in order to increase the range without necessarily increasing the maximum altitude. During the gliding phase, the control effort will increase in order to provide extra lift to the missile. This increase will lead to an increment in the control surface deflections and consequently in the angle of attack. Thus, the missile will deviate more from the trim points that the controllers are designed and the controllers are also tested for this deviation.

7.2 Simulation Results

Simulation results of the two autopilots are presented in the same graphics in sections 7.2.1, 7.2.3 and 7.2.4. Also the simulation results are given in unit simulation time.

Line style (_ _ _ _) represents Autopilot 1.
Line style (_____) represents Autopilot 2.

7.2.1 No Disturbance Case

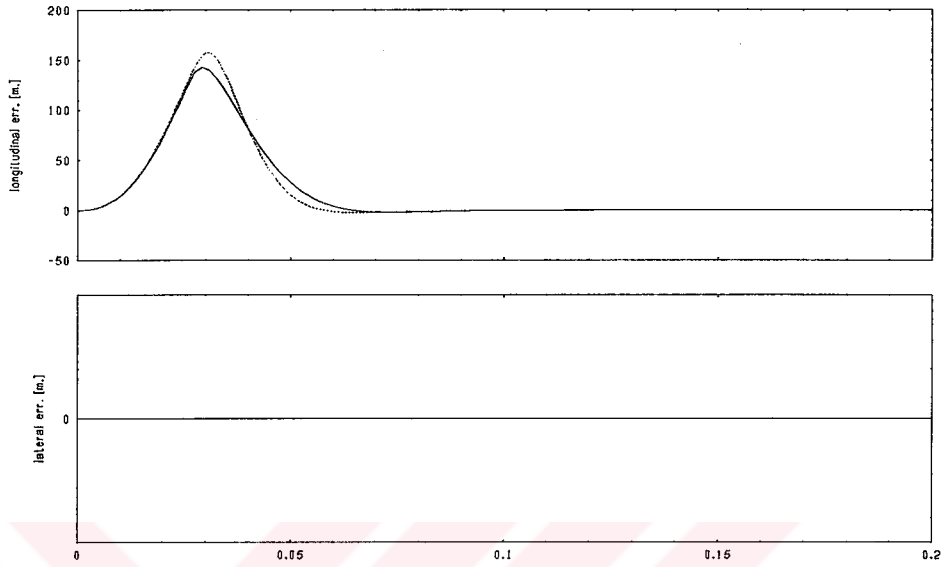

Figure 7.1 Trajectory Errors

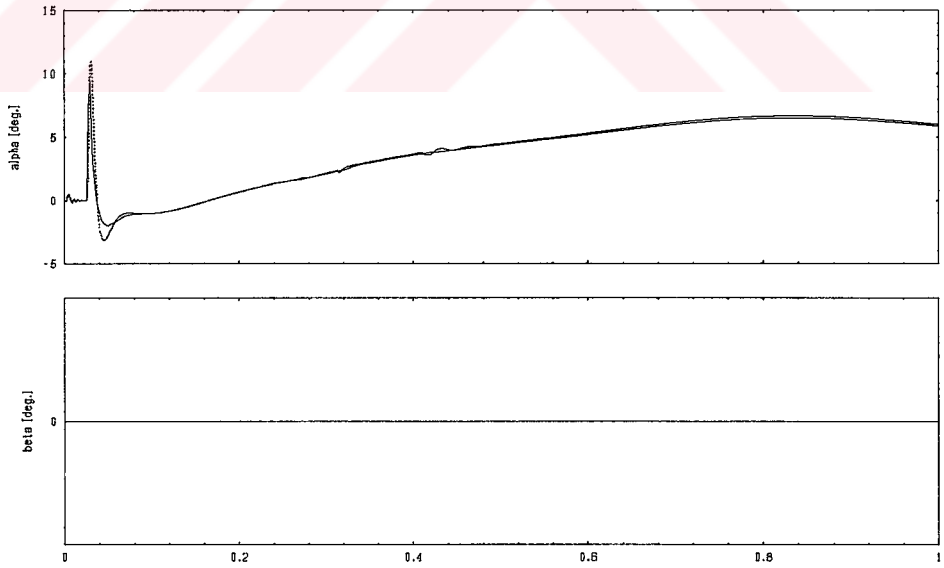

Figure 7.2 Angle of Attack and Side Slip Angles

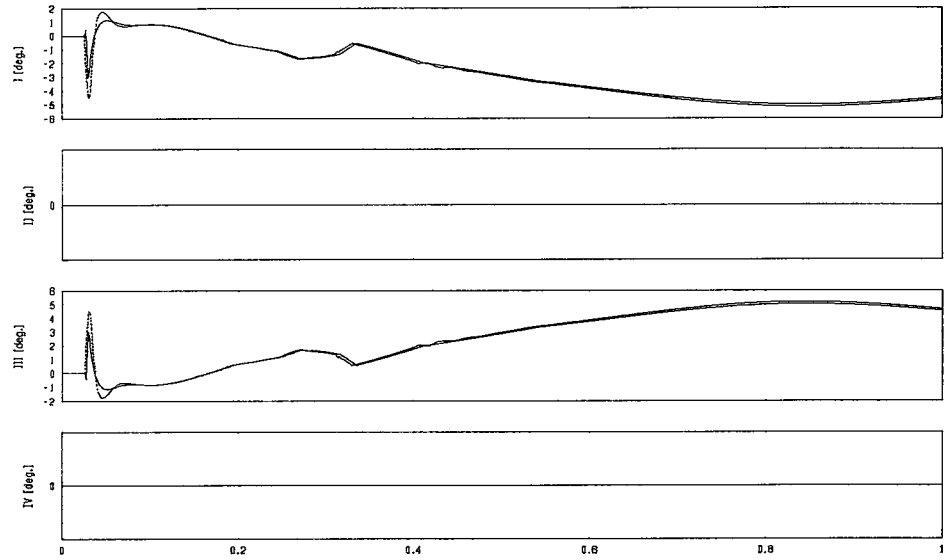

Figure 7.3 Canard Deflections

7.2.2 Random Aerodynamic Derivative Perturbation

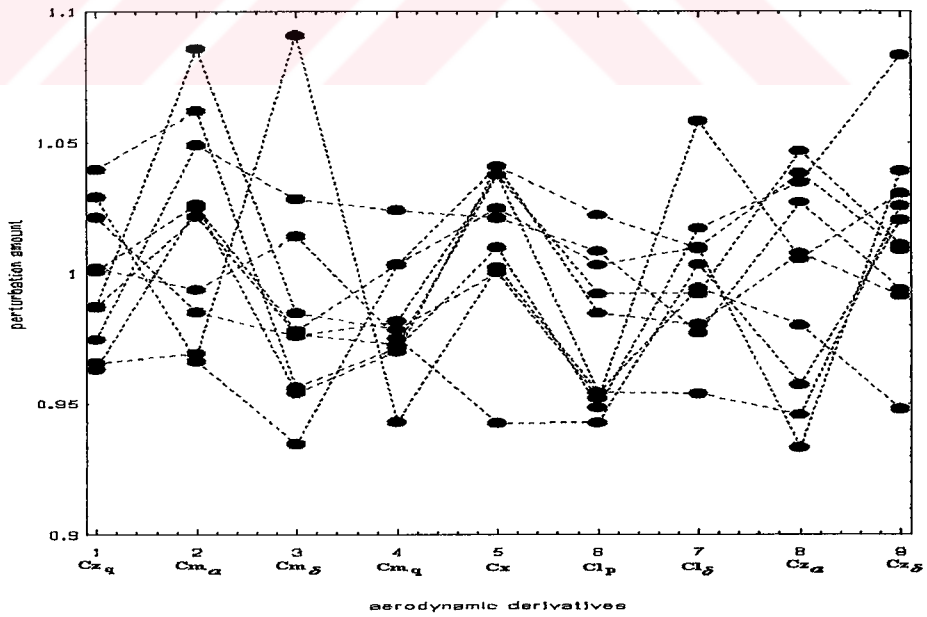

Figure 7.4 Random Perturbation for Aerodynamic Derivatives

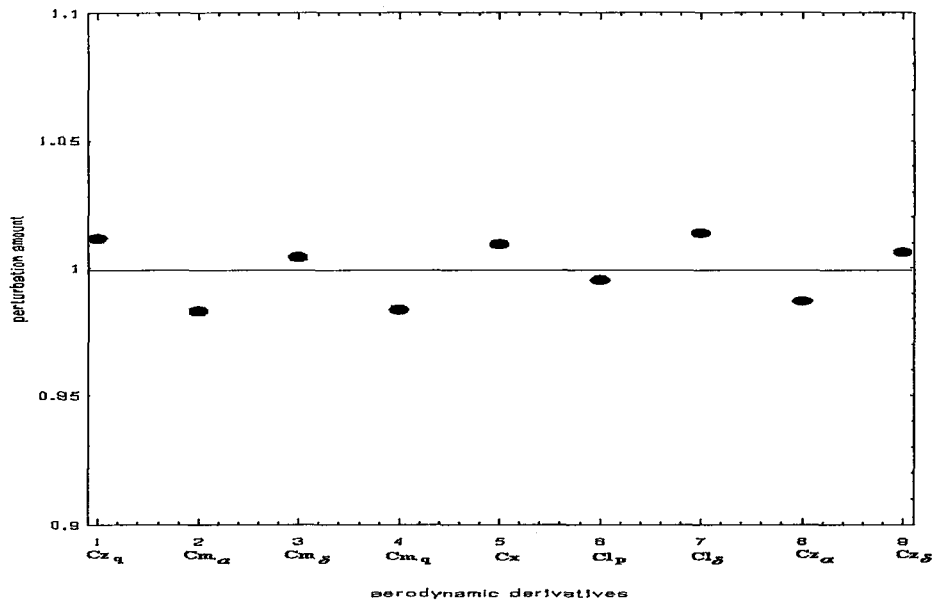

Figure 7.5 Mean Perturbation Amount for Aerodynamic Derivatives

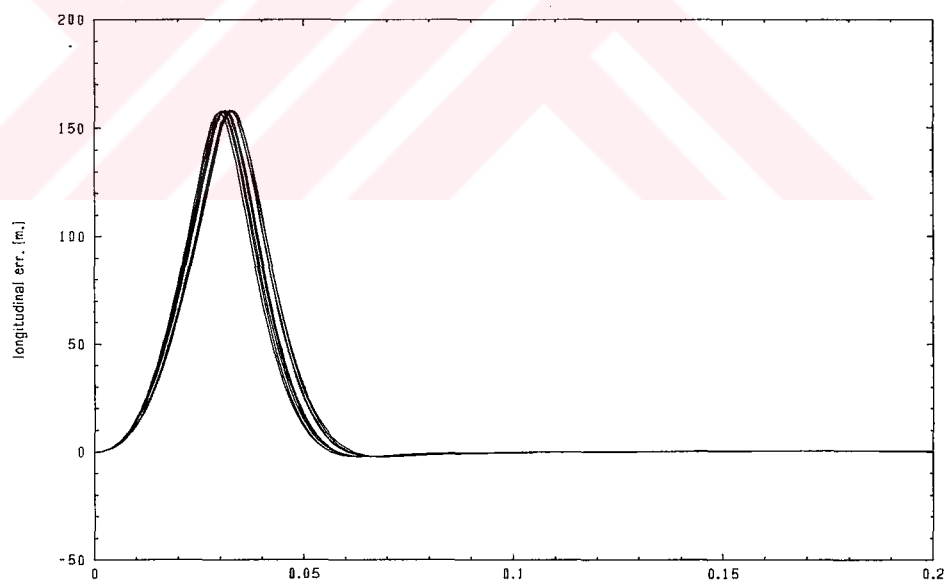

Figure 7 6 Longitudinal Trajectory Errors for Autopilot1

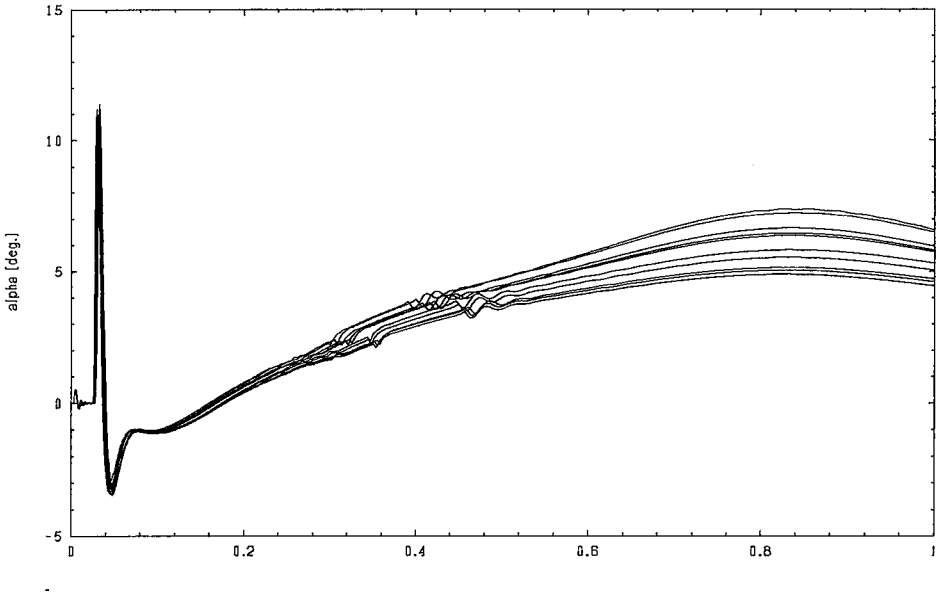

Figure 7.7 Angle of Attacks for Autopilot 1

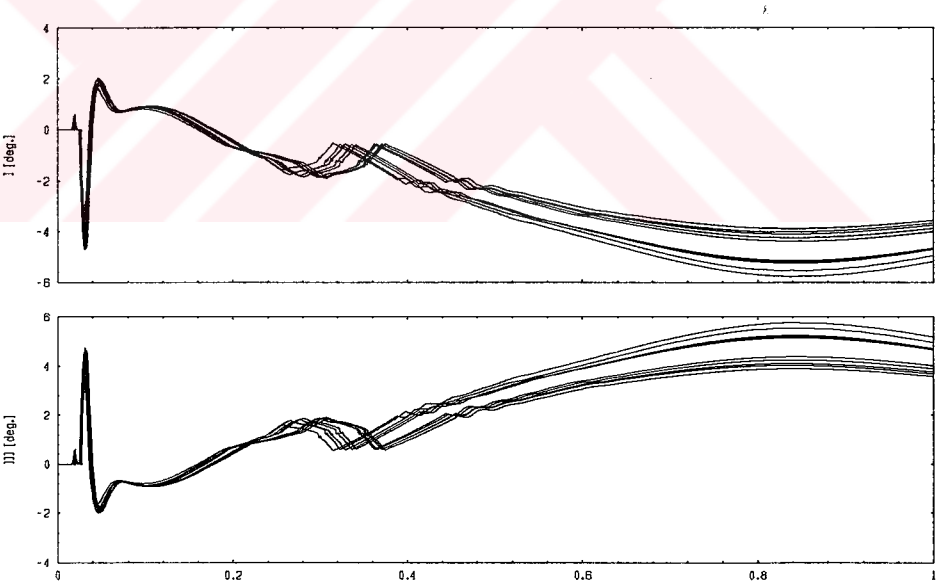

Figure 7.8 Canard Deflections for Autopilot 1

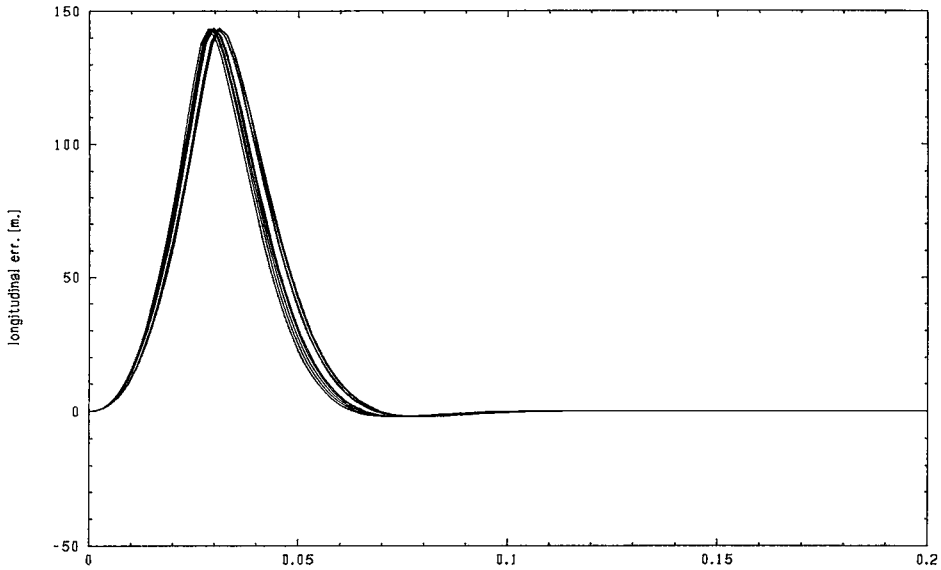

Figure 7.9 Longitudinal Trajectory Errors for Autopilot 2

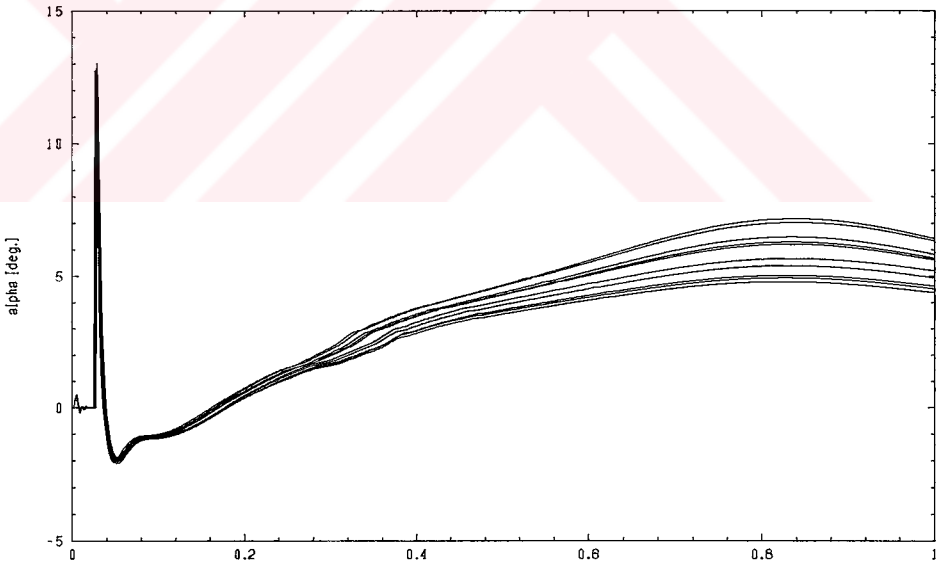

Figure 7.10 Angle of Attacks for Autopilot 2

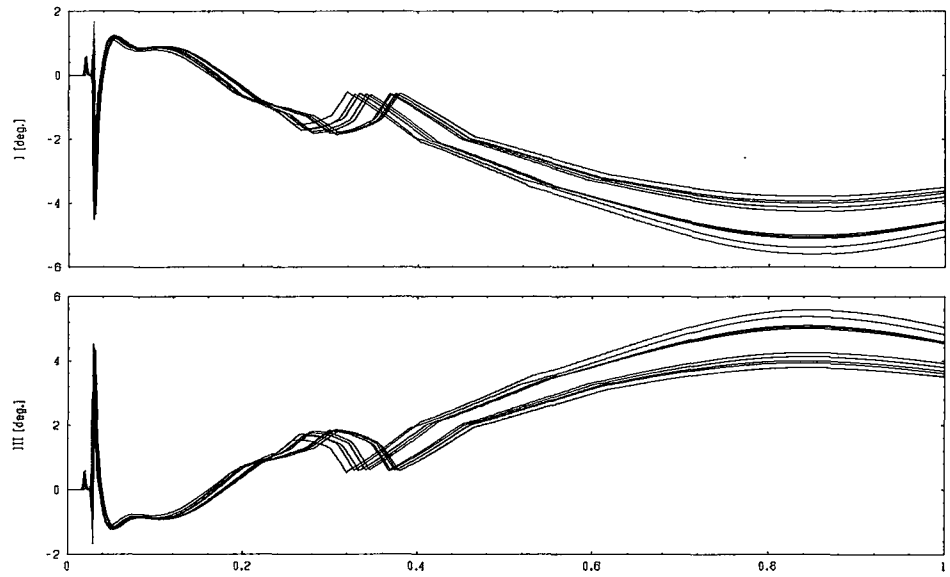

Figure 7.11 Canard Deflections for Autopilot 2

7.2.4 Yaw Plane Disturbances

7.2.4.1 Case 1: Side Wind and Thrust Misalignment are in the Same Sense

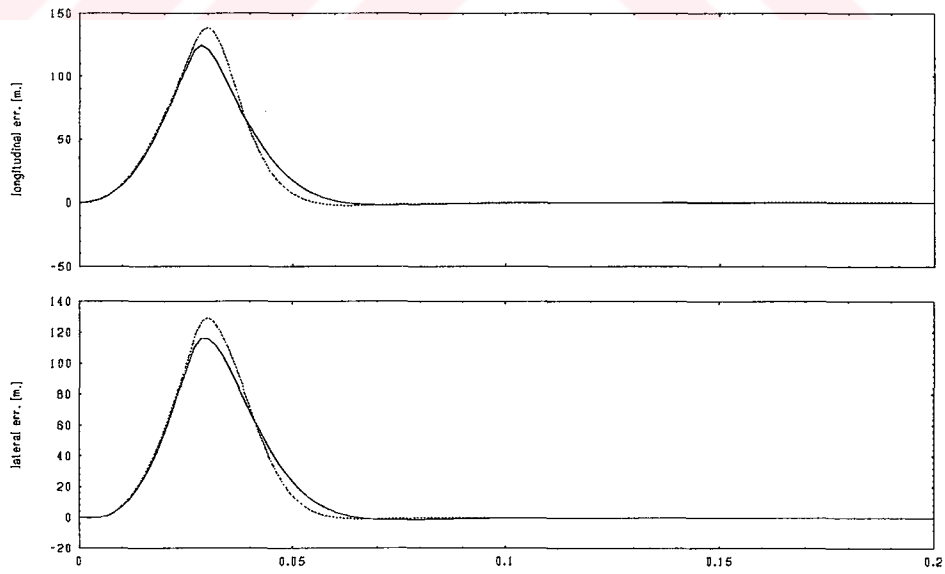

Figure 7.12 Trajectory Errors

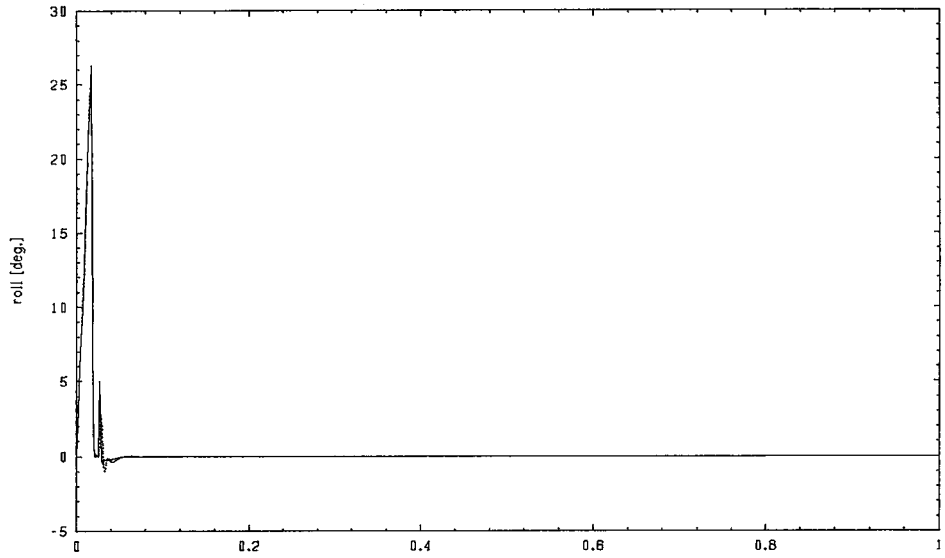

Figure 7.13 Roll Angles

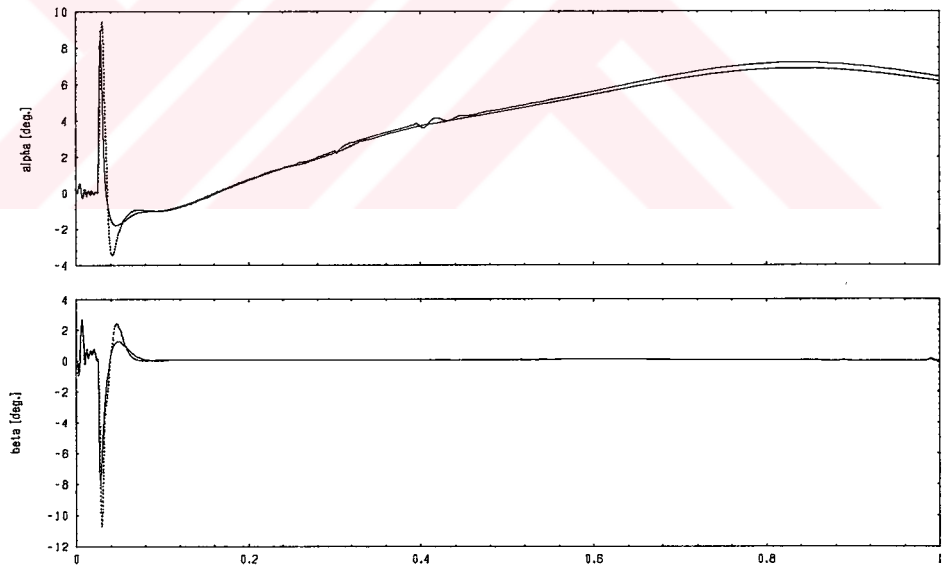

Figure 7.14 Angle of Attack and Side Slip Angles

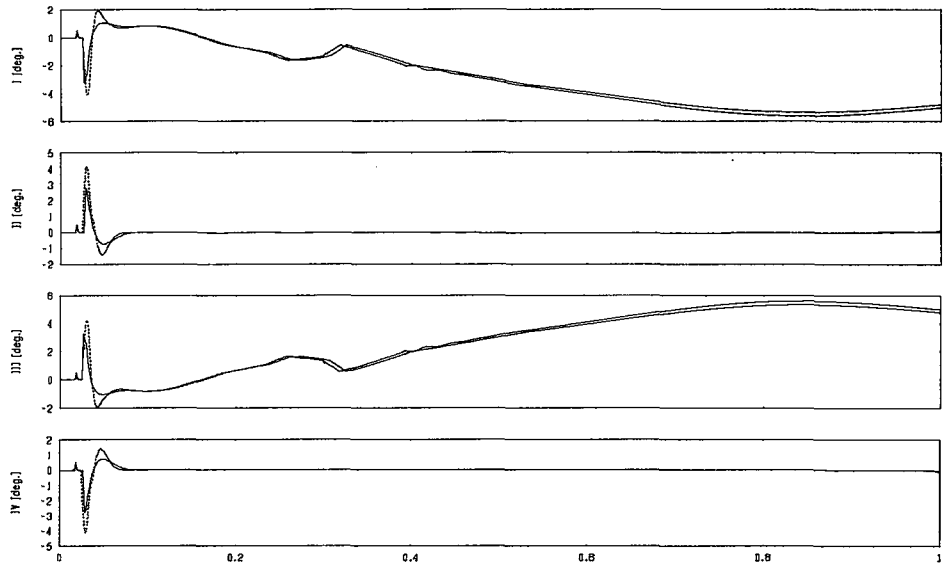

Figure 7.15 Canard Deflections

7.2.4.2 Case 2: Side Wind and Thrust Misalignment are in the Opposite Sense

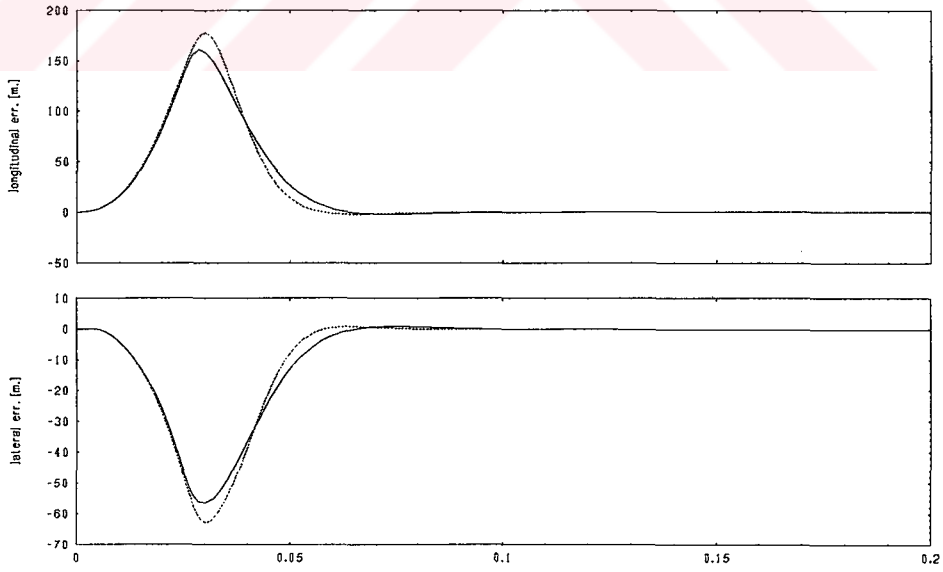

Figure 7.16 Trajectory Errors

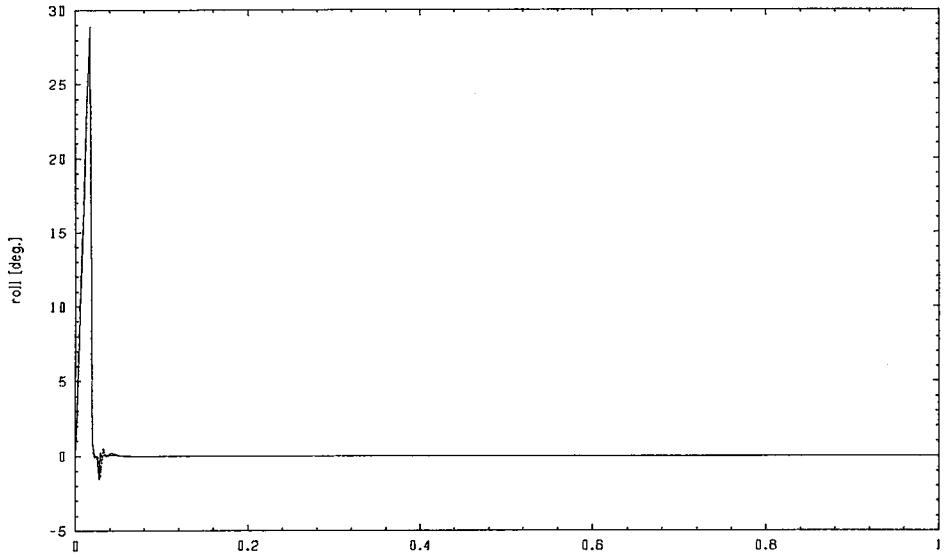

Figure 7.17 Roll Angles

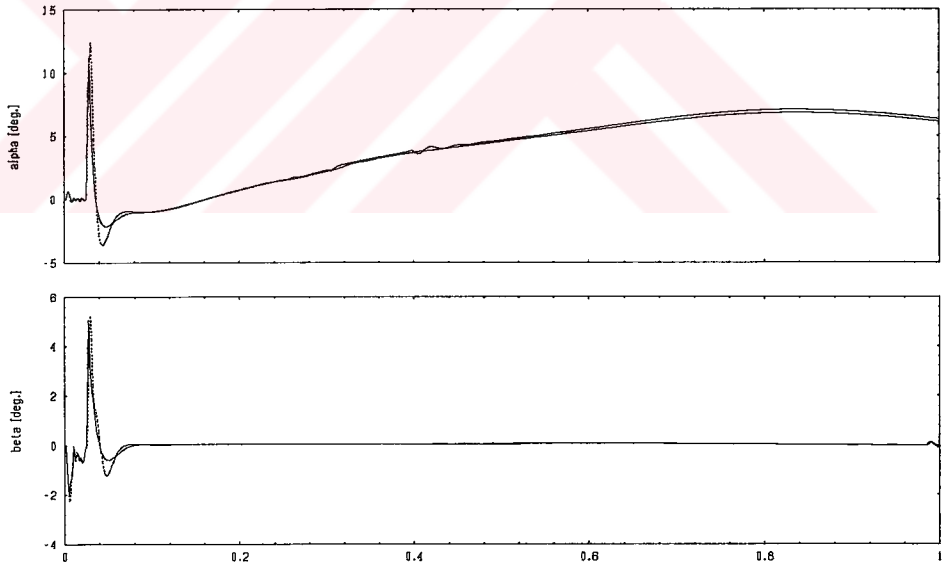

Figure 7.18 Angle of Attack and Side Slip Angles

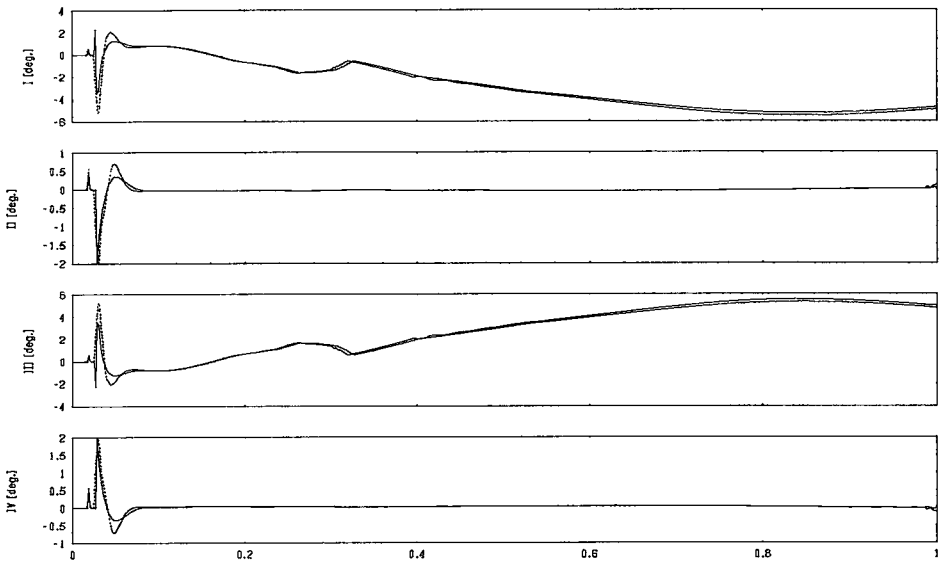

Figure 7.19 Canard Deflections

7.2.5 Worst Case

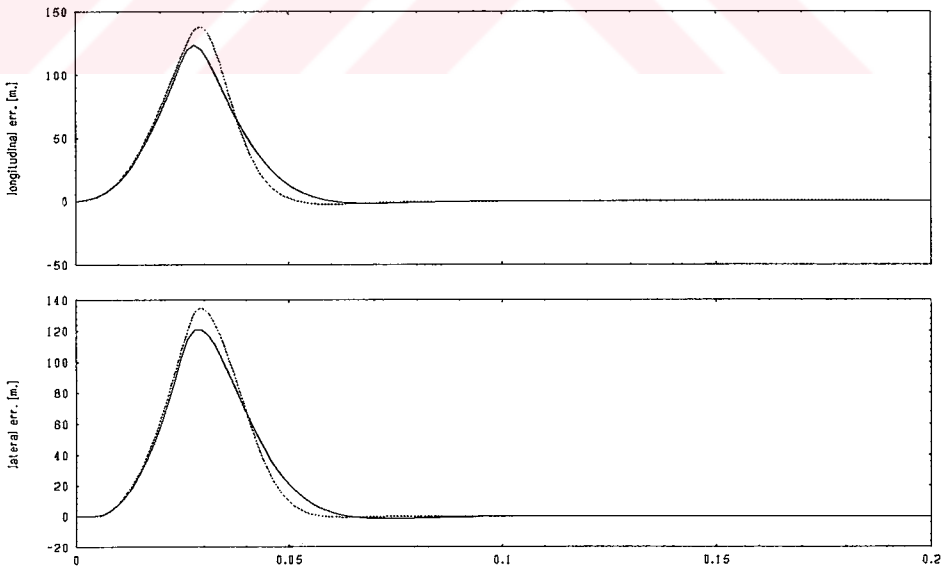

Figure 7.20 Trajectory Errors

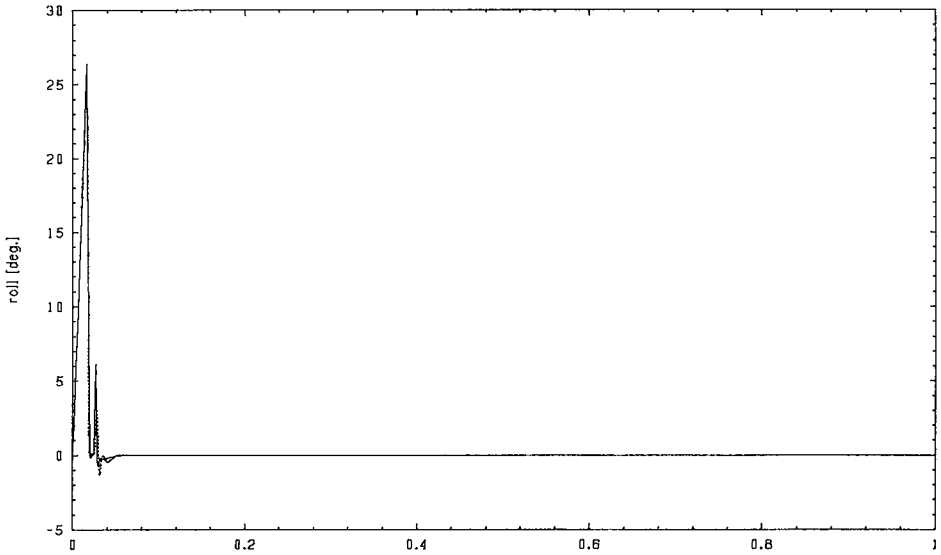

Figure 7.21 Roll Angles

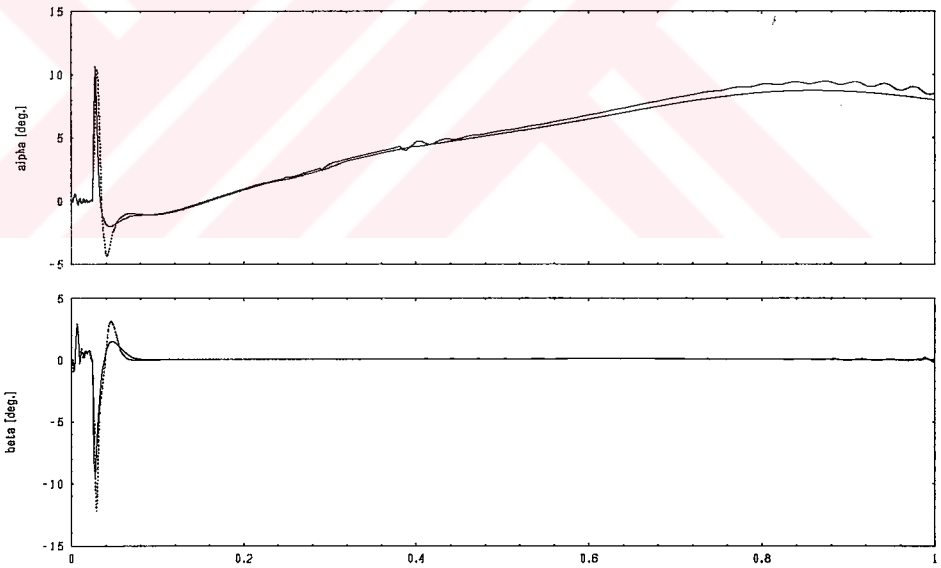

Figure 7.22 Angle of Attack and Side Slip Angles

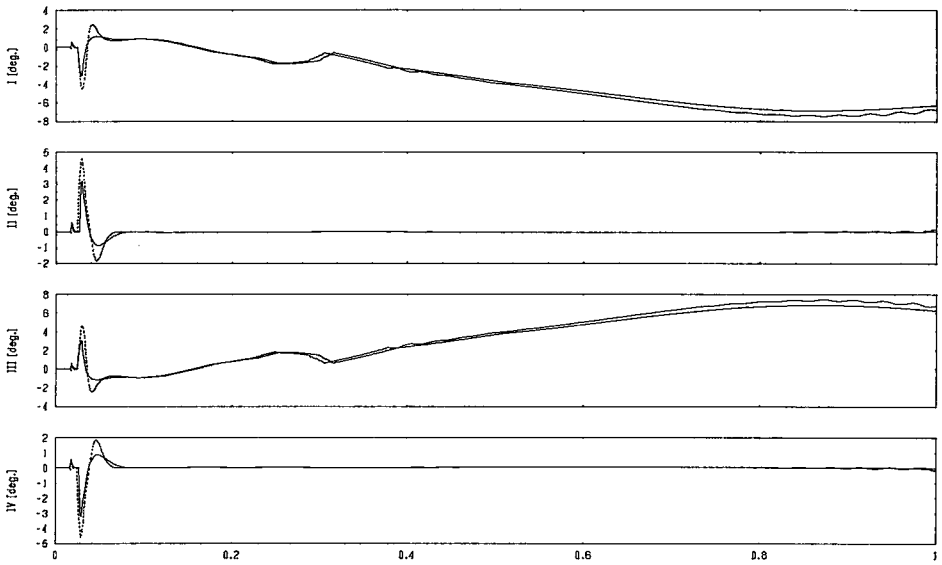

Figure 7.23 Canard Deflections

CHAPTER 8

CONCLUSION

In this thesis, a guidance system, two different lateral and longitudinal autopilots and a roll autopilot are designed for a trajectory tracking canard controlled surface to surface missile. The guidance system is designed using inverse dynamics methodology in order to null the error between the desired and the actual trajectories of the missile both in the pitch and yaw planes. In the guidance design, the same parameters are used for both of the pitch and yaw planes, in order to produce the desired normal acceleration commands in these planes.

Two acceleration autopilots are designed to fulfill the desired acceleration commands. Both of the autopilots are designed using the linearized and decoupled dynamics of the missile.

The decoupled dynamics of the missile is maintained by a roll autopilot which tries to keep the missile always at zero roll angle. Roll control of missiles with canard surfaces are problematic due to the roll reversal effect which is caused by the downwash effect of the canards on the missile tail fins. However, canard surfaces are still preferred because the canards have the advantage of being located far from the tail and the motor sections of the missile. This provides more space for packaging of the control actuation system and the guidance unit. This roll

reversal effect is also studied within the scope of this thesis and a proper roll control is designed using a simple PD controller for the generic missile under study.

A modification is applied on the conventional linearized dynamics of the missile in order to handle the normal acceleration and the canard deflection as state variables. This brings not only the direct availability of the state variables from the sensors in the inertial measuring unit and the control actuation system of the missile, but also a freedom to design a full state feedback controller without having angle of attack and side slip sensors or an extra on - line computation algorithm for these angles.

The first autopilot, Autopilot 1, is designed using the modified linear dynamics of the missile, and a state feedback with integral controller is applied. The closed loop transfer function of the autopilot is found and some adjustments both on the numerator and denominator dynamics are made. The numerator has a third order dynamics and the two zeros of this dynamics are determined by the plant parameters of the missile dynamics. Thus, only one zero can be placed freely. This zero is placed such that it has the same magnitude as the natural frequency of the other two complex conjugate zero pairs. There are four poles to place in the denominator dynamics. Since there are four controller gains, and one is used for zero placement, only three poles can be placed as desired. The three poles are placed as the dominant ones and the fourth pole is checked and verified that it does not come closer to the imaginary axis than the dominant complex conjugate pole pairs. This way, there will not be any sensible effect of the numerator dynamics up to the cut off frequency of the autopilot and a flat Bode magnitude plot for the autopilot closed loop transfer function is obtained again up to the cut off frequency of the autopilot.

Design of Autopilot 1 is carried out for twenty Mach numbers in the range between 0.1 and 3. This is done for a gain scheduling in the six degrees of freedom simulations. For different Mach numbers, different numerator and denominator natural frequencies are obtained in order to satisfy the desired zero and

pole placement form described above. Satisfactory placements have been achievable because the nature of the uncontrolled missile dynamics have mostly been favorable, except may be at the very early and very late phases of flight where the Mach numbers are rather low, and low Mach numbers lead to low autopilot bandwidths according to the described pole and zero placement procedure.

The second autopilot, Autopilot 2, is designed using quadratic performance index minimization scheme. The same modified state space formulation is used throughout the design. This brings the minimization of the canard deflection easily, since it is a state variable in the modified system. A prescribed stability degree criterion is also included in the design so that the closed loop poles do not come closer to the imaginary axis than a pre - specified border. A root locus approach is integrated into the study and the changes in the closed loop pole locations are also investigated as the relative weightings of the state variables are changed.

Design of Autopilot 2 is also carried out for the same Mach numbers for a gain scheduling in the six degrees of freedom simulations.

Two of the autopilots are integrated into the six degrees of freedom simulations and simulated for a given pre - specified trajectory under four simulation cases. These are; no external disturbance case, side wind and thrust misalignment case, aerodynamic data perturbation case and the worst case in which all the disturbances are effective. The simulation results for both of the autopilots are taken out graphically.

The simulation results show that, the guidance system, the two kinds of the lateral and longitudinal autopilots (Autopilot 1 and Autopilot 2) and the roll autopilot show satisfactory responses in order to satisfy the desired reference commands. All of the external disturbances are rejected by the robustness characteristics of the designed autopilots throughout the specified trajectory. The time histories of the angle of attack, the side slip angle and the canard deflection

angles are maintained at small amounts through all phases of flight and the canard surfaces operate within their saturation limits for all elevator, rudder and aileron deflections. Thus, the autopilots does not deviate much from the trim values for which they are designed for.

In all of the simulation results, it is seen that the angle of attack, the side slip angle and the canard deflection values for Autopilot 2 are somewhat smaller when compared with those of Autopilot 1. There are also some small wiggles in those values for Autopilot 1 around Mach number 1 and toward the end of the flight where the Mach number reaches to smaller values such as 0.4 and 0.3. Also the peak values of the trajectory errors are higher for Autopilot 1 than Autopilot 2.

Autopilot 2 becomes slightly better than Autopilot 1 due to its quadratic performance index minimization characteristics which leads to smaller angle of attack, side slip angle and canard deflection values. The small wiggles in these values for small Mach numbers for Autopilot 1 occur due to small bandwidths that come out by the design procedure of Autopilot 1 which forces the dominant poles to the right of the zeros. If this enforcement is released to some extend for small Mach numbers, then Autopilot 1 could be improved by preventing its bandwidth from falling below some minimum allowable value.

If the autopilots are considered with the question whether they achieve the desired trajectory tracking mission, they are all successful.

In future studies, both of the autopilots has to be tested in discrete time simulations using fixed point arithmetic calculations with specified sampling frequencies. After these software simulation tests, the autopilot algorithms can be put in the hardware and tested in the hardware in the loop simulations in order to use in the real time flight mission of the missile.

REFERENCES

1. Indirect Off - Set Program Notes by Martin Marietta, "Guidance and Control, Autopilot Design, Part 1, Book 1",Orlando, 1993.
2. Indirect Off - Set Program Notes by Martin Marietta, "Guidance and Control, Autopilot Design, Part 2",Orlando, 1993.
3. Integrated Systems Inc. $Matrix_x$, Product Family, "Xmath Reference, Part Number 000 - 0026 - 003", January 1996.
4. Integrated Systems Inc. $Matrix_x$, Product Family, "SystemBuild User's Guide, Part Number 000 - 0051 - 005", January 1996.
5. Saffel, B. F., Millard, H., L., Brooks, E., N., "A Method for Predicting the Static Aerodynamic Characteristics of Typical Missile Configuration for Angles of Attack to 180 Degrees", Naval Ship Research and Development Center Report, Washington DC, 1971.
6. Burns, K. A., Deters, K. J., Stoy, S. L., Vukelich, S. R., Blake, W. B., "MISSILE DATCOM, User's Manual, Revision 6/93, Final Report for Period August 1992 - March", Wright Patterson Air Force Base, Ohio, 1993.
7. Tanrıkulu, Ö., Önen, C., Mahmutyazıcıoğlu, G., Bektaş, İ., "Linear Stability Analysis of Unguided Missiles with Wrap - Around Tail Fins in Free Flight", AGARD - FVP - 1995 Spring Activities, Ankara.

8. McLean, D., "Automatic Flight Control Systems", Prentice Hall International (UK) Ltd., 1990, ISBN 0 -13- 054008 - 0.

9. Ateşoğlu, Ö., Özgören, K., "Autopilot Design For A Trajectory Tracking Missile Using Optimal Control With Prescribed Degree of Stability", Proceedings of the Ankara International Aerospace Conference and Symposia, pp.202 - 209, Ankara, September 19 - 21 1996.

10. Gur, I., Shinar, J., Rom, J., "A Model for the Evaluation of Induced Rolling Moments and Side Forces in Slender Cruciform Canard Configurations at Small Angle of Incidence", Israel Journal of Technology, Vol. 14, pp.74 - 85, 1976.

11. Shinar, J., "Roll Control Feasibility of a Slender Cruciform Configuration by Canard Surfaces at Mach Number 2.25", Israel Journal of Technology, Vol. 12, pp.31 - 39, 1974.

12. Mikhail, A., G., "Roll Damping for Finned Projectiles Including Wrap Around, Offset, and Arbitrary Number of Fins", Propulsion and Flight Division Weapons Technology Directorate U. S. Army Research Lab. Aberdeen Proving Ground, Maryland 21005 - 5066.

13. Mahmutyazıcıoğlu, G., "Dynamics and Control Simulation of an Inertially Guided Missile", M.S. Thesis in M.E.T.U. Mechanical Engineering Dept., Ankara, 1994.

14. Anderson, L., Andersson, J., "Development of the S - 19 Guidance System for the Reduction of Sounding Rocket Dispersion", AIAA 4th Sounding Rocket Technology Conference Proceedings, June 1976, pp. 172 - 178.

APPENDIX

MODELING OF OTHER COMPONENTS OF THE SIX DEGREE OF FREEDOM SYSTEM

A.1 Variable Mass and Inertia Model

Due to the burning of the propellant, the mass, the rotational inertia and the location of the mass center of the missile change in time.

This variation can be modeled as shown below:

For $t < t_{boost}$,

$$m(t) = m_0 - \frac{m_0 - m_1}{Imp_{total}} . Imp(t) \tag{A.1}$$

$$I(t) = I_0 - \frac{I_0 - I_1}{Imp_{total}} . Imp(t) \tag{A.2}$$

$$x_c(t) = x_{c0} - \frac{x_{c0} - x_{c1}}{Imp_{total}} . Imp(t) \tag{A.3}$$

m_0, I_0, x_{c0} are the initial, and m_1, I_1, x_{c1} are the final values of the mass, the rotational inertia and the mass center location. Imp_{total} is the total impulse given by the rocket motor, i.e. the total area under the trust - time curve. Imp(t) is the impulse at time t generated by the trust force (T) and is found by

$$Imp(t) = \int_0^t T(\tau).d\tau \tag{A.4}$$

A.2 Thrust Misalignment Model

Ideally the thrust vector is assumed to be aligned with the center line (x axis) of the missile. But due to inaccuracies in the production and the burning of the propellant, misalignment of the thrust with the x axis can be unavoidable. Hence, this has to be modeled in the six degrees of freedom simulations.

The misaligned thrust force components (T_x, T_y, T_z) and moment components (L_T, M_T, N_T) in the x, y and z directions can be expressed as

$$\begin{bmatrix} T_x \\ T_y \\ T_z \end{bmatrix} = \begin{bmatrix} T.\cos\delta_1 \\ -T.\sin\delta_1.\sin\delta_2 \\ T.\sin\delta_1.\cos\delta_2 \end{bmatrix} \tag{A.5}$$

$$\begin{bmatrix} L_T \\ M_T \\ N_T \end{bmatrix} = \begin{bmatrix} 0 \\ T_z.(l - x_c) \\ T_y.(l - x_c) \end{bmatrix} \tag{A.6}$$

The angles δ_1, δ_2 and the misaligned thrust and force components can be seen in Figure A.1. l is the length of the missile.

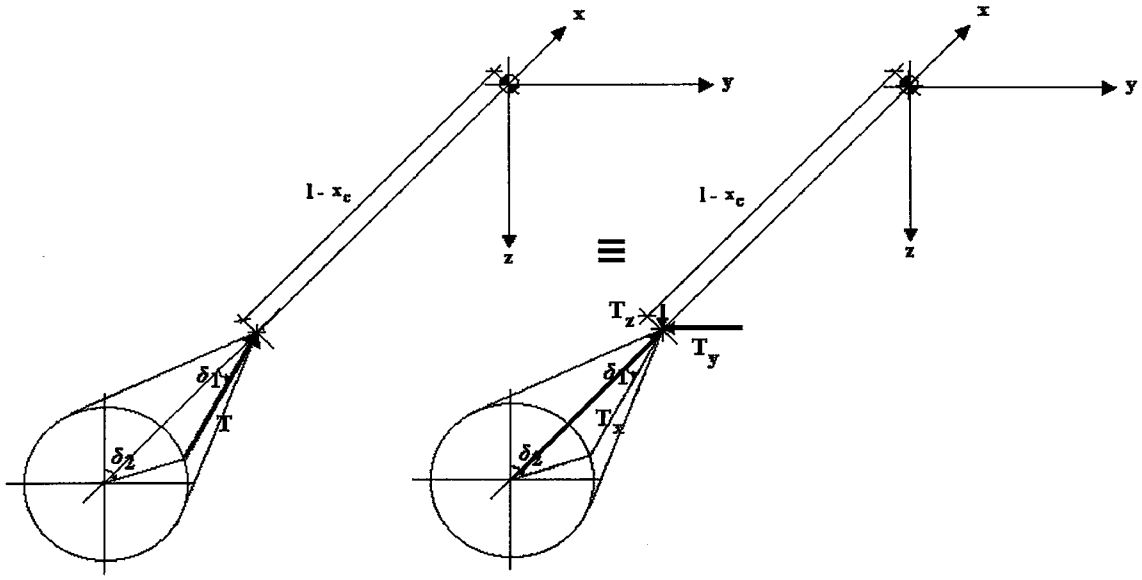

Figure A.1 Thrust Misalignment Model.

In the simulations a side thrust misalignment is modeled by taking the misalignment angles as

$$\delta_1 = 0.1^\circ \tag{A.7}$$

$$\delta_2 = 90^\circ \tag{A.8}$$

A.3 Sensor Models

Accelerometers and gyroscopes are used to measure the body accelerations and rotation rates respectively. As an ideal case, the accelerometers all in the three directions have to be located at the center of mass of the missile not to measure some induced components due to body rotations. But this is not feasible in almost every application due to the changing center of mass location throughout the flight and placement of the inertial measuring unit in the guidance section of the missile. Therefore the measured accelerations can be expressed as [13]

$$\begin{bmatrix} a_{xm} \\ a_{ym} \\ a_{zm} \end{bmatrix} = \begin{bmatrix} (F_{ax} + T_x)/m - (x_c - l_a).(q^2 + r^2) \\ (F_{ay} + T_y)/m + (x_c - l_a).(\dot{r} + p.q) - 2.r.\dot{x}_c \\ (F_{az} + T_z)/m - (x_c - l_a).(\dot{q} + p.r) + 2.q.\dot{x}_c \end{bmatrix} \tag{A.9}$$

where a_{xm}, a_{ym}, a_{zm} are the measured acceleration values, l_a is the distance of the accelerometers from the nose and $\dot{x}_c$ is the time rate of change of mass center position.

Since the accelerometers do not measure gravitational acceleration components they have to be compensated for gravity effect. Also the gyroscopic terms measured by accelerometers must be compensated to achieve the true value of the accelerations to use in the strapdown system algorithms. This is done as,

$$\begin{bmatrix} a_x \\ a_y \\ a_z \end{bmatrix} = \begin{bmatrix} a_{xm} + g_x + (x_c - l_a).(q^2 + r^2) \\ a_{ym} + g_y - (x_c - l_a).(p.q) + 2.r.x_c \\ a_{zm} + g_z + (x_c - l_a).(p.r) - 2.q.x_c \end{bmatrix} \tag{A.10}$$

The $\dot{q}$ and $\dot{r}$ terms are ignored in the above equation since they are neither measured nor numerically estimated without high noise levels. They are assumed to be small in magnitude in the compensation process.

Both the accelerometers and the gyroscopes are modeled as second order dynamic systems. The transfer functions for gyroscopes and accelerometers can be expressed as,

$$G_a(s) = \frac{\omega_{na}^{\ 2}}{s^2 + 2.\zeta_a.\omega_{na}.s + \omega_{na}^{\ 2}} \tag{A.11}$$

$$G_g(s) = \frac{\omega_{ng}^{\ 2}}{s^2 + 2.\zeta_g.\omega_{ng}.s + \omega_{ng}^{\ 2}} \tag{A.12}$$

The undamped natural frequency of these systems can be taken in the range of 500-700 rad./sec. and the related damping values are taken in the range of 0.5-0.8. Their dynamics are very fast when compared to the guidance, the three autopilots and the control actuation system.

The error modeling of these systems is a very important subject to study. The typical errors on gyroscopes are bias, g sensitive drift and random noise and typical errors on accelerometers are bias and random noise. These error sources can be modeled as a total drift on the sensors. These total drift values can be taken as 100 deg./hr. for the gyroscopes and 100 μg for the accelerometers.

A.4 Strapdown Model

In inertial navigation systems, strapdown system algorithms are used to achieve the position information. In these systems the information coming from the strapdown accelerometers and gyroscopes are used to calculate the position.

The measured angular rates are converted into changes in attitude of the vehicle with respect to its initial orientation. The resulting attitude transformation matrix is used to convert the measured accelerations from body reference frame to inertial reference frame. The transformed accelerations are numerically integrated twice with a high computation speed to obtain the position data with respect to the inertial reference frame. On the other hand, the transformation matrix is obtained by Equation (2.10), using the measured angular rates as inputs.

The computational logic of the strapdown system algorithm used in the six degrees of freedom simulations can be seen in Figure A.2.

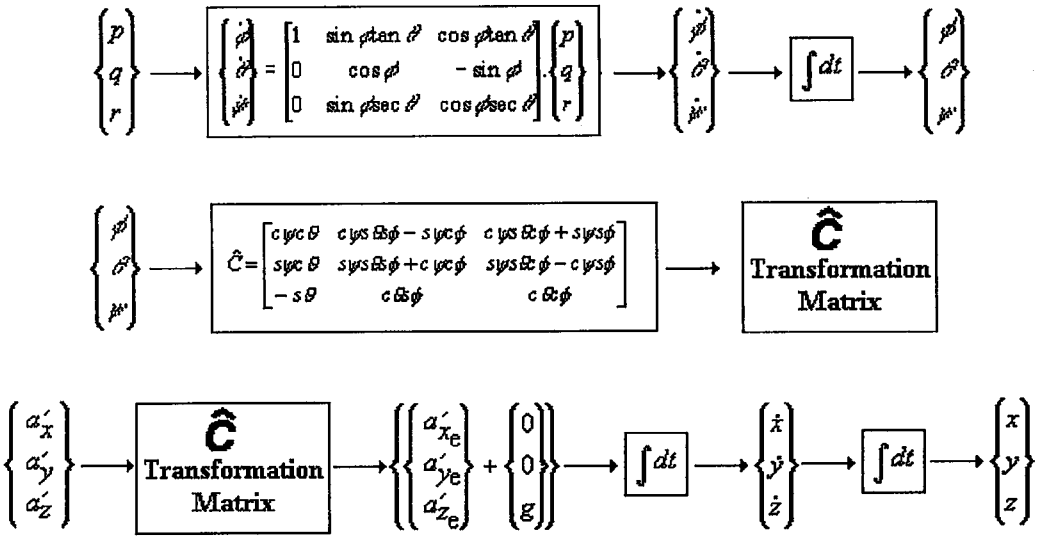

Figure A.2 Strapdown System Algorithm Computational Logic.

The a'_x, a'_y, a'_z values in Figure A.2 are the accelerometer outputs which are not compensated for gravitational acceleration, but compensated for the induced accelerations from the body rotations. The p, q, r values are the gyroscope outputs in the missile body reference frame.

A.5 Control Actuation System Model

The dynamics of the control actuation system is also included in the overall simulation model. The control actuation system itself is a closed loop control system. Its dynamics can also be expressed as a second order system as shown in Equation (A.13).

$$\frac{\delta(s)}{\delta_c(s)} = \frac{\omega_{nc}^{\ 2}}{s^2 + 2.\zeta_c.\omega_{nc}.s + \omega_{nc}^{\ 2}} \qquad \text{(A.13)}$$

The fin deflection $\delta(t)$ in a missile is generally limited to $\pm\ 10^0$ - 15^0. Outside this range, the aerodynamic flow separation on the control surfaces cause a decrease in their lifting force performance, i.e. their control effectiveness. Also,

because of the actuator constraints, the rate of the fin deflection $\delta(t)$ is limited. This brings a nonlinear modeling of control actuation system as shown in Figure A.3. The limiting values for the fin deflections and their rates are taken to be 10^0 and 1200^0/sec. respectively in the six degrees of freedom simulations.

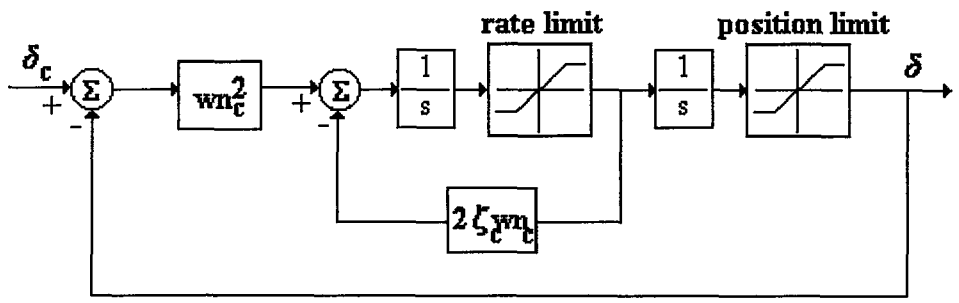

Figure A.3 Nonlinear Control Actuation System Model.

A.5.1 Aerodynamic Control Surface Arrangements

The movable fins in this study are located at the front of the missile and they are called canards. Due to the roll reversal effect described in Chapter 6 the canards and tails are in a "interdigitated" position which can be seen in Figure A.4.

In the simulation models, each of the four canards is taken to be driven by a separate actuator. The roll, yaw and pitch movements are realized by the effective aileron, rudder and elevator deflections which are conventionally defined as the following combinations of the actual control surface deflections :

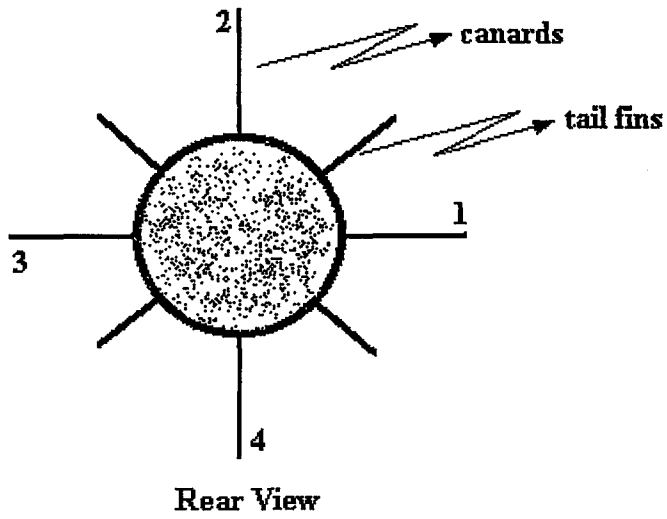

Figure A.4 Interdigitated Configuration.

$$\delta_a = \frac{1}{4}.(\delta_1 + \delta_2 + \delta_3 + \delta_4) \tag{A.14}$$

$$\delta_r = \frac{1}{2}.(\delta_2 - \delta_4) \tag{A.15}$$

$$\delta_e = \frac{1}{2}.(\delta_1 - \delta_3) \tag{A.16}$$

As noted, this convention leads to a redundancy in the control surfaces, which originates from the fact that there are four control surfaces to achieve three motions. This redundancy can be used in minimization of the control surface deflection magnitudes. The outputs of the yaw, pitch and roll autopilots are δ_e, δ_r and δ_a respectively. Equations (A.14), (A.15) and (A.16) can be rewritten as

$$\begin{bmatrix} 1 & 0 & -1 & 0 \\ 0 & 1 & 0 & -1 \\ 1 & 1 & 1 & 1 \end{bmatrix} . \begin{Bmatrix} \delta_1 \\ \delta_2 \\ \delta_3 \\ \delta_4 \end{Bmatrix} = \begin{Bmatrix} 2.\delta_e \\ 2.\delta_r \\ 4.\delta_a \end{Bmatrix} \tag{A.17}$$

or more compactly as

$$\hat{A}.\bar{k} = \bar{b} \tag{A.18}$$

Minimizing a performance index such as

$$f = \frac{1}{2}.\bar{k}^T.\hat{Q}.\bar{k} \tag{A.19}$$

will give,

$$\bar{k} = \hat{Q}^{-1}.\hat{A}^T.(\hat{A}.\hat{Q}^{-1}.\hat{A}^T)^{-1}.\bar{b} \tag{A.20}$$

Taking,

$$\hat{Q} = \text{diagonal}(a, b, a, b) \tag{A.21}$$

The optimal fin deflection commands for the control actuation system will be,

$$\begin{Bmatrix} \delta_1 \\ \delta_2 \\ \delta_3 \\ \delta_4 \end{Bmatrix} = \begin{Bmatrix} \frac{2.b}{a+b}.\delta_a + \delta_e \\ \frac{2.a}{a+b}.\delta_a + \delta_r \\ \frac{2.b}{a+b}.\delta_a - \delta_e \\ \frac{2.a}{a+b}.\delta_a - \delta_r \end{Bmatrix} \tag{A.22}$$

By tuning the weightings a and b, the minimization level of (1, 3) and (2, 4) pairs of the fins can be changed as desired. Also the roll motion deflection can be done either by (1, 3) or (2, 4) pairs only, instead of all four of them by taking one of the weightings a and b as zero. This will increase the roll effectiveness of the aileron deflection due to the reasons explained in Section 6.2.

A.5.2 Roll Resolvation Model

During the flight the missile may roll due to some external disturbances and manufacturing misalignments of the control surfaces. Although there is a roll autopilot which is roll stabilizing the missile there may still be a certain amount of offset in the roll angle. The autopilot outputs has to be compensated for this roll effect since, the autopilot outputs are produced for the non rolling frame. This compensation is done in a way as shown below.

Let the deflection signals that are produced by the autopilots for the non - rolled frame (F_0) be :

$$\bar{r}^{(0)} = \begin{bmatrix} \delta_{ac} \\ \delta_{ec} \\ \delta_{rc} \end{bmatrix} \tag{A.23}$$

Suppose the missile has instantaneously a roll offset of ϕ. Then, the rotation matrix from F_0 to the rolled frame F_1 will be

$$\hat{C}^{(0,1)} = \begin{bmatrix} 1 & 0 & 0 \\ 0 & \cos\phi & \sin\phi \\ 0 & -\sin\phi & \cos\phi \end{bmatrix} \tag{A.24}$$

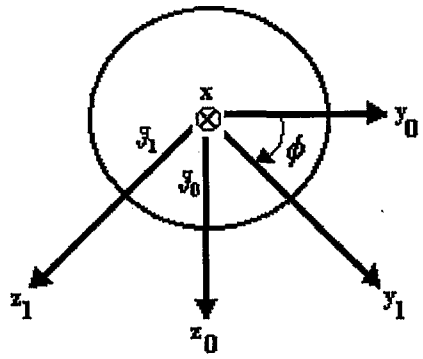

Figure A.5. Roll Resolvation Frames.

Consequently, the resolved autopilot commands will be

$$\bar{r}^{(1)} = \hat{C}^{(1,0)}.\bar{r}^{(0)} \tag{A.25}$$

or more explicitly,

$$\begin{bmatrix} \delta'_{ac} \\ \delta'_{ec} \\ \delta'_{rc} \end{bmatrix} = \begin{bmatrix} 1 & 0 & 0 \\ 0 & \cos\phi & -\sin\phi \\ 0 & \sin\phi & \cos\phi \end{bmatrix} . \begin{bmatrix} \delta_{ac} \\ \delta_{ec} \\ \delta_{rc} \end{bmatrix} = \begin{bmatrix} \delta_{ac} \\ \delta_{ec}.\cos\phi - \delta_{rc}.\sin\phi \\ \delta_{ec}.\sin\phi + \delta_{rc}.\cos\phi \end{bmatrix} \tag{A.26}$$

The autopilot commands will be resolved as shown in Equation (A.26) and $\bar{r}^{(1)}$ will be used instead of $\bar{r}^{(0)}$ in Equation (A.22) for the optimal fin deflections.

A.6 Wind Model

The atmospheric winds acting on the missile are treated as external disturbances. These disturbances try to deviate the missile from its desired trajectory throughout the flight. The transformation of the wind velocity in the earth fixed reference frame to the body fixed reference frame is done by using the direction cosine matrix from earth to body in Chapter 2 as shown below :

$$\begin{bmatrix} U_{wx} \\ U_{wy} \\ U_{wz} \end{bmatrix} = \hat{C}^{(b,e)} . \begin{bmatrix} V_{wx} \\ V_{wy} \\ V_{wz} \end{bmatrix} \tag{A.27}$$

The aerodynamic forces and moments arise due to the relative motion of the missile with respect to the surrounding air. So, when there are winds, the following relative velocity components should be used in computing the aerodynamic force and moment coefficients :

$$\begin{bmatrix} u_r \\ v_r \\ w_r \end{bmatrix} = \begin{bmatrix} u - U_{wx} \\ v - U_{wy} \\ w - U_{wz} \end{bmatrix} \tag{A.28}$$

The wind profile used in the simulations is generated with the help of the suggestion in [8] and [14]. This is a side wind profile which changes with altitude as shown in Table A.1.

A random noise with a standard deviation of $\sigma_w = 1 m/s$ is added on this wind profile and integrated in to the six degree of freedom simulations. The side wind profile used in the simulations, can be seen in Figure A.6.

Table A.1 Side Wind Profile.

Altitude [m.]	Side Wind Velocity [m./s]
0	0
10	3
100	6
700	9
1500	10
2400	11
5000	12

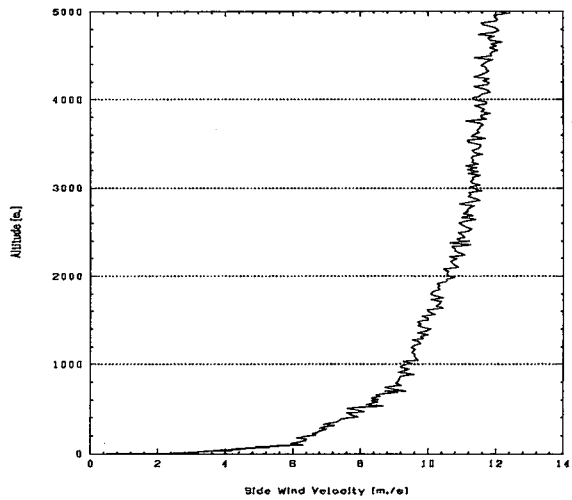

Figure A.6 Side Wind Profile.

A.7 Effect of Center of Mass Change on the Pitch and Yaw Moments

The aerodynamic force and moment coefficients explained in Chapter 3 are found from Missile Datcom [6], by specifying the mass center of the missile as the one after the boost phase i.e. as the final center of mass. This means that the forces and moments are found as if they are acting on the final center of mass of the missile even in the boost phase. This effect can be compensated by using the following formulation for pitching and yawing moments :

$$M' = M + (x_c - x_{c1}).F_{az} \tag{A.29}$$

$$N' = N - (x_c - x_{c1}).F_{ay} \tag{A.30}$$

Here, M and N are the pitching and yawing moments. F_{az} and F_{ay} are the normal and side forces as explained in Chapter 3. x_c is the center of mass location

at any instant during the flight and x_{c1} is the final center of mass position after the boost phase as explained in A.1.